

QUANTITATIVE OBSERVATIONS ON MULTIPLE FLOW STRUCTURES INSIDE
RANQUE HILSCH VORTEX TUBE

by

SACHIN UTTAMRAO NIMBALKAR

A Dissertation submitted to the
Graduate School-New Brunswick
Rutgers, The State University of New Jersey

In partial fulfillment of the requirements

For the degree of

Doctor of Philosophy

Graduate Program in Mechanical & Aerospace Engineering

Written under the direction of

Dr. MICHAEL R. MULLER

And approved by

New Brunswick, New Jersey

[May, 2009]

ABSTRACT OF THE DISSERTATION
QUANTITATIVE OBSERVATIONS ON MULTIPLE FLOW STRUCTURES INSIDE
RANQUE HILSCH VORTEX TUBE

By SACHIN U. NIMBALKAR

Dissertation Director:

Dr. MICHAEL R. MULLER

Ranque-Hilsch vortex tube is a device that separates a flow of gas into two streams simultaneously, one hotter than the inlet and one cooler. Traditionally vortex tubes are mostly operated at high entrance pressures (>10 psig) and always used for cooling operations. There are industrial applications that result in unused pressurized gases. Using vortex tube energy separation may be a method to recover waste pressure energy from high and low pressure sources. In various industrial systems, magnitudes of waste pressure may be lower but may have significant mass flow rates. Hence it is important to make sure that vortex tube provides the required energy separation while harnessing the low pressure but high mass flow rate waste energy and utilizes it for not only cooling but also for heating purposes.

Our recent experimental observations show that in the low inlet pressure regime (<10 psig); vortex tubes behave differently and produce multiple flow structures rather than expected re-circulating cold stream and the columnar hot stream type of flow (simply “Vortex Tube flow” or VT-flow).

This thesis characterizes industrial waste pressure as a reclaimable form of energy, analyzes the effectiveness of ‘vortex tube energy separation’ in recovering waste energy from low pressure sources, and explores experimentally and theoretically the possibility of multiple flow structures (like Reverse, Elbow, T-flow or VT-flow) inside vortex tube in a low inlet pressure regime.

First time, a study of flow modes in low pressure vortex tubes with small cold fractions has been presented which yielded quantitative confirmation of simple one dimensional model for these flows allowing both predictive capabilities and guidance in design.

PREFACE

The vortex tube (also called the Ranque-Hilsch vortex tube) is a mechanical device operating as a refrigerating and heating machine simultaneously without any moving parts, by separating a compressed gas stream into a low total temperature region and a high one. Traditionally vortex tubes are mostly operated at high entrance pressures and always used for cooling operations. There are industrial applications that result in unused pressurized gases. Using vortex tube energy separation may be a method to recover waste pressure energy from high and low pressure sources. “Waste pressure energy” may come in the form of pressurized exhaust gases (including non-condensable gases), steam, blow off compressed air, or even in the form of pressurized hot water. In various industrial systems, magnitudes of waste pressure may be lower but may have significant mass flow rates. Hence it is important to make sure that vortex tube provides the required energy separation while harnessing the low pressure but high mass flow rate waste energy and utilizing it for not only cooling but for heating purpose also. Purpose of this thesis is to present our recent experimental observations showing that in the low inlet pressure regime (<10 psig), vortex tubes behave differently and produce multiple flow structures rather than the expected re-circulating cold stream and the columnar hot stream (VT-flow).

This thesis is written for vortex tube manufacturers, researchers working on solar cyclone generators, vortex burners, vortex heat exchangers and vortex rockets, scientists with interest in vortex dynamics and computational fluid dynamics.

This thesis characterizes industrial waste pressure as a reclaimable form of energy, analyze the effectiveness of ‘vortex tube energy separation’ in recovering waste energy

from low pressure sources, and explores experimentally and theoretically the possibility of multiple flow structures (like Reverse/Venturi flow, Elbow flow, T-flow or VT-flow) inside vortex tube in a low inlet pressure regime.

ACKNOWLEDGEMENT

Early in the process of completing my master's thesis (January 2005), it became quite clear to me that a researcher cannot complete a PhD thesis alone. The actual list of individuals I wish to thank extends beyond the limits of this page. By keeping the one page limit in mind, I would like to thank the following persons for their dedication, prayers, and support:

My greatest advisor, Dr. Michael R. Muller, has been a significant presence in my life. His ability to probe beneath the text and the messy charts is a true gift, and his insights have strengthened this study significantly. I will always be thankful for his wisdom, knowledge, and deep concern not only for me, but also for his constant insistence that I should never give up the obsession for new knowledge. It has been an honor to work with him.

I would also like to thank the other members of my PhD committee who monitored my work and took effort in reading and providing me with valuable comments on earlier versions of this thesis: Dr. Haim Baruh, Dr. Tobias Rossmann, Dr. Jerry Shan and Dr. Anthony Wright (ORNL). I thank you all.

I am most grateful to my parents, brother, sister and sister-in-law who were always there to encourage me and my choices financially and psychologically. Last but not least, I wish to express my great appreciation to Michaela Martin, Donald Kasten, Joshua Kace, Mike B. Muller, Kunjal and Baking Oza, Siddika Pasi, Jill Mesonas, Malik Khan, Prakash Rao, Sara Salahi and Mindy Ren for their encouragement at the end of this journey and for their emotional and psychological support during the crucial portion of this project.

TABLE OF CONTENT

ABSTRACT OF THE DISSERTATION.....	ii
PREFACE	iii
ACKNOWLEDGEMENT.....	v
TABLE OF CONTENT.....	vi
LIST OF TABLES	ix
LIST OF ILLUSTRATIONS.....	x
NOMENCLATURE.....	xiii
CHAPTER 1 INTRODUCTION	1
1.1 OBJECTIVES OF THE THESIS.....	1
1.2 MOTIVATION - UTILIZING WASTE PRESSURE ENERGY IN INDUSTRIAL SYSTEMS	2
1.2.1 <i>Concept of waste pressure energy</i>	2
1.2.2 <i>Sources of waste pressure energy</i>	2
1.2.3 <i>Use of Ranque Hilsch vortex tube for utilizing waste pressure</i>	4
1.3 BASIC DESCRIPTION OF VORTEX TUBE AND HOW IT WORKS	5
1.4 ESSENTIAL LITERATURE REVIEW	7
1.4.1 <i>Experimental research on vortex tube</i>	8
1.4.2 <i>Theoretical Research on vortex tube</i>	11
1.4.3 <i>A study on temperature separation in a large vortex tube</i>	15
1.4.4 <i>Literature on axial and radial stagnation points inside vortex tube</i>	18
1.5 SUMMARY OF LITERATURE REVIEW	20
CHAPTER 2 THEORETICAL AND EXPERIMENTAL BACKGROUND	22
2.1 EXPERIMENTAL APPARATUS	22
2.2 APPROPRIATE NON-DIMENSIONALIZATION OF ENERGY SEPARATION EFFECT	25
2.3 RESULTS AND DISCUSSION	27
2.4 QUANTIFYING PERFORMANCE OF THE VORTEX TUBE SYSTEM.....	31

2.4.1	<i>Energy separation efficiency</i>	31
2.4.2	<i>Energy flux separation efficiency</i>	31
2.5	TOTAL PRESSURE DROP ACROSS THE VORTEX TUBE	32
CHAPTER 3 DESCRIPTION OF EXPERIMENTS PERFORMED AND RESULTS.....		33
3.1	EXPERIMENTAL APPARATUS	33
3.2	THERMAL AND FLUID DYNAMICAL TIME SCALES.....	37
3.3	EFFECT OF THE FRICTIONAL COEFFICIENT (K VALUE) OF THE TAPERED VALVE.....	40
3.4	QUANTITATIVE OBSERVATIONS ON MULTIPLE FLOW STRUCTURES INSIDE VORTEX TUBE.....	42
3.5	OBSERVED FLOW STRUCTURES INSIDE VORTEX TUBE	43
3.6	HYSTERESIS BEHAVIOR OF THE VORTEX TUBE & THE THERMAL TIME CONSTANT	48
CHAPTER 4 ANALYTICAL MODELING AND APPLICATION OF MODELING.....		54
4.1	COLD END ORIFICE ENTRANCE PRESSURE AND MULTIPLE FLOW STRUCTURES.....	54
4.2	A THEORETICAL MODEL EXPLAINING MULTIPLE FLOW MODES	55
4.3	CRITERIA FOR DIFFERENT FLOW STRUCTURES.....	59
4.4	TRANSITION FROM T-FLOW TO VT-FLOW	60
4.5	LOCATION OF AXIAL STAGNATION POINT INSIDE VORTEX TUBE	62
4.5.1	<i>Carriage and slider method</i>	62
4.5.2	<i>Experimental Setup and Procedure</i>	63
4.5.3	<i>Axial Stagnation Point Test Results</i>	63
4.6	A THEORETICAL MODEL TO PREDICT THE LOCATION OF AN AXIAL STAGNATION POINT.....	66
4.7	T TO VT-FLOW TRANSITION – A THEORETICAL UNDERSTANDING	70
4.7.1	<i>T to VT-flow transition and Linderstrom-Lang’s work</i>	70
4.7.2	<i>T to VT-flow transition and the traveling vortex breakdown</i>	74
CHAPTER 5 CONCLUSIONS AND DISCUSSION		76
5.1	USING VORTEX TUBE FOR UTILIZING INDUSTRIAL WASTE PRESSURE ENERGY	76
5.2	APPROPRIATE NON-DIMENSIONALIZATION OF ENERGY SEPARATION EFFECT	76
5.3	THERMAL AND FLUID DYNAMICAL TIME-SCALES	76

5.4	QUANTITATIVE OBSERVATIONS ON MULTIPLE FLOW MODES INSIDE VORTEX TUBE	77
CHAPTER 6	FUTURE WORK.....	79
CHAPTER 7	APPENDIX.....	80
7.1	APPENDIX 1: CATALOGUE OF VORTEX TUBE APPLICATIONS.....	80
7.2	APPENDIX 2: INSTRUMENTATION FOR VORTEX TUBE EXPERIMENTS	81
7.2.1	<i>Thermistors.....</i>	<i>81</i>
7.2.2	<i>Pressure Transducer: (211-B-RF-7/CR/GA-GP-50).....</i>	<i>82</i>
7.2.3	<i>Precision Turbine Flow-meters with direct signal conditioner.....</i>	<i>83</i>
7.2.4	<i>Direct signal conditioner (FLSC-64).....</i>	<i>85</i>
7.2.5	<i>Vortex Tube: (Model # 3499)</i>	<i>85</i>
7.2.6	<i>Vortex Tube performance</i>	<i>86</i>
7.2.7	<i>Data acquisition and signal conditioning.....</i>	<i>87</i>
7.2.8	<i>Lab-view program</i>	<i>88</i>
7.3	APPENDIX 3: EXPERIMENTAL PROCEDURES	90
7.3.1	<i>Experiment 1 - Thermal and fluid dynamical time scales.....</i>	<i>90</i>
7.3.2	<i>Experiment 2 - Flow meter calibrations.....</i>	<i>91</i>
7.3.3	<i>Experiment 3 - The frictional coefficient (k value) of the hot fraction control valve.....</i>	<i>94</i>
7.3.4	<i>Experiment 4 - Quantitative observations on multiple flow structures.....</i>	<i>97</i>
7.3.5	<i>Experiment 5 – Hysteresis behavior of the vortex tube</i>	<i>99</i>
7.4	APPENDIX 4: MULTIPLE FLOW STRUCTURES – A THEORETICAL MODEL	101
7.4.1	<i>Multiple flow structures - A theoretical model.....</i>	<i>101</i>
7.4.2	<i>A generalized vortex sink solution.....</i>	<i>102</i>
7.4.3	<i>Introduction to the generalized vortex sink solution.....</i>	<i>102</i>
7.4.4	<i>Need for an inner solution.....</i>	<i>104</i>
CHAPTER 8	BIBLIOGRAPHY.....	111
	CURRICULUM VITA	116

LIST OF TABLES

TABLE 1: VARIOUS APPLICATIONS AND AVAILABLE WASTE PRESSURES.....	3
TABLE 2: LENGTHS AND DIAMETERS OF THE VORTEX TUBES USED BY OTHER RESEARCHERS.....	15
TABLE 3: GEOMETRIC PARAMETERS AND TEST SEQUENCE	24
TABLE 4: VORTEX TUBE DIMENSIONS USED BY OTHER RESEARCHERS.....	36
TABLE 5: THERMO-PHYSICAL CONDITIONS FOR THE MULTIPLE FLOW STRUCTURES INSIDE VORTEX TUBE.....	47
TABLE 6: CATALOGUE OF VORTEX TUBE APPLICATIONS.	80

LIST OF ILLUSTRATIONS

FIGURE 1: SCHEMATIC DRAWING OF VORTEX TUBE.....	4
FIGURE 2: UTILIZING WASTE PRESSURE ENERGY BY USING VORTEX TUBE	5
FIGURE 3: SCHEMATIC ILLUSTRATION OF THE THERMAL CONDUCTIVITY DUE TO THE PRESSURE GRADIENT. ...	6
FIGURE 4: COUNTER FLOW AND UNI-FLOW VORTEX TUBES.....	9
FIGURE 5: COMPARISON BETWEEN AMITANI [5]'S AND TAKAHAMA'S EXPERIMENTAL WORK.....	16
FIGURE 6: ENERGY SEPARATION CAN BE ACHIEVED WITH 7 & 21 FT LONG VORTEX TUBES.....	17
FIGURE 7: OBSERVATION MADE BY AHLBORN AND GROVES	18
FIGURE 8: EXPERIMENTAL RESULTS BY C. M GAO AND ET.AL	19
FIGURE 9: EXPERIMENTAL APPARATUS USED DURING M.S. RESEARCH.....	22
FIGURE 10: LAB MANUFACTURED GENERATORS WITH VARYING ORIFICE DIAMETER	24
FIGURE 11: EFFECT OF P_i/P_a ON TEMPERATURE SPLITTING EFFECT FOR VARIOUS COLD FRACTIONS.....	26
FIGURE 12: APPROPRIATE NON-DIMENSIONALIZATION OF THE ENERGY SPLITTING EFFECT.....	27
FIGURE 13: EFFECT OF ORIFICE DIAMETER ON THE ENERGY SEPARATION	28
FIGURE 14: EFFECT OF ORIFICE DIAMETER ON THE ENERGY FLUX SEPARATION EFFICIENCY.	29
FIGURE 15: EFFECT OF NUMBER OF NOZZLES AND ORIFICE DIAMETER ON THE PERFORMANCE OF VORTEX TUBE.....	30
FIGURE 16: CHARACTERIZING PRESSURE DROPS IN VORTEX TUBES.....	32
FIGURE 17: EXPERIMENTAL APPARATUS USED TO MEASURE THERMAL & FLUID DYNAMICAL TIME SCALES AND FRICTIONAL COEFFICIENT OF THE TAPERED HOT FRACTION CONTROL VALVE.	34
FIGURE 18: SCHEMATIC OF THE EXPERIMENTAL APPARATUS AND THE HOT FRACTION CONTROL VALE CONSTRUCTION.....	35
FIGURE 19: THERMAL AND FLUID DYNAMICAL TIME SCALES	37
FIGURE 20: THERMAL TIME CONSTANT	38
FIGURE 21: DRAMATIC EFFECT OF FRICTIONAL COEFFICIENTS (K) ON COLD FRACTIONS.	40
FIGURE 22: EFFECT OF BACK PRESSURE ON COLD END ORIFICE ENTRANCE PRESSURE (P_o).....	42
FIGURE 23: REVERSE OR VENTURE FLOW	43

FIGURE 24: ELBOW FLOW.....	43
FIGURE 25: T FLOW.....	44
FIGURE 26: VORTEX TUBE TYPE OF FLOW (OR VT-FLOW).....	44
FIGURE 27: MULTIPLE FLOWS AND THE CRITICAL COLD FRACTIONS.....	45
FIGURE 28: MULTIPLE FLOWS AND THE CRITICAL BACK PRESSURES.....	46
FIGURE 29: OBSERVING MULTIPLE FLOW STRUCTURES INSIDE VORTEX TUBE – TIME PLOT.....	47
FIGURE 30: DUAL VALUED BEHAVIOR IN TEMPERATURE GRADIENT.....	48
FIGURE 31: DUAL VALUED BEHAVIOR IN COLD FRACTION.....	49
FIGURE 32: HYSTERESIS BEHAVIOR OF THE VORTEX TUBE AND THE FLOW TRANSITION.....	50
FIGURE 33: HYSTERESIS BEHAVIOR IN TEMPERATURES AND THE FLOW TRANSITION.....	51
FIGURE 34: LINEAR (NON-DUAL VALUED) BEHAVIOR OF FLOW METER RAW DATA.....	51
FIGURE 35: NON-LINEAR (DUAL VALUED) BEHAVIOR IN COLD FRACTIONS DUE TO UNSTEADY TEMPERATURES	53
FIGURE 36: LINEAR (NON-DUAL VALUED) BEHAVIOR OF FLOW METER.....	53
FIGURE 37: LAMINAR FLOW ASSUMPTION AND BERNOULLI’S EQUATION.....	56
FIGURE 38: MAPPING MULTIPLE FLOW STRUCTURES ON INLET PRESSURE AND BACK PRESSURE PARAMETRIC PLANE.....	58
FIGURE 39: RELATING BACK PRESSURE (PB) WITH COLD END ORIFICE ENTRANCE PRESSURE (Po).....	59
FIGURE 40: CARRIAGE AND SLIDER METHOD.....	62
FIGURE 41: FLOW VISUALIZATION BY CARRIAGE AND SLIDER METHOD.....	63
FIGURE 42: THEORIZED AXIAL FLOW STRUCTURES WHEN THE WALL IS AT DIFFERENT POSITIONS THE TUBE END.....	64
FIGURE 43: FLOW VISUALIZATION EXPERIMENT.....	65
FIGURE 44: OBSERVED MULTIPLE FLOW STRUCTURES AND THE PROBABLE AXIAL STAGNATION POINT LOCATIONS.....	66
FIGURE 45: TRANSITION FROM T TO VT-FLOW AND THE EFFECT OF AXIAL STAGNATION POINT LOCATION ON THE PRESSURE DROP ACROSS THE COLD END SIDE.....	68
FIGURE 46: EFFECT OF D_H/D_C ON THE GAS SEPARATION EFFECT.....	71

FIGURE 47: FLOW PATTERNS; VISUALIZED BY LINDERSTROM-LANG.	72
FIGURE 48: WALL PRESSURES AS FUNCTIONS OF HOT FRACTION.....	73
FIGURE 49: THE POSSIBILITY OF VORTEX BREAKDOWN INSIDE VORTEX TUBE.....	74
FIGURE 50: THE EFFECT OF AN AXIAL PRESSURE DISTRIBUTION INSIDE THE PIPE ON THE LOCATION OF VORTEX BREAKDOWN BUBBLE OR VICE VERSA,.....	74
FIGURE 51: SCHEMATIC DIAGRAM OF THE EXPERIMENTAL APPARATUS	81
FIGURE 52: OMEGA PRECISION THERMISTOR.....	82
FIGURE 53: PRESSURE TRANSDUCER	82
FIGURE 54: PRECISION TURBINE FLOW METER WITH SIGNAL CONDITIONER	83
FIGURE 55: DIRECT SIGNAL CONDITIONER	85
FIGURE 56: VORTEX TUBE.....	86
FIGURE 57: MODEL # 3499 – DIMENSIONS AND PERFORMANCE CHART.	86
FIGURE 58: E SERIES MULTIFUNCTION	87
FIGURE 59: LAB-VIEW PROGRAM – FRONT PANEL AND PROGRAM.....	89
FIGURE 60: FLOW METER RAW FREQUENCY DATA	93
FIGURE 61: CALIBRATED MASS FLOW RATE DATA.....	93
FIGURE 62: PRESSURE DROPS AND MASS FLOW RATES ACROSS THE TAPERED VALVE FOR DIFFERENT OPENING POSITIONS.....	95
FIGURE 63: FRICTIONAL COEFFICIENTS (K) OF THE TAPERED VALVE FOR DIFFERENT OPENING POSITIONS	95
FIGURE 64: QUANTITATIVE OBSERVATIONS ON MULTIPLE FLOW STRUCTURES INSIDE VORTEX TUBE	97
FIGURE 65: THE EFFECT OF AXIAL STAGNATION POINT LOCATION ON THE PRESSURE DROP ACROSS THE COLD END SIDE.....	108
FIGURE 66: THE EFFECT OF AXIAL STAGNATION POINT LOCATION ON THE PRESSURE DROP ACROSS THE COLD END SIDE.....	109

NOMENCLATURE

m_c, m_h	: Mass flow leaving cold-end and hot end respectively.
m_i	: Total mass flow entering the system, $(m_c + m_h)$.
cf	: Cold air fraction, (m_c / m_i) .
D	: Inside diameter of Vortex Tube, $2r_i$
d_o	: Diameter of cold end orifice.
N	: Number of nozzles on the Generator.
w_n	: Width of nozzle opening.
l_n	: Length of nozzle opening.
P_t, P	: Total and Static pressure, respectively.
V	: Velocity.
T	: Static temperature.
T_t	: Total temperature, $T + \frac{V^2}{2 \times C_p}$
C_p	: Specific heat of air at constant pressure and constant volume
K	: The ratio of specific heats, C_p / C_v .
γ	: Specific weight of air.
H	: Enthalpy of air, $C_p T$.
H_t	: Total enthalpy of air, $C_p T_t$.
η	: Efficiency of energy separation defined by equation number 1
ε	: Performance factor of vortex tube, defined by equation
a	: Speed of sound.
f	: Frequency in Hz.
h	: Convective heat transfer coefficient.
k	: Thermal conductivity of a fluid.

Ma	: Mach number, = $\frac{V}{a}$
Pr	: Prandtl number of a fluid, = $\frac{\nu}{\alpha}$
Re	: Reynolds number, = $\frac{VD}{\nu}$
α	: Thermal diffusivity of a fluid.
ν	: Kinematic viscosity of a fluid.
ρ	: Density of a fluid.
Tu	: Turbulence intensity, = $\frac{v'}{V}$
s	: Specific entropy of a fluid.
Γ	: Circulation inside a fluid.
ω	: Vorticity of a fluid.

Subscripts

i	: Inlet of vortex tube.
n_i	: Entrance of nozzle.
h	: Hot end of vortex tube.
c	: Cold end of vortex tube.
o	: Cold end orifice.

Chapter 1 Introduction

In Chapter 1, main objectives and motivation of the present research work, the general background of energy separation inside vortex tube and previous studies related to it are reviewed.

1.1 Objectives of the thesis

The objectives of the present research work are to:

- Characterize industrial waste pressure as a reclaimable form of energy,
- Analyze the effectiveness of ‘vortex tube energy separation’ in recovering waste energy from low pressure sources,
- Present an appropriate non-dimensionalization scheme for energy separation effect,
- Make a distinction between thermal and fluid dynamical time scales,
- Explore experimentally and theoretically the possibility of multiple flow structures (like Reverse/Venture flow, Elbow flow, T-flow or VT-flow) inside vortex tube in a low inlet pressure regime,
- Identify Reverse flow, T-flow and VT-flow zones in inlet and back pressure parametric space.
- Investigate dual valued or hysteresis behavior of vortex tube and relate it with the multiple flow structures inside the tube.

1.2 Motivation - Utilizing waste pressure energy in industrial systems

1.2.1 Concept of waste pressure energy

Waste pressure, similar to waste heat, can be defined as the pressure energy which is generated in a process but then “dumped” to the environment even though it could still be reused for some useful and economic purpose. In various industrial processes, waste pressure may come in the form of pressurized exhaust gases (including non-condensable gases), steam, blow off compressed air, or even in the form of pressurized hot water. The essential quality of waste pressure energy is not the amount but rather the “value”.

This thesis begins with an introduction to various applications that typically result in waste pressure and will analyze the effectiveness of vortex tube technology in recovering waste pressure energy from high and low pressure sources (P. A. Domanski, 1995) [1] and achieve energy and gas separation.

1.2.2 Sources of waste pressure energy

The strategy of how to recover this waste pressure depends in part on the pressure and source of waste pressure gases, type of the gas and the economics involved. Sources of waste pressure energy can be divided according to pressure magnitude into two categories: High pressure and low pressure sources.

Based on the pressure energy applications, sources of waste pressure energy can be classified into the following categories:

Back pressure applications, two phase flashing applications, low and high pressure non-condensable exhaust gases, and industrial low and high pressure applications.

Table 1 lists various waste pressure applications. In most of these applications available pressure energy is low in magnitude. To recover energy from high magnitude (pressure and mass flow both) there are already so many proven technologies currently available and successfully implemented (like back pressure turbines, flash steam turbines etc. Hence, throughout our studies, our primary focus was on low pressure applications. The preliminary analysis done in the laboratory (Selin Arslan, 2005 [2]) shows that the vortex tube technology can be used to harness this low magnitude waste pressure energy for some useful economic purposes.

Application	Average available waste pressures (bar)
[a] Back pressure applications:	
1. Gas turbine exhaust	2 – 6
2. Forced air- blast furnace exhaust	2 – 10
3. Positive pressure furnaces:	
i. Envelope furnaces	6.5 – 10
ii. Laboratory furnaces	1.15 – 1.4
iii. Powder metallurgy, air furnaces and sintering furnaces.	2 – 5
[b] Two phase flashing applications	
1. Vapor compression liquid chiller	2 – 10
2. Multistage flashing- desalination	1.15 – 1.40
3. Geothermal steam flashing	6 – 8
[c] Non-condensable gas exhausts	
1. Fossil thermal power plants, H ₂ production.	5 – 30
2. Geothermal steam flashing, CO ₂ production.	6 – 10
3. Air separation units (Pressure swing adsorption) O ₂ or N ₂ production.	6 – 80

Table 1: Various applications and available waste pressures.
[2], [3] & [4]

1.2.3 Use of Ranque Hilsch vortex tube for utilizing waste pressure

The Ranque-Hilsch tube is a device that separates a flow of gas into two streams simultaneously, one hotter than the inlet and one cooler. The lack of moving parts and no need of electricity make the vortex tube attractive for a number of specialized applications where simplicity, robustness and reliability are desired. Historically, the design of commercially available vortex tubes has been optimized to supply the cool stream fraction for a variety of applications including integrated circuit board cooling, cabinet cooling, cooling ultrasonic welds, and cooling small parts after brazing. (Selin Arslan, 2002) [2].

A schematic drawing of a typical vortex tube is shown in figure 1. Inlet nozzles are tangent to the main tube which causes the entering air to acquire the vortical motion which gives the device its name. At one side of inlet nozzle is a fixed flow restriction called the ‘cold orifice’, and at the other end of the main tube there is a variable flow restriction (called the hot fraction control valve).

These names derive from the essence of the vortex tube, namely, that the air leaving the tube through the orifice is colder than the entering air while the air leaving through the valve is hotter.

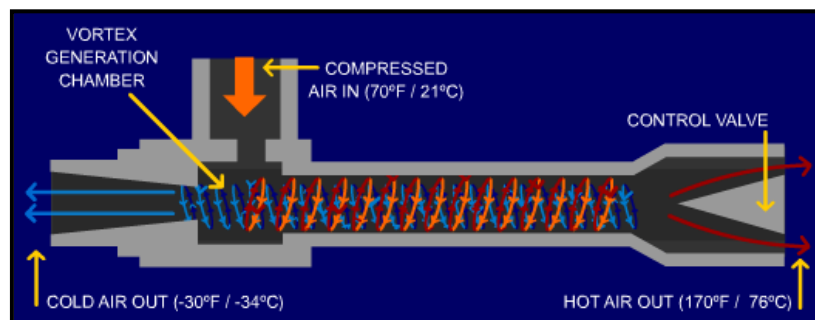


Figure 1: Schematic drawing of vortex tube.
(Source: Exair Corp. USA)

The degree of heating and cooling depends upon the relative amount of air leaving each end of the tube. Cold airflow and temperature are easily controlled by adjusting the slotted tapered valve in the hot air outlet. Opening the valve reduces the cold airflow and cold air temperature. Closing the valve increases the cold airflow and cold air temperature. The percentage of air directed to the cold outlet of the vortex tube is called the “cold fraction” and the percentage of air directed to the hot outlet is called the “hot fraction”.

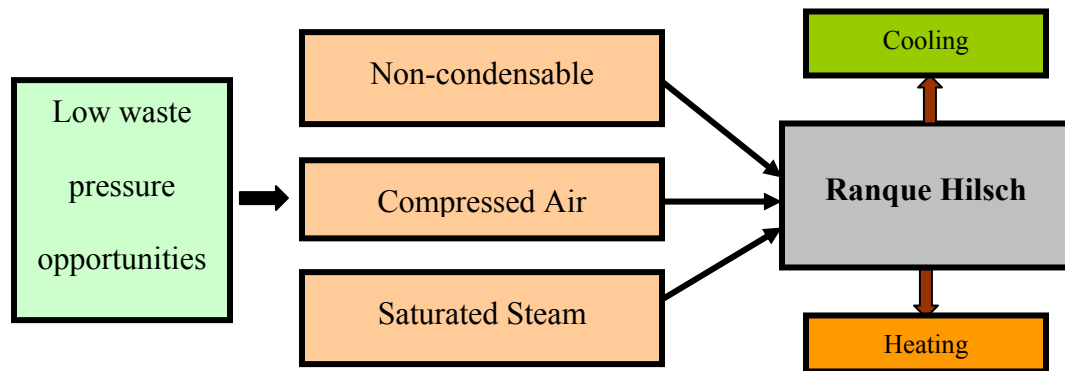


Figure 2: Utilizing waste pressure energy by using vortex tube

1.3 Basic Description of vortex tube and how it works

1.3.1.1 Energy separation inside vortex tube

“Energy separation” is the re-distribution of the total energy in a fluid flow without external work or heat, so that some portion of the fluid has higher and other portion has lower total energy than the surrounding fluid. Since this interesting phenomenon was first observed in the 1930’s [34], many researchers have reported that energy separation could be observed in various flow situations like impinging jets, boundary layer flow past a cylinder and simple boundary layer flow over a flat plate. However, the detailed

mechanism of energy separation is not fully understood yet. In the present study, instantaneous mechanism of energy separation is explained in a vortex tube by both theoretical and experimental methods.

1.3.1.2 Fluid dynamics behind vortex tube

Energy separation in the Ranque-Hilsch tube can be accounted for by two phenomena. Firstly, the formation of an approximately forced vortex near the tangential inlets to the tube initially provides a kinetic energy separation, the peripheral gas having a much higher velocity than that near the centre. Secondly the strong radial pressure gradient produced by the forced vortex enables turbulent fluctuations to transport thermal energy radially outwards and re-enforce the existing energy separation until the thermal and pressure gradients have come into equilibrium

The effects of the two processes are modified by axial convection and by viscous dissipation of the kinetic energy of the flow to produce the characteristic distributions found within the vortex tube.

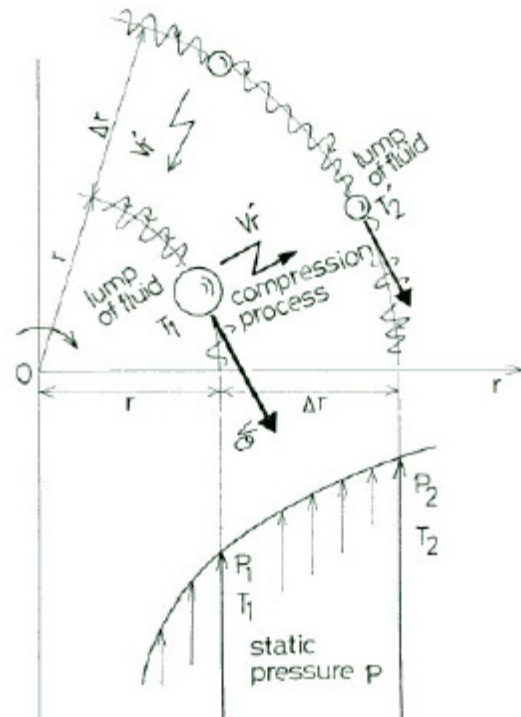


Figure 3: Schematic illustration of the thermal conductivity due to the pressure gradient.

(Source: Deissler R. G. and Perlmutter) [42]

Axial convection extends the turbulent thermal transport process over a significant length of the tube, and is responsible for the observed axial development of the energy separation. Viscous dissipation converts the kinetic energy separation into a thermal separation, and serves to produce a temperature rise in both the hot and cold streams as their kinetic energy is reduced.

The energy separation is maintained by the flow so long as the swirl is strong enough to provide a substantial radial pressure gradient to help offset the effects of turbulent conduction. As the swirl decays, for example towards the end of a uni-flow tube, the energy separation declines.

Such an explanation is consistent with many observed features of vortex tubes, essentially attributing the existence of a radial stagnation enthalpy gradient to the formation of a forced vortex, and the cooling of the central flow below the inlet temperature to a turbulent transport process that depends on the compressibility of the fluid. In particular it would explain why a vortex tube operated on high pressure water produces an energy separation, but with no net cooling of the central flow (Balmer [24]).

1.4 Essential literature review

From 1934, almost 200-215 articles are published on Ranque Hilsch vortex tube. Not all the articles are directly related to our work, especially, those articles which were focused on computational work. Many articles addressed experimental findings and remaining discussed various theories explaining energy separation phenomenon. In this subsection, we are going to discuss only those articles (experimental and/or theoretical work) which are directly related to current work.

1.4.1 Experimental research on vortex tube

In the past, many researchers tried to study energy separation phenomenon and the resulting enrichment of the inlet gas inside the vortex tube. Most of the researchers conducted experiments to study the effect of the following parameters on the energy separation characteristics of the vortex tube:

- Thermo-physical parameters (like the fluid, inlet pressure, temperature, etc.) and
- The geometry (like number of nozzles, diameter, length, etc.)

1.4.1.1 Thermo-physical parameters

It was very important to conduct experiments with different working mediums to determine the effect of compressibility on the energy separation. The first study on the separation of mixtures with the Ranque Hilsch vortex tube was published in 1967 by Linderstrom-Lang [18] and in 1977 by Marshall [19]. The gas mixtures (oxygen and nitrogen, carbon dioxide and helium, carbon dioxide and air, and other mixtures) were used as the working medium in their work. In 2001 the vortex tube system was used for carbon-dioxide separation by K. T. Raterman [20]. In 2002 the Ranque Hilsch vortex tube system was used to enrich the concentration of methane by Manohar [21]. In 2004, natural gas was used as working medium and with the vortex tube natural gas was liquified by Poshernev [22].

In 1979 steam was used as working medium by Takahama [7]. In 1979, two-phase propane was used as the working medium by Collins [23]. It was found that when the degree of dryness (defined as the ratio of the mass of gaseous part over the total mass) of the liquid and gaseous propane is higher than 0.80, a significant temperature difference is maintained. With two-phase working medium, the degree of dryness is an important

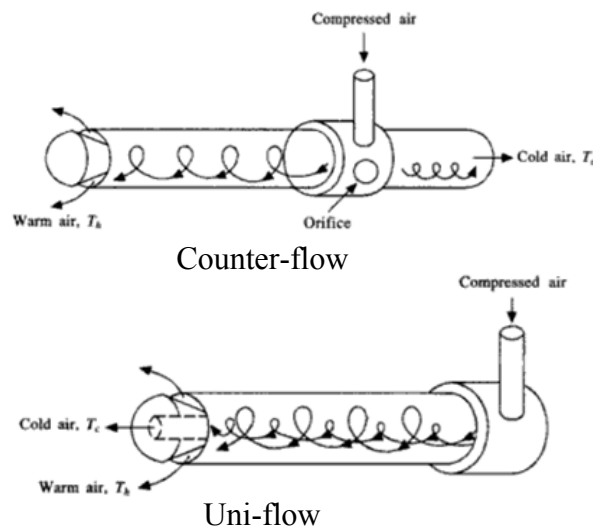
parameter, when the degree of dryness is larger than some critical value, energy separation occurs.

In 1988, Balmer [24] used liquid water as the working medium. It was found that when the inlet pressure is high, for instance 20 to 50 bars, then and then we get the energy separation. So it proves that for the energy separation process, compressibility is vital.

Experimental results obtained by varying thermo-physical parameters can be summarized as follows:

- The working media is very important in the operation of the vortex tube system.
- By selecting different working media, the performance of the system can be optimized, and
- The vortex tube can be used for utilizing waste pressure energy even if the pressure energy is in the form of non-condensed gases, inert gases or liquid vapors.

1.4.1.2 Geometrical Parameters



Geometrical parameters include the positioning of components like the cold exhaust, control valves and inlet nozzles. Depending upon the position of cold exhaust, we can call vortex tube as counter-flow or uni-flow vortex tube.

Figure 4: Counter flow and uni-flow vortex tubes.

If the cold exhaust is placed completely opposite to the hot exhaust, it is called “counter-flow vortex tube. If the cold exhaust and the hot exhaust are on the same side, it is called a “uni-flow” vortex tube.

From the experimental investigation (T. Cockerill, [25]), it was found that the performance of the uni-flow vortex tube is inferior to that of the counter-flow vortex tube. So, most of the time, the counter-flow geometry was chosen.

The literature concerning the design, operation and performance of vortex tubes is extensive, with descriptions first appearing in 1948 (Hilsch, [26]) with excellent review papers by H. Takahama (1965) [6], Boye Ahlborn, Stuart Groves (1997) [27], and C. M. Gao et. al. (2005) [28]. Studies focusing on the role of internal geometry include: Takahama (1960) [29], Hartnet and Eckert (1976) [30], J. Marshall (1977) [19], M. H. Saidi (2003) [12] and Eiamsa-ard, S. et.al. (2007) [31].

During 1960s, Takahama carried out experimental studies on pressure and temperatures inside the vortex tube and studied the effect of various geometric factors on its energy separation characteristics [6, 7, and 8]. In 1977, J. Marshall [19] confirmed experimentally that separation is primarily dependent upon centrifugation. His results appear substantially to indicate in comparing the standard and large tubes that the gas separation performance is the same if the effect of overall pressure drop is considered. In 2003, M. H. Saidi [12] found that generator with more flow intakes causes the cold air temperature and the efficiency of the vortex tube to decrease.

Finally, of importance to the work discussed here, several researchers have sought to characterize the internal flow details including the existence of a secondary flow circulation. Specifically, in 1997, Ahlborn and Groves [27] used a pitot tube to observe a

secondary flow within the vortex tube. From the measured velocity field they determined that the return flow at the center of the tube is much larger than the cold mass flow emerging out of the cold end. Therefore, the vortex tube must have a secondary circulation imbedded into the primary vortex, which moves fluid from the back flow core to the outer regions.

1.4.2 Theoretical Research on vortex tube

Theoretical studies have been carried out in parallel with experiments. Most theories are based on results obtained from the related experimental work; some are based on numerical simulations. In 1997 Gutsol [32] and in 2002 Leont'ev [33] have published detailed reviews about the Ranque Hilsch vortex tube theories. So, the summary on the theories given here will be brief.

1.4.2.1 Adiabatic compression and adiabatic expansion model

The first explanation was given by Ranque [34]. He hypothesized that the energy separation is due to adiabatic expansion in the central region and adiabatic compression in the peripheral region. In 1947 Hilsch [26] used similar ideas to explain the phenomenon in the vortex tube, but introduced the internal friction between the peripheral and internal gas layers. He used this model to explain his experimental results rather well. Because the process in the vortex tube is not truly adiabatic [26], this model was later rejected (see Fulton [35]).

1.4.2.2 Effect of friction and turbulence

In 1950, Fulton [35] hypothesized that the energy separation is due to the free and forced vortex flow generated inside the system. He stated that “Fresh gas before it has traveled

far in the tube succeeds in forming an almost free vortex in which the angular velocity or rpm is low at the periphery and very high toward the center. But friction between the layers of gas undertakes to reduce all the gas to the same angular velocity, as in a solid body.” During the internal friction process between the peripheral and central layers, the outer gas in turn gains more kinetic energy than it loses internal energy and this leads to a higher gas temperature in the periphery; the inner gas loses kinetic energy and so the gas temperature is lower.

Lay [37] used the potential and forced vortex motion for the vortex tube analysis and proposed via an elegant mathematical formalization that the internal friction effect and turbulence are the main reason for the energy separation. Kreith [38], Alimov [39] also attributed the friction effect as reason for the energy separation. Reynolds [40], [41], Deissler [42] also pointed out that the energy separation is due to friction and turbulence. Van Deemter [43] in 1951 performed numerical simulation work based on the extended Bernoulli equation. He had similar ideas as Fulton [35] and calculated the temperature profile as scaled by the turbulent Prandtl number. There is a remarkable agreement between his model and Hilsch’s measurements.

Deissler [42], Reynolds [41], Sibulkin [9], and Lewellen [44] all presented mathematical analysis based on the turbulent Navier Stokes (N-S) equation. Based on their analysis, they come to the common conclusion that heat transfer between flow layers by temperature gradients and by pressure gradients due to turbulent mixing, turbulent shear work done on elements are the main reasons for the energy separation. At the author’s former university, Xi’an Jiaotong University, this theory was further investigated with numerical simulation method and experimental studies [44]. The work concluded that the

energy separation is mainly due to internal friction and turbulence characterized by the turbulent viscosity number.

Gutsol [32] summarized many existent Russian theories in the past in a critical review. He proposed a turbulence model with exchange of the micro-volumes motion effect to explain the energy separation. Gutsol explained that due to the turbulent motion at the exhaust of the inlet nozzle, turbulent vortex motion exists inside the vortex tube at different layers. Via this turbulent mass transfer an exchange of kinetic energy and heat takes place between fluid layers. This theory is similar to the inner friction theory proposed by Fulton [35] but more mathematical.

The internal friction, mentioned in the friction and turbulence models, is the viscous friction between different gas layers. This is different from the roughness and friction mentioned by Paruleker [45]. The friction referred to in Paruleker is the friction between the wall surface and flow.

The friction and turbulence models are incomplete. The relationships proposed by different authors include a lot of turbulent parameters, which are difficult to determine and rely on assumptions. Another disadvantage is that the models do not consider geometrical effects. All these difficulties limit the applications of these models.

1.4.2.3 Acoustic streaming model

Kurosaka, Chu and Kuroda [46] from the University of Tennessee explained the VT with the phenomenon of acoustic streaming. They focused their research on the fundamental functions of ordered/disordered turbulence and found a relationship between the acoustic resonance frequencies and the forced vortex motion frequency. They proposed that the energy separation inside the vortex tube is due to the damping of the acoustic streaming

along the axis of the tube towards the hot exhaust. In 2005, the frequencies found from the spectral analysis (C. M. Gao [28]) on the samples taken by the hot-wire anemometry also have these relationships and indicate the existence of the acoustic phenomena.

1.4.2.4 Secondary circulation model

Ahlborn [27] proposed a secondary circulation model based on his experimental results. He found that the cumulative mass flow over the cross section of the vortex tube in the cold end direction is larger than the cold exhaust flow, which implies the existence of a secondary circulation flow in the VT. With this secondary circulation model, the vortex tube can be considered as a classical refrigeration device and the secondary circulation flow can be thought as a classical cycle [27].

The secondary flow pattern has also been noted experimentally by Linderstrom-Lang [18], Fulton [35], Scheper [36], Ahlborn [27] and Gao [28], and numerically explained by Cockerill [25], Gutsol [32] and Aljuwayhel [47]. The main difference among all these secondary flow patterns is whether the secondary flow is a closed cycle or not.

Linderstrom-Lang, Fulton, Scheper and Cockerill suggested it as an open cycle, while Ahlborn, Gao, Gutsol, and Aljuwayhel suggested a closed cycle. More detailed analysis on the secondary circulation model is discussed in later Chapters.

In summary, as pointed out by van Deemter [48] and Gutsol [32] most of these theories can only either explain their own works and could not match with the others, or could be used for qualitative analysis only. This indicates also that the above theories are incomplete. The above mentioned theories point out two directions of theoretical research, which gives hints for further investigations. One is focusing on thermodynamics

(compression and expansion), turbulent flow, viscous friction, internal heat transfer, and acoustics. The other one is concerning the flow pattern, like secondary circulation.

1.4.3 A study on temperature separation in a large vortex tube

Sr. No.	Author	Year	D (Inner Dia.) ft.	L (Length) ft.	Fluid
1	Tatsuo Amitani [5]	1983	2.62	21.65	Blast furnace exhaust gas
2	Tatsuo Amitani [5]	1983	0.51	7.38	Blast furnace exhaust gas and air
3	H. Takahama [6]	1965	0.26	5.20	air
4	H. Takahama [7]	1979	0.06	3.42	air
5	M. Sibulkin [9]	1961	0.13	3.00	air
6	H. Takahama [8]	1980	0.18	2.00	air
7	H. Bruun [10]	1969	0.31	1.73	air
8	K. Stephan [11]	1983	0.06	1.17	air
9	M. Saidi [12]	2003	0.06	0.93	air
10	Our vortex tube [2]	2004-08	0.06	0.83	air
11	Exair Corp. [13]	-	0.08	0.83	-

Table 2: Lengths and diameters of the vortex tubes used by other researchers

The largest obstacle in using vortex tube for waste pressure utilization in industrial systems is its physical size. The largest vortex tube which is available commercially today is 0.83 ft long (L) and 0.08 ft in diameter (D). In table 2, we have listed lengths and diameters of the vortex tubes used by other researchers. The largest vortex tube ever used in the lab for research purpose was by Tatsuo Amitani [5] in year 1983. Interestingly, he used this largest sized test apparatus in a blast furnace to utilize the waste pressure in the

form of pressurized blast furnace flue gases. He used two different sized vortex tubes, one was ~ 21 feet long and another was 7 feet long.

Figure 5 shows a variation in efficiency (equation 1) of the vortex tube with cold fraction for 7 feet long vortex tube. He compared his results with Takahama's [6, 7, & 8] results.

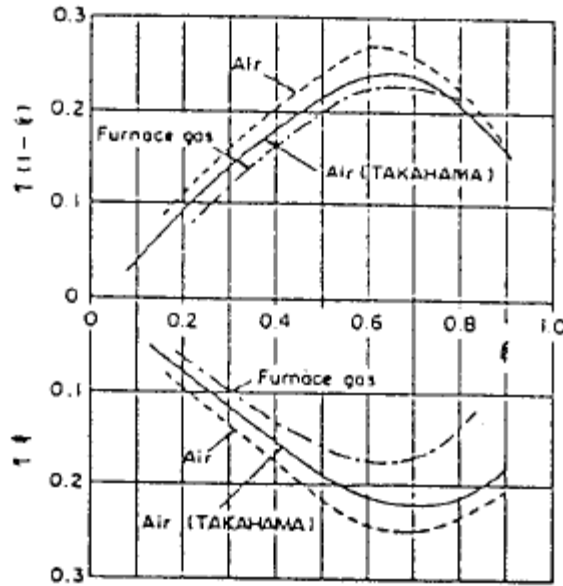


Figure 5: Comparison between Amitani [5]'s and Takahama's experimental work.

$$\eta = \frac{(T - T_{mi})}{\Delta T_{ns} + \Delta T_{cs}} \dots\dots 1$$

Where T is the temperature (T_h or T_c), T_{mi} is the total temperature before the nozzle, ΔT_{ns} is the adiabatic temperature drop to the nozzle outlet pressure, and ΔT_{cs} is the adiabatic temperature drop from the nozzle outlet pressure to atmospheric pressure.

But the important point is energy separation can be achieved by using 21 and 7 feet long vortex tubes (figure 5 and 6). Hence, if we need to construct large vortex tubes for utilizing industrial waste pressure energies with large mass flows but less pressure

It can be observed from the figure 5 that refrigeration $[\eta(\xi)]$ and heating efficiencies $[\eta(1-\xi)]$ of the vortex tube drops by a small amount if we use hot flue gases coming out of the blast furnace.

magnitudes it's feasible. Amitani's [5] (1983) work is preliminary in nature and lots of progress needs to be done to develop large sized vortex tube systems. Current research findings are not sufficient to address completely some design related issues, role of compressibility, turbulence and swirl intensity on the size limit of vortex tube.

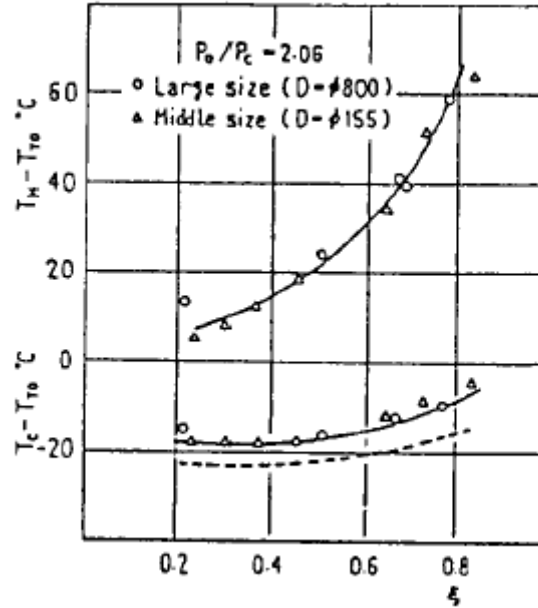
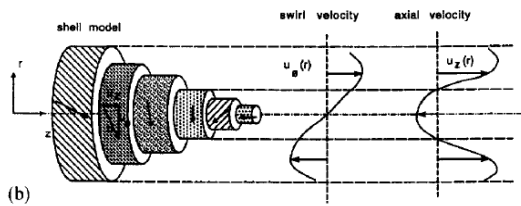


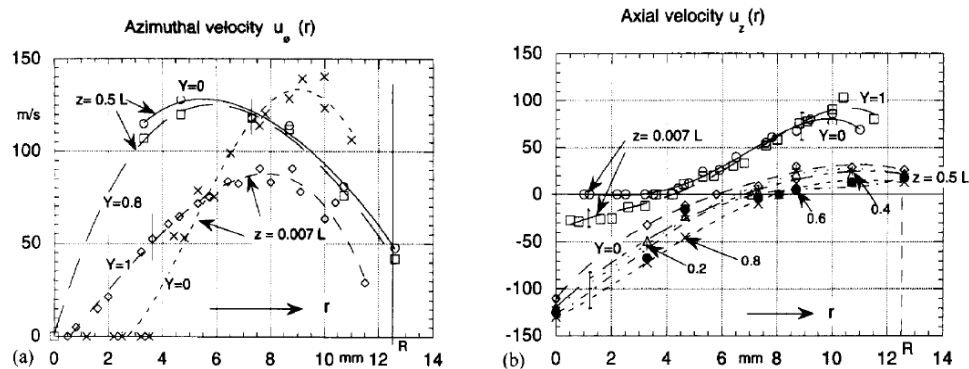
Figure 6: Energy separation can be achieved with 7 & 21 ft long vortex tubes.
[Diameters are shown in the brackets.]

1.4.4 Literature on axial and radial stagnation points inside vortex tube

In 1997, Ahlborn and Groves [27] used a pitot tube to observe a secondary flow within the vortex tube. From the measured velocity field they determined that the return flow at the center of the tube is much larger than the cold mass flow emerging out of the cold end. Therefore, the vortex tube must have a secondary circulation imbedded into the primary vortex, which moves fluid from the back flow core to the outer regions.



3. (a) Flow angle and (b) cartoon of the velocity field for $Y \approx 0$ and $z = 0.007L$.



4. (a) Azimuthal and (b) axial velocity components at $z = 0.007L$ and $z = 0.5L$ for various mass flow ratios.

Figure 7: Observation made by Ahlborn and Groves (1997)

[Azimuthal and axial velocity components at $z = 0.007L$ and $z = 0.5L$ for various mass flow ratios.]

Along with the existence of secondary flow, they also found that the location of an axial stagnation point (a point where axial flow changes direction) depends upon the cold fraction. Please note that the cold fraction is the function of the frictional coefficient (k -value) of the hot fraction control valve at constant inlet pressure. For low cold fractions

($Y = cf \rightarrow \text{zero}$) stagnation point is located near the inlet region of the vortex tube and it moves downstream as cold fraction increases ($Y = cf \rightarrow 1$). Figure 7 is showing their quantitative results for the azimuthal and axial velocity components for $z = 0.007$ to $0.5L$. It can be observed from the figure 7 that for $z = 0.007L$ and for cold fractions (Y) almost equal to zero, we have elbow type of flow inside the vortex tube and the axial stagnation point is located somewhere near the inlet region. As cold fraction increases, larger portion of the central core gets negative axial velocity. Negative axial velocity means flow is going towards cold end side and axial stagnation point is located somewhere in the downstream region ($z > 0.5L$).

In year 2005, C. M . Gao [28] did similar experiments on vortex tube. In order to investigate pressures, temperatures and flow structure inside the vortex tube, C.M. Gao and et.al built a simple vortex tube and used pitot tube for their measurements.

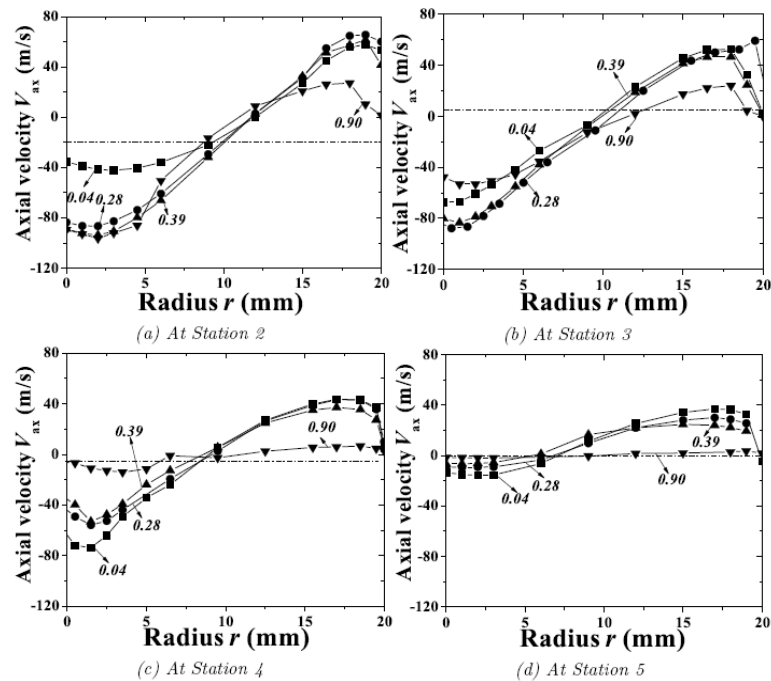


Figure 8: Experimental results by C. M Gao and et.al (2005)
 [The distribution of the axial velocity component for different cold fractions.]

Based on their experimental results, they claimed the existence of secondary circulating region inside the vortex tube. Figure 8 shows distribution of the axial velocity components for different cold fractions and at different test locations along the length of the vortex tube. In his experimental setup, station 5 was located about 67.5 mm (almost 5 times the vortex tube diameter) from the inlet of the vortex tube. It can be observed from the figure 8 that the location of an axial stagnation point depends upon the cold fraction. For lower cold fractions, axial stagnation point is located near the inlet region of the vortex tube and the location moves downstream as cold fraction increases.

1.5 Summary of Literature Review

- The working fluids (air, CO₂, methane, etc) and their compressibility properties play crucial roles in the operation of vortex tube system. By selecting the appropriate working media, the performance of the vortex tube system can be optimized. As long as the waste pressure energy is in the form of non-condensable gases, inert gases or liquid vapors (all compressible gases), the vortex tube can be used to utilize this waste energy for some useful and economic purposes.
- Many researchers observed that the performance of the uni-flow vortex tube is inferior to that of the counter-flow vortex tube. Hence during all of our experimental work, we used the counter-flow type of vortex tube.
- Most of the theories developed to explain energy separation phenomenon inside the vortex tube can only either explain their own works and could not match with the others, or could be used for qualitative analysis only. This indicates also that the most of these theories are incomplete which gives hints for further investigations.

- The largest obstacle in using vortex tubes for waste pressure utilization in industrial systems is their physical size. Work done by the previous researchers is preliminary in nature and lots of progress needs to be done to develop large sized vortex tube systems. Current research findings are not sufficient to address completely some design related issues, role of compressibility, turbulence and swirl intensity on the size limit of vortex tube.
- Based on the experimental work done by Ahlborn (1997) and Gao (2005) it can be concluded that the location of an axial stagnation point inside the vortex tube is controlled by only two parameters: Inlet pressure (P_i) and the back pressure (P_b) exerted by the hot fraction control valve.
- Previously reported vortex tubes were mostly operated at high entrance pressures (>10 psig) and the pressures never dropped closer to or below one atmosphere. In various industrial systems, magnitudes of waste pressure may be lower but may have significant mass flow rates. It is important to make sure that vortex tube provides the required energy separation while harnessing the low pressure but high mass flow rate waste energy and utilizing it for heating or cooling purposes. Experimental observations in the past (S. Nimbalkar, 2005 [3], [54]) show that in the low inlet pressure regime, vortex tubes behave differently and produce multiple flow structures (like Venture flow, Elbow flow or T-flow) rather than the expected re-circulating cold stream and the columnar hot stream (VT-flow). Our initial speculation is that the existence of multiple flow structures inside the vortex tube is related to the relocation of an axial stagnation point.

Chapter 2 Theoretical and Experimental Background

This section presents the important results from the series of experiments conducted by the author in the past during his Master of Science research (S. Nimbalkar [3], [54]) focusing on various geometries of the “cold end side” for different inlet pressures and cold fractions. These experiments helped us in selecting the appropriately sized vortex tube and correctly designing the experimental setup for the PhD research work.

2.1 Experimental apparatus



Figure 9: Experimental apparatus used during M.S. research. (S. Nimbalkar [3], [54]).

The typical experimental setup is shown in figure 9. Clean, dry air from a compressed air system is reduced through a pressure reduction valve to the desired value and is then dumped into a plenum chamber. From there flow accelerates into the inlet port of the vortex tube. The flow is then forced into an energetic vortex through multiple jets or a single jet oriented tangentially. This spinning fluid is turned 90 degrees and can exit from either end of the tube. Flow out of the hot-end side is restricted by a tapered valve which creates back pressure and preferentially selects fluid near the outer wall. Flow out of the cold-end side is restricted by a disk with a circular hole in its center. This “orifice” preferentially selects flow from the center of the tube which will be colder due to the adiabatic expansion associated with turbulence contained within the vortex.

The purpose of this study was to examine the effect of the cold end orifice diameter on the overall energy separation of the vortex tube. Different generators with varying cold end orifices were manufactured in the lab (See table 3 and figure 10) tests were conducted using a commercially manufactured vortex tube (Exair Corp., Model No. 3299, maximum mass flow rate 11 lbm/min at 100 psig inlet pressure) for different inlet mass flow rates (1, 1.5 and 1.8 lbm/min).

The temperature of the air entering into the vortex tube and the air leaving at hot and cold end sides were measured by thermistors. The total mass flow entering the system, the mass flow leaving the cold end and the mass flow leaving the hot-end were measured by turbine type of flow meters. Turbine type of flow meter produces less pressure drop across it as compared to variable area flow meters. It was observed that the back pressures generated at cold and hot ends due to the variable area flow meters affect the flow characteristics of the vortex tube, and may force a recirculating flow inside it. Inlet

pressure was measured with the help of a diaphragm type pressure transducer which was calibrated by the manufacturer and cross checked with the help of a dead weight calibrator in the measurement lab.

Generator No.	Inner diameter D (inch)	Generator Nozzle			Cold end orifice diameter d_c (inch)	$d_r = \frac{d_c}{D}$
		width (inch)	length (inch)	nozzles		
Generator 1	0.75	0.125	0.160	4	$d_{c_1} = 0.136$	0.18
Generator 2	0.75	0.125	0.160	4	$d_{c_2} = 0.2750$	0.37
Generator 3	0.75	0.125	0.160	4	$d_{c_3} = 0.3770$	0.50
Generator 4	0.75	0.125	0.160	4	$d_{c_4} = 0.4975$	0.66

Table 3: Geometric parameters and test sequence

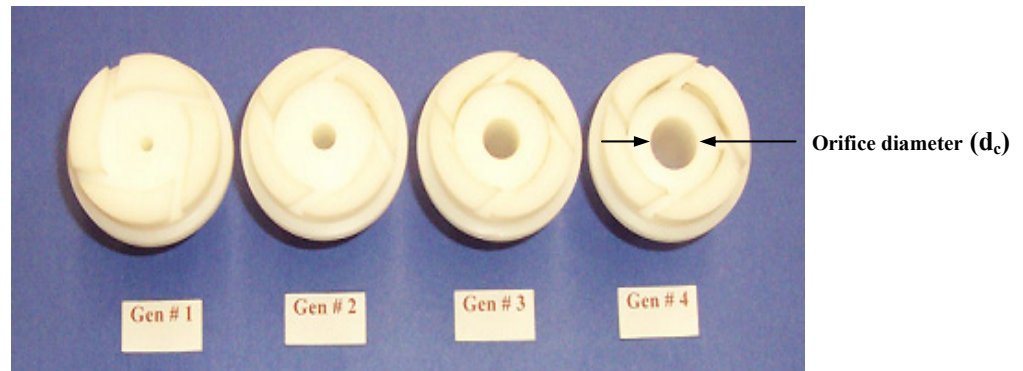


Figure 10: Lab manufactured generators with varying orifice diameter

The vortex tube used while performing all experiments had an internal diameter $D = 0.75$ inch and a length $L = 10$ inches (L/D ratio equal to 13.33). The tube was made of stainless steel and thermally insulated from the atmosphere to avoid errors due to heat conduction and to maintain repeatable steady-state.

2.2 Appropriate non-dimensionalization of energy separation effect

To recover characteristic properties of the vortex tube and its energy separation effect, it is necessary to non-dimensionalize various geometric and thermo-physical parameters involved. These parameters are: inlet pressure (P_i), orifice diameter (d_c), inlet mass flow rate (m_i), cold end mass flow rate (m_c) and pressure drop across the hot fraction control valve.

In the past, most of the researchers did not use the dimensionless parameters in their research work and remaining of them used improper scaling parameters for non-dimensionalization. For example, use of inlet temperature to non-dimensionalize temperature splitting effect (figure 11). Temperature splitting effect is defined as the difference between hot and cold end side temperatures (equation 2). Basically, it is the maximum possible temperature gradient achieved by vortex tube. If the compressed air is generated at some remote location, then the inlet temperature would not change with the inlet pressure. Hence, it would be inappropriate to use the inlet temperature to scale the temperature gradients. But if compression is done onsite, inlet temperature would change with inlet pressure (due to compressor work) and it would be appropriate to use the inlet temperature to scale the temperature splitting effect. Temperature splitting effect is defined as,

$$\text{Temperature splitting effect} = (T_h - T_c) \dots \dots 2$$

More properly, we should use input energy (which is compressor work) to non-dimensionalize the temperature gradients as shown in figure 12. Input energy is the compression work required to compress air from atmospheric pressure (P_{atm}) to the inlet pressure (P_i) isentropically which is given by:

$$CW = \frac{k}{k-1} \times R \times T_{atm} \times \left\{ \left(\frac{P_i}{P_{atm}} \right)^{\frac{(k-1)}{k}} - 1 \right\} J / kg \dots\dots 3$$

where, k is specific heat ratio for air =1.4, R is gas constant = 53.34 ft-lbf/lbm-°R.

Hence non-dimensionalized version of the energy splitting effect is:

$$\text{Energy splitting effect} = \frac{c_p(T_h - T_c)}{CW} \dots\dots 4$$

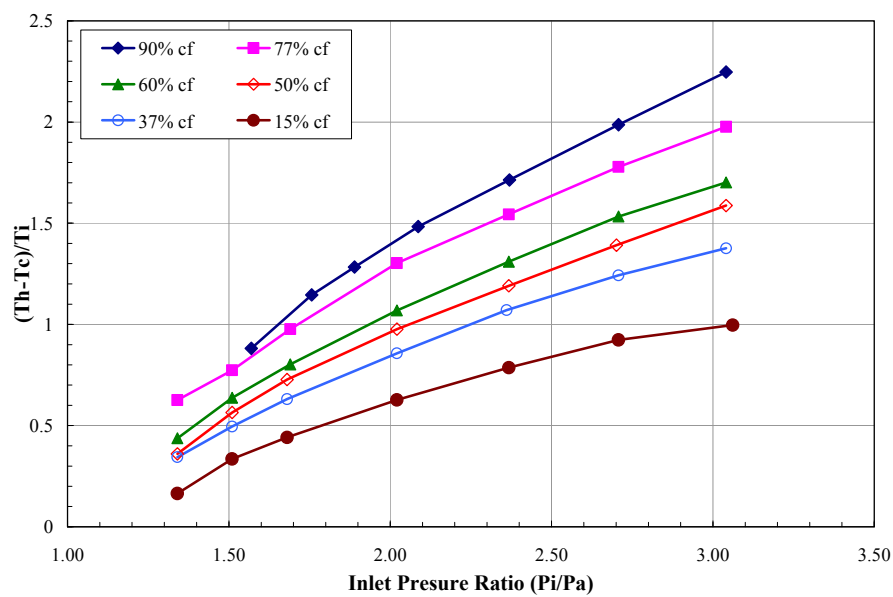


Figure 11: Effect of Pi/Pa on temperature splitting effect for various cold fractions.

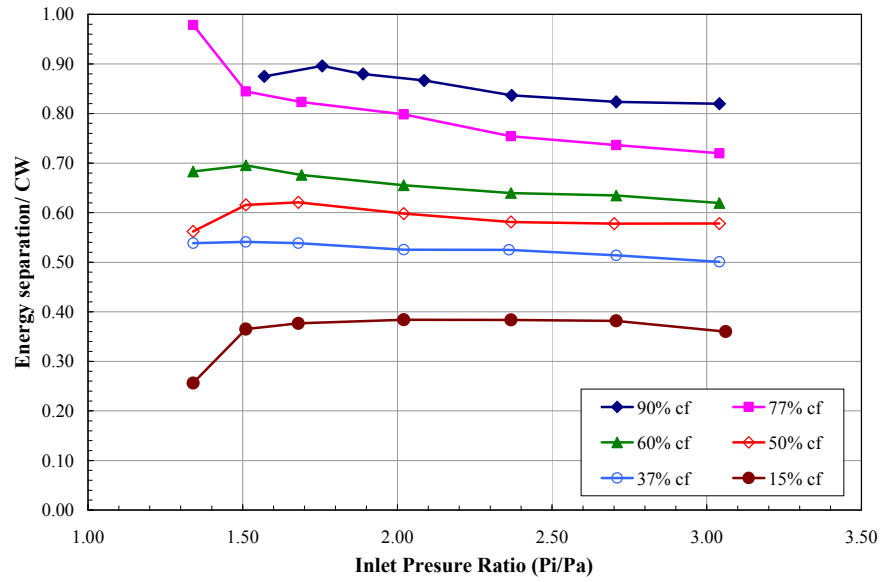


Figure 12: Appropriate non-dimensionalization of the energy splitting effect.

2.3 Results and discussion

In figure 13, energy separation efficiency is plotted against the cold fraction for various cold end orifice diameters [$d_r = (d_c/D) = 0.18$ to 0.66] at inlet mass flow rate of 1 lbm/min. Energy separation efficiency can be defined as the ratio of energy separation effect (either cold end or hot end) to the isentropic compression work per unit mass.

$$\text{Energy separation efficiency (cold end)} = \frac{c_p(T_i - T_c)}{CW} \dots\dots\dots 5$$

Inlet mass flow rate is already non-dimensionalized in the form of cold fraction (m_c/m_i). So by defining energy separation efficiency and the cold fraction, dimensional quantities like temperatures, inlet pressure, and inlet and cold mass flow rates are non-dimensionalized.

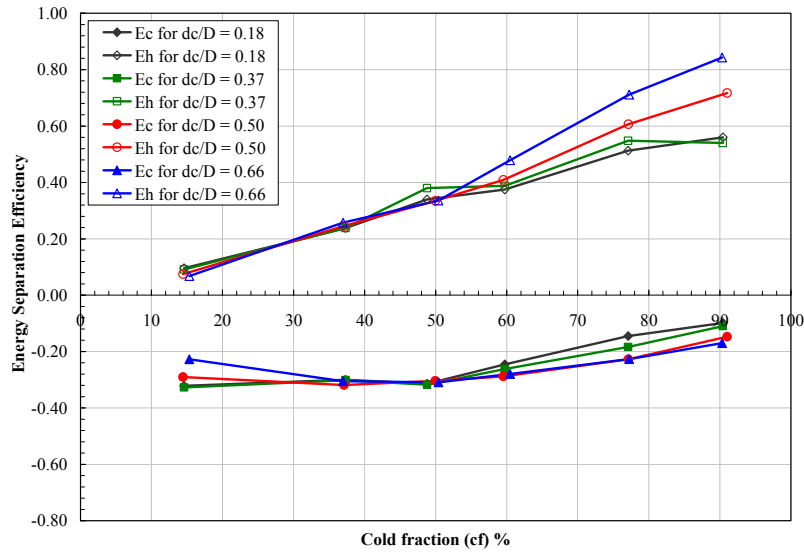


Figure 13: Effect of orifice diameter on the energy separation

From figure 13, it can be observed that hot side energy separation efficiencies behave linearly with respect to the cold fractions. For high cold fractions (above 60%) and smaller cold end orifice diameters, hot side energy separation efficiencies drop asymptotically relative to low cold fraction efficiencies. Certainly, energy separation efficiencies for different orifice diameters collapse on each other more at low cold fraction showing, what we believe to be, similar fluid mechanics. On the other hand, cold side energy separation efficiencies should keep increasing with drop in cold fraction as observed by K. Stephan and et. al. in 1983 [8]. But on the contrary, below 60% cold fraction energy separation efficiencies are either constant or decreasing asymptotically. Above observations indicate that effect of orifice diameter on energy separation efficiency is negligible for cold fraction less than 60%.

Another important observation is that at 50% cold fraction both cold and hot end energy separation efficiencies are almost equal as expected. But at the same time, at 50% cold

fraction almost every curve representing different orifice diameter, is passing through the same point. That means, for 50% cold fraction vortex tube shows similar energy separation performance irrespective of orifice diameter.

To take into consideration effect of the mass flow rates on the performance of the vortex tube, let us define energy flux separation efficiency. It is defined as the ratio of cold end energy flux (or hot end energy flux) to the isentropic compressor work.

$$\text{Energy flux separation efficiency (cold end)} = cf \times \frac{c_p(T_i - T_c)}{CW} \dots\dots\dots 6$$

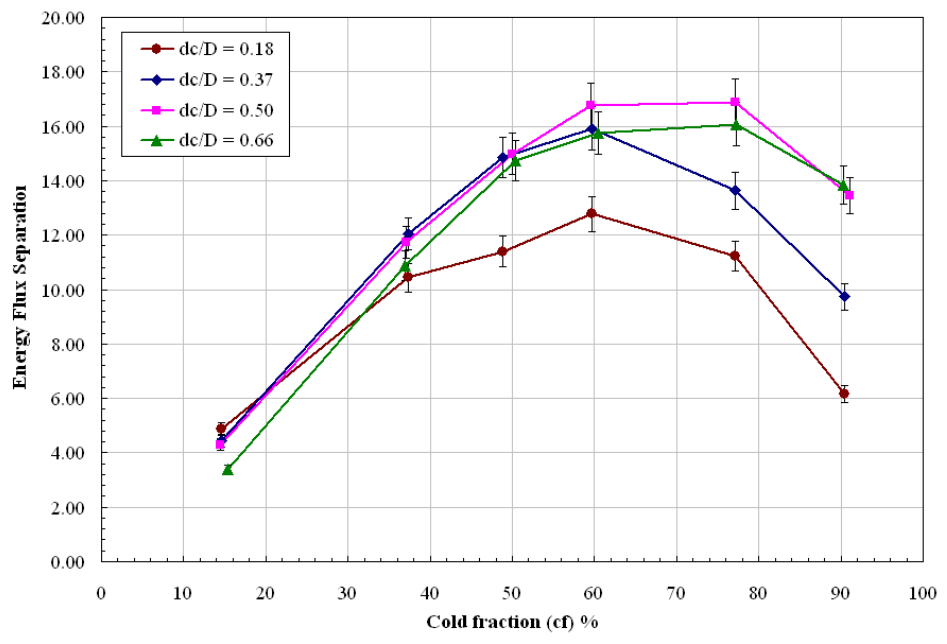


Figure 14: Effect of orifice diameter on the energy flux separation efficiency (mi = 1 lbm/min).
[Error bars in the graph indicate 5% of experimental error]

Figure 14 shows the dependence of energy flux separation efficiency of the vortex tube on the cold fraction, the orifice diameter at the inlet mass flow rate of 1 lbm/min. As discussed earlier, effect of inlet mass flow rate is washed out because of its presence in the cold fraction.

Results are showing that below 60% cold fraction energy fluxes are varying almost linearly and the effect of orifice diameter is very insignificant. Beyond 60% cold fraction, effect of orifice diameter is dominant. Firstly, energy flux separation efficiency is dropping with an increase in cold fraction and secondly for constant cold fraction it is increasing with orifice diameter. Hence it can be concluded that while operating the vortex tube for cold fraction above 60%, selecting larger orifice diameter will give better energy flux separation efficiency.

During our PhD research work we used a generator with 8 nozzles during all our experiments because our past experiments (S. Nimbalkar, 2005 [3]) show that vortex tube produces optimum energy separation with 8 nozzles (figure 15).

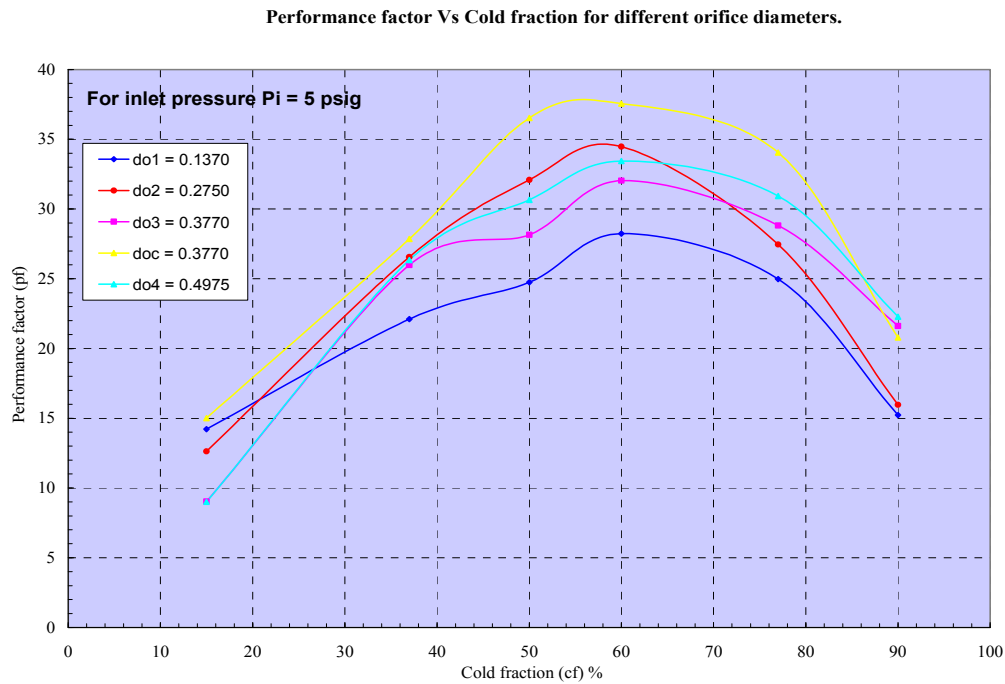


Figure 15: Effect of number of nozzles and orifice diameter on the performance of vortex tube.

As shown in figure 15, there are two generators with same orifice diameter ($do_c = do_3 = 0.377$ inch) but different number of nozzles. Generator c is with 8 numbers of nozzles

and generator 3 with only 4 numbers of nozzles. It clear from the figure 15 that at $P_i = 5$ psig, generator with 8 numbers of nozzles show better performance than a generator with 4 number of nozzles.

2.4 Quantifying performance of the vortex tube system

Performance of the vortex tube system can be defined many ways. Most of the researchers used traditional ways to quantify the efficiency of vortex tube without worrying about proper non-dimensionalization. In this subsection the efficiencies of the vortex tube system are appropriately defined and presented.

2.4.1 Energy separation efficiency

It can be defined as the ratio of energy separation effect (either cold end or hot end) to the isentropic compression work per unit mass.

$$\text{Energy separation efficiency (cold end)} = \frac{c_p(T_i - T_c)}{CW} \dots\dots 7$$

2.4.2 Energy flux separation efficiency

To take into consideration effect of the mass flow rates on the performance of the vortex tube, let us define energy flux separation efficiency. It is defined as the ratio of cold end energy flux (or hot end energy flux) to the isentropic compressor work.

$$\text{Energy flux separation efficiency (cold end)} = cf \times \frac{c_p(T_i - T_c)}{CW} \dots\dots 8$$

2.5 Total pressure drop across the vortex tube

Total pressure balance inside the vortex tube is well discussed by William J. Love in 1974 [16] and A. Piralishvili et. al. in 2005 [17].

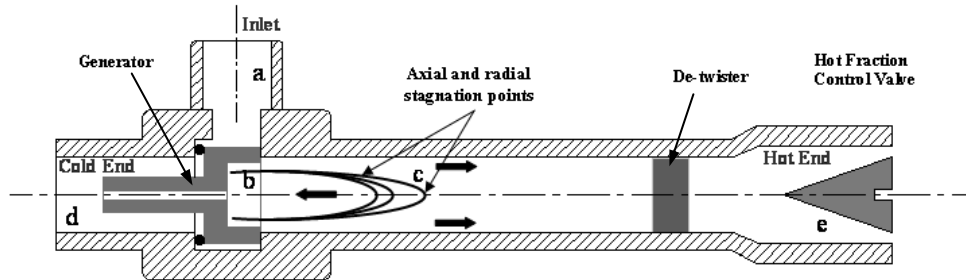


Figure 16: Characterizing pressure drops in vortex tubes.

- a. Pressure drop at the inlet,
- b. Pressure drop through the generator,
- c. Pressure drop due to flow,
- d. Pressure drop through the cold end orifice,
- e. Pressure drop across the hot fraction control valve.

As shown in figure 16, the total pressure drop across vortex tube is the addition of pressure drop at the inlet (a), pressure drop due to the generator (b), the flow (c), pressure drop through the cold end orifice (d) and due to the hot fraction control valve (e). Pressure drop across the generator takes into account the geometry of the generator and number of nozzles machined on its surface. Pressure drop due to the flow takes into consideration not only the decay of the vorticity in the swirling flow but it also considers the reduction or reversal of the axial velocity in the core of the vortex. Pressure drop across the hot fraction control valve decides the cold fraction and the location of axial stagnation point. We will discuss in detail the effect of pressure drop across the hot fraction control valve on the location of axial stagnation point and the resulting multiple flow structures in the next section.

Chapter 3 Description of Experiments Performed and Presentation of Experimental Results

3.1 Experimental apparatus

There are inherent limitations to the experimental study of vortex flow inside Ranque Hilsch tube which have kept the systematic investigation of it from progressing very far.

Similar to Ranque Hilsch (1934) [34], we used small scale models of vortex tube which are available commercially. Such small scale models, however, are not suitable to any internal measurements (figure 17b) of the vortex phenomenon, since they do not lend themselves to any velocity, pressure, or temperature traverses. To perform these observations, considerably larger size models have to be designed, and this in turn requires very high pressures and very high flow rates of supply air. Even for larger models, great care must be given to the fact that whatever probes are to be inserted in the tube, the flow pattern must not be disturbed.

To get around these obstacles and to keep the experimental setup straightforward, without affecting the actual flow structures inside the vortex tube, we decided to carry out only external measurements. Not only the simplicity but keeping the vortex tube model smaller allowed us to conduct our tests at small inlet pressures too. The main consideration in the test program was the flexible design of a test apparatus which would allow pressure, temperature and the flow measurements without causing major disturbances in the flow field.

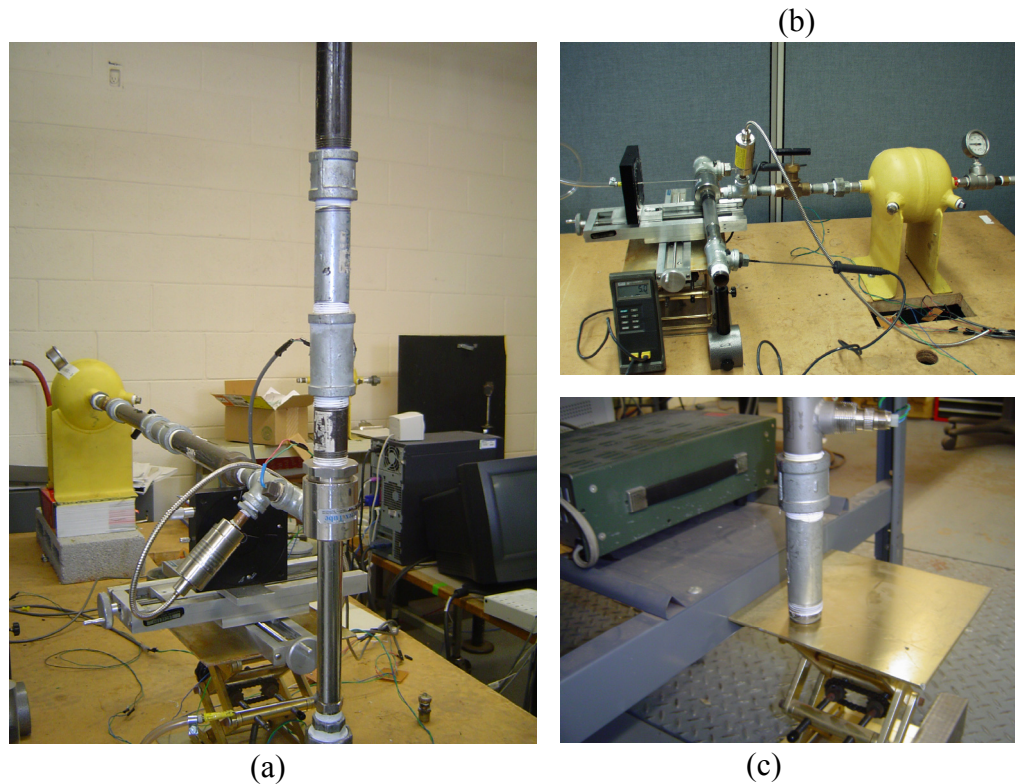


Figure 17: Experimental apparatus used to measure thermal & fluid dynamical time scales and frictional coefficient of the tapered hot fraction control valve.

[(a) Experimental setup used for external measurements, (b) A setup for internal static and dynamic pressure measurements using a pitot tube, and (c) a hot end and the moving wall setup].

The main experimental setup shown in figure 17(a) and (c) was constructed:

- To measure thermal and fluid dynamical time scales,
- To calibrate the turbine type of flow meters and
- To determine the frictional coefficients (k values) of the tapered hot fraction control valve for different opening positions.

Clean, dry air from a compressed air system was reduced through a pressure reduction valve to the desired value and was then dumped into a plenum chamber (figure 17a). From there flow accelerated into the inlet port of the vortex tube. The flow was then forced into an energetic vortex through 8 nozzles oriented tangentially. This spinning fluid was turned 90 degrees and could exit from either end of the tube. Flow out of the

hot-end side was restricted by a tapered valve which creates back pressure (P_b) and preferentially selects fluid near the outer wall. Flow out of the cold-end side was restricted by a disk with a circular hole in its center. This “orifice” preferentially selects flow from the center of the tube which will be colder due to the expansion associated with turbulence contained within the vortex.

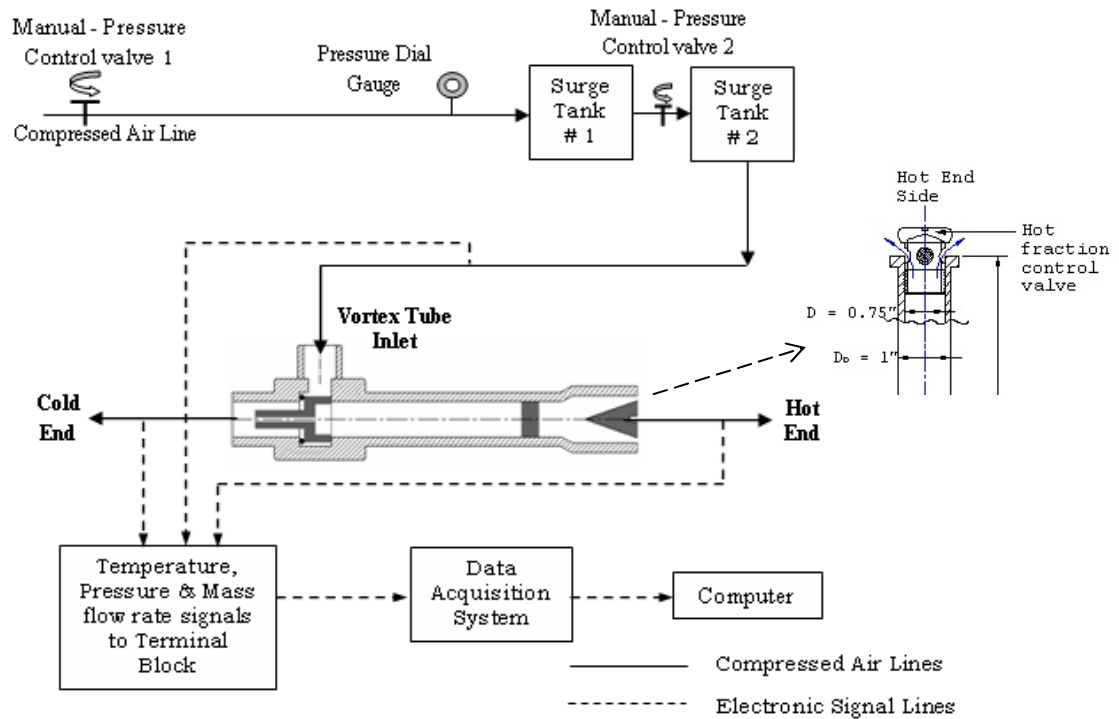


Figure 18: Schematic of the experimental apparatus and the hot fraction control vane construction.

During all of these experiments, temperatures were measured on inlet and the exhausts of the vortex tube by using thermistors. Inlet pressure (or inlet mass flow rate) was controlled by using a needle valve. Fluctuations in the compressed air line were damped by using the plenum chamber. Inlet and hot end mass flow rates were measured by using turbine type of flow-meters. All the experiments were conducted at low inlet pressures and for small cold fractions; and hence cold end side flow meter failed to pick up the flow data. Therefore we used inlet and hot end mass flow rates to calculate cold end mass

flow rate ($m_c = m_i - m_h$). In addition to hot end side pressure transducer which was located after the tapered valve, we installed Pitot tube and the liquid manometer to measure pressure right before the tapered valve. Pressure before and after the tapered valve along with the hot end mass flow rate helped us to figure out frictional coefficient of the hot fraction control valve.

Tests were conducted using a commercially manufactured vortex tube (Exair Corp., Model No. 3299, maximum mass flow rate 11 lbm/min at 100 psi inlet pressure) for different inlet mass flow rates (1, 1.5 and 1.8 lbm/min). The details of the present set-up and those of other researches are given in Table 4.

Author	Length L (inch)	Inner diameter D (inch)	Generator Nozzle		Cold end orifice diameter d_c (inch)	$d_r = \frac{d_c}{D}$
			Equivalent Diameter (inch)	nozzles		
Takahama	317	2	0.5	4	-	-
Reynolds	48	3	0.12	8	1.27	0.42
Ahlborn	24	1	-	-	0.328	0.33
C. Gao	8	0.63	0.12	1	0.16	0.25
Our work	10	0.75	0.162	8	0.38	0.50

Table 4: Vortex tube dimensions used by other researchers.
(Length unit: inch; “-” means that value is unknown)

3.2 Thermal and fluid dynamical time scales

Figure 19 shows the actual time required for the temperature and the flow data to achieve a steady state condition, when the inlet pressure is suddenly varied from 0 psig to 6 psig. The thermal time constant (τ_t) is defined as the time required for instantaneous temperature gradient ($\Delta T_t - \Delta T_i$) to achieve 63.33 % of its final value or ($\Delta T_s - \Delta T_i$) and can be calculated by fitting data to.

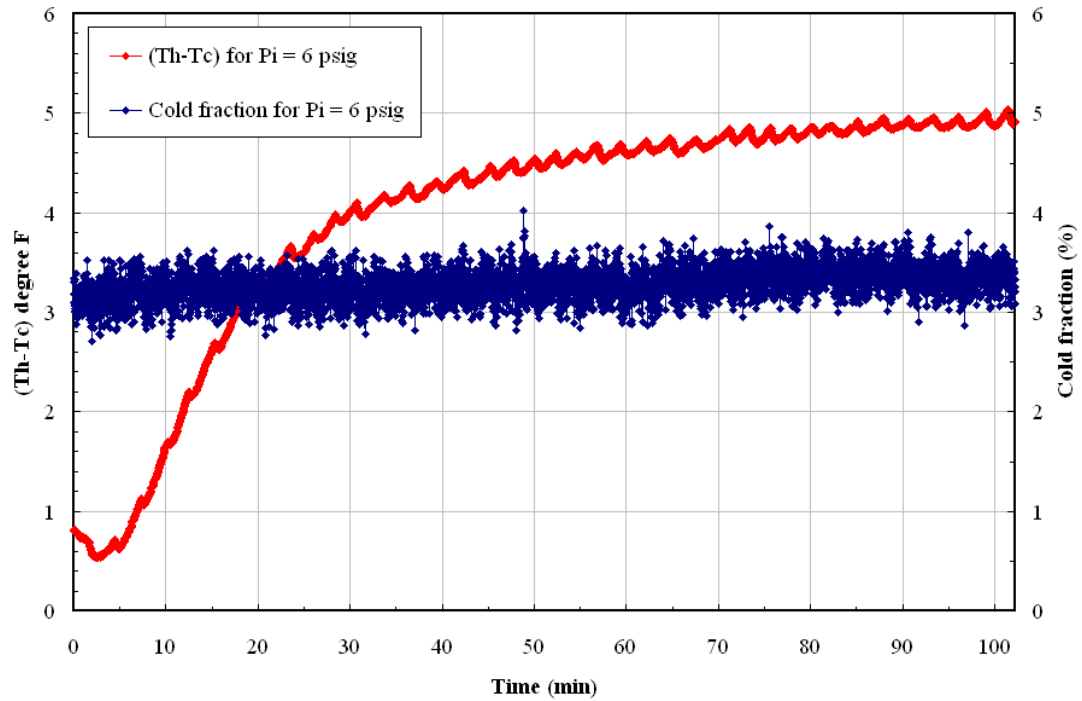


Figure 19: Thermal and fluid dynamical time scales

$$\frac{\Delta T_t - \Delta T_i}{\Delta T_s - \Delta T_i} = \left(1 - e^{-\frac{t}{\tau_t}} \right)$$

Where, $\Delta T = T_h - T_c$; °F.

$\Delta T_i = T_{hi} - T_{ci}$ or initial $\Delta T = 0.81$ °F for above data.

$\Delta T_t = T_{ht} - T_{ct}$ or instantaneous ΔT at time t; °F.

$$\Delta T_s = T_{hs} - T_{cs} \text{ or final } \Delta T ; ^\circ\text{F.}$$

t = instantaneous time; minute.

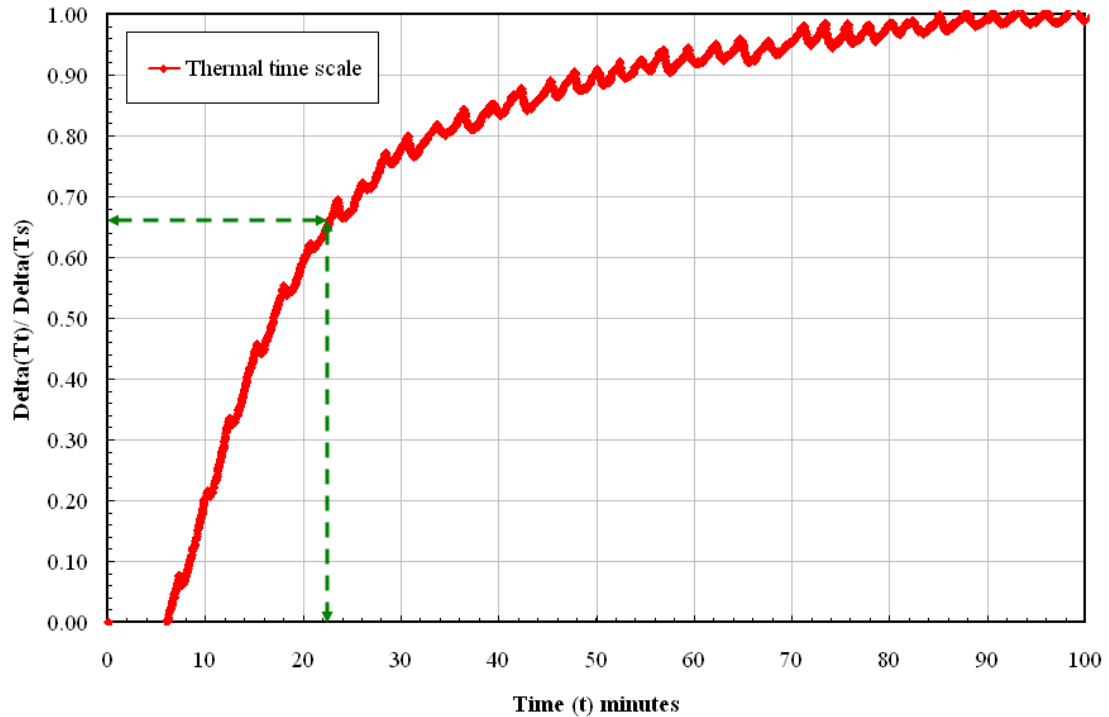


Figure 20: Thermal time constant

Figure 20 show that the time required for instantaneous temperature gradient ($\Delta T_t - \Delta T_i$) to reach 63.33 % of its final value (or $\Delta T_s - \Delta T_i$) is equal to 22 minutes. After putting value of t = 22 minutes and temperature ratio equal to 0.6333 ($\frac{\Delta T_t - \Delta T_i}{\Delta T_s - \Delta T_i} = 0.6333$) value of time constant turns out to be 21.97 minutes. It means that within 22 minutes, temperature values achieve 63.33 % of their final values.

The fluid dynamical time constant (τ_f) can be defined as the time required for instantaneous cold fraction ($cf_t - cf_i$) to achieve 63.33 % of its final value or ($cf_s - cf_i$). From figure 19, it can be observed that time constant for the flow is very small (less than

3 minutes) as compared to thermal time constant. Large amount of fluctuations were found in the mass flow rate data due to the turbulence caused by a needle valve located right before the inlet mass flow meter. Turbulence problem at higher pressures (> 5 psig) was later solved by inserting a piece of foam after the needle valve. This will be discussed in detail later in the next section.

On the whole, the thermal time scale for the vortex tube is larger (~ 22 minutes) than the fluid dynamical timescale (< 3 minutes).

3.3 Effect of the frictional coefficient (k value) of the tapered valve

During our preliminary experiments it was observed that the back pressure (P_b) exerted by the hot fraction control valve has more dominant effect on the cold fractions as compared to the inlet pressure (P_i) (figure 21).

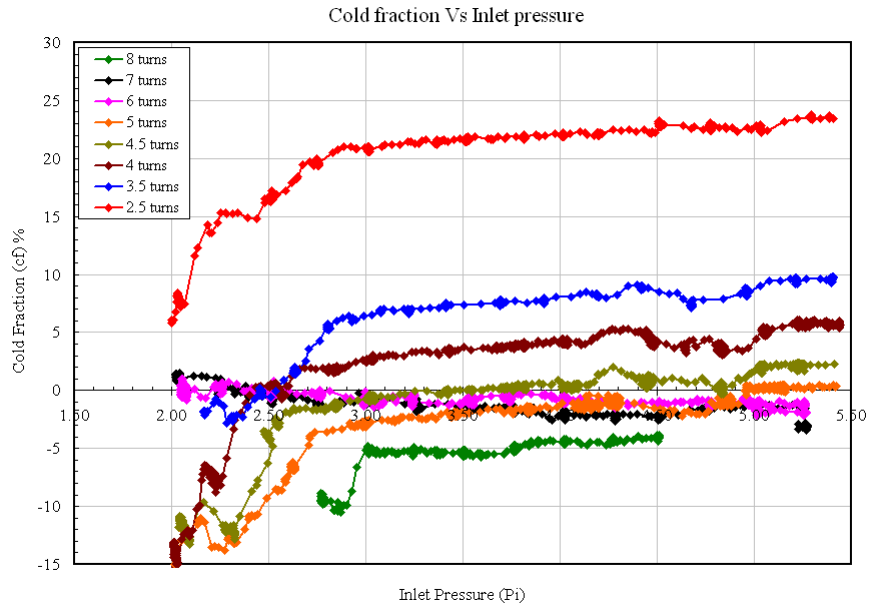


Figure 21: Dramatic effect of frictional coefficients (k) on cold fractions.

By opening or closing the hot fraction control valve by just a small amount it was simple to see more dramatic effect on the flow patterns as compared to the inlet pressure. Hence, we decided to vary tapered valve position ('k' value) to study various possible flow structures inside the vortex tube without changing the inlet pressure. Refer to Appendix 3 (Experiment 3) to understand the experimental procedure followed to measure 'k' values of the tapered valve for various open positions.

For instance, (figure 21) at a constant inlet pressure of 4 psig, by opening the tapered valve by 5 turns ($k = 0.39$), we get suction effect at the cold end side. The suction effect

at the cold end side means atmospheric air gets drawn in from the cold end side. For the same inlet pressure, and for 4.5 turns open ($k = 0.44$), we get no flow going in or coming out of the cold end and for 4 turns open ($k = 0.48$), flow starts coming out of the cold end side and we get the normal energy separation effect. As discussed before 'k' is frictional coefficient of the hot fraction control valve located at the hot end of the vortex tube and measured in the laboratory for different valve opening positions (Refer to Appendix 3). Please refer section 3.5 for more detailed explanation of various flow modes observed inside the vortex tube.

Looking at the effect of inlet pressure on the cold fraction, it is very minimal as the slopes of cold fraction and inlet pressure curves for a constant tapered valve position are almost zero.

Experimental findings so far can be summarized as follows:

- There are two critical independent parameters which need to be addressed while dealing with vortex tube systems. One is inlet pressure (P_i) and the other one is 'k' value of the hot fraction control valve.
- At constant inlet pressure and for the fixed geometry of the vortex tube, 'k' value of the valve plays very vital role in deciding the type of the flow structure and resulting energy separation inside the vortex tube.

3.4 Quantitative observations on multiple flow structures inside vortex tube

After calibrating the flow meters, measuring the time scales and measuring the ‘k’ values of the tapered valve, we somewhat modified the experimental setup to observe the multiple flow structures quantitatively (figure 22).

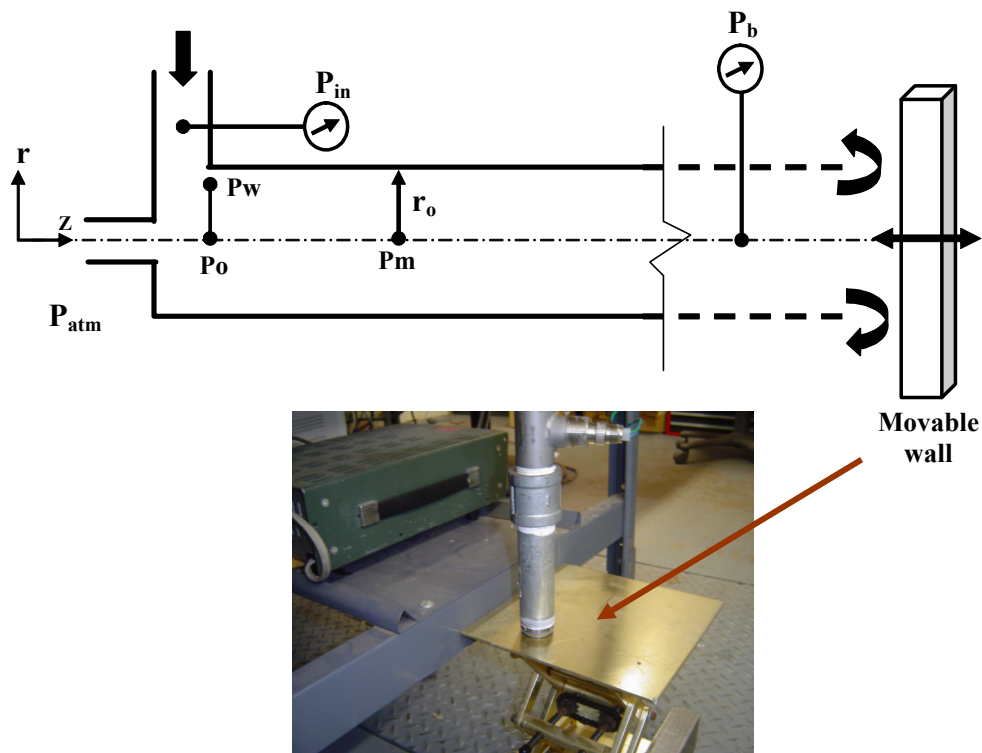


Figure 22: Effect of back pressure on cold end orifice entrance pressure (P_o)

[Primary experimental setup to obtain different flow structures inside the vortex tube. Vortex tube is vertical in this experimental setup with the hot end side near the ground]

It was difficult and time taking to change the position of the hot fraction control valve without disassembling the whole hot end side of the experimental setup. Hence, we decided to replace the hot fraction control valve with a movable wall (figure 22).

Movable wall does the same job of controlling the back pressure but with more convenience and the control.

3.5 Observed flow structures inside vortex tube

Case 1: Reverse or Venturi flow (Please refer to figure 22 for the definition of P_o)

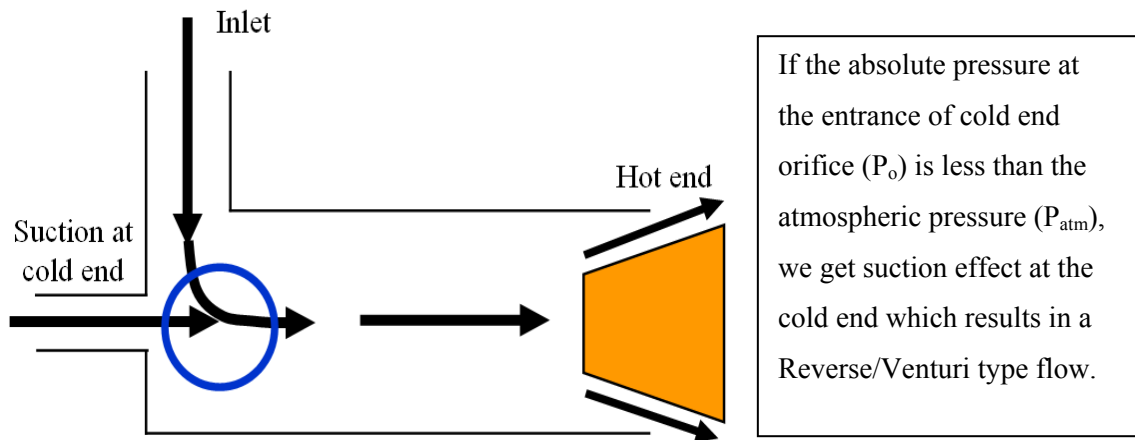


Figure 23: Reverse or Venture flow

Case 2: Elbow flow

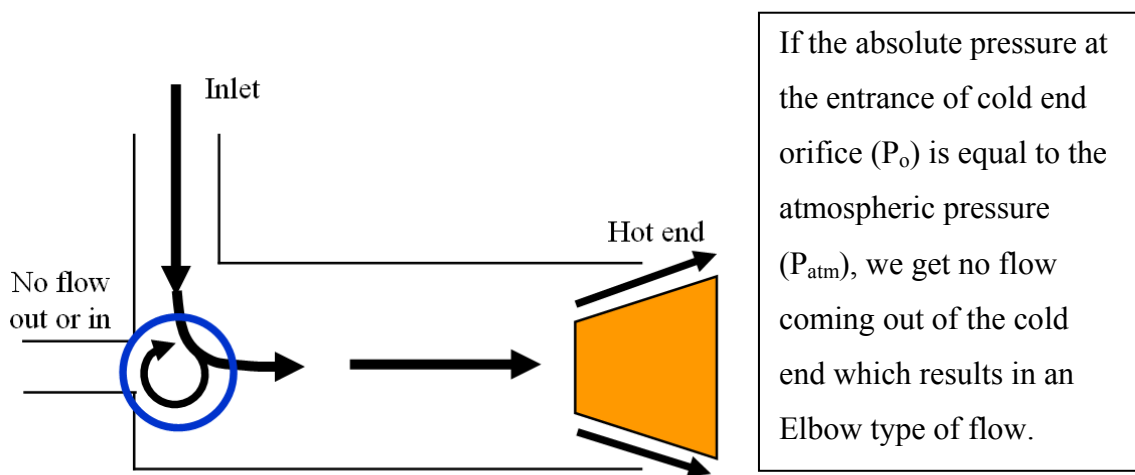


Figure 24: Elbow flow

Case 3: T-Flow

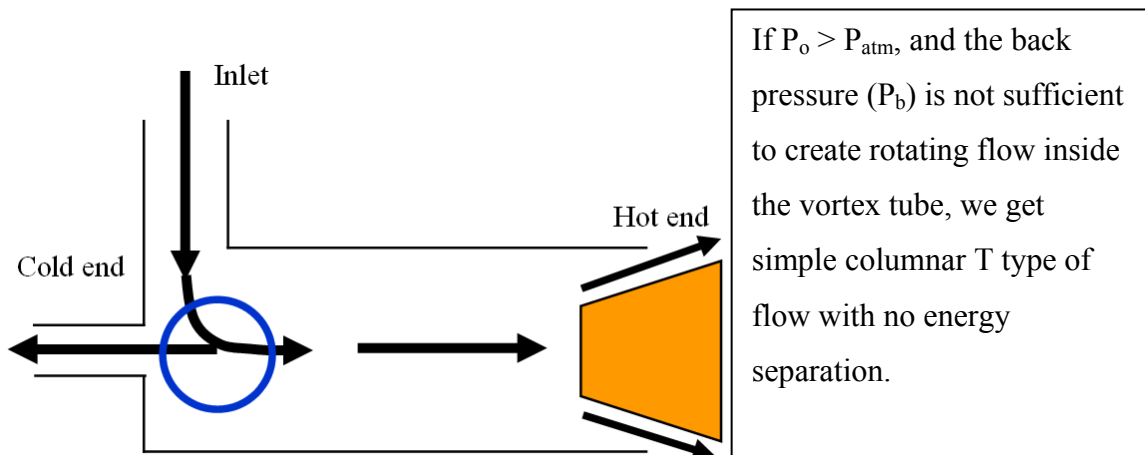


Figure 25: T flow

Case 4: Vortex Tube flow (or VT-flow)

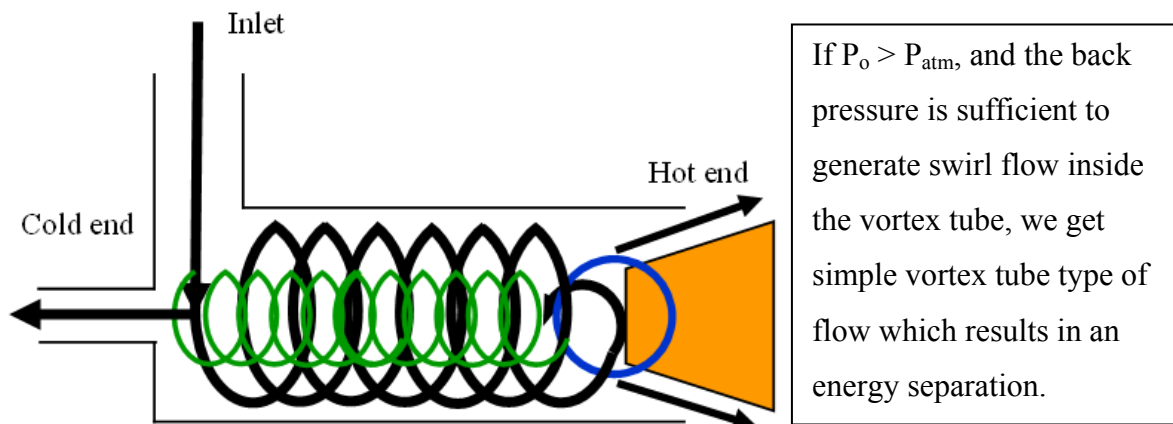


Figure 26: Vortex Tube type of flow (or VT-flow)

As shown in figure 27 and 28, for various constant inlet pressures ($P_i = 2$ to 8 psig), the back pressure (P_b) was changed by moving the wall closer or away from the hot end. Flow transitions from Reverse to Elbow, Elbow to T-flow and from T-flow to VT-flow were observed respectively. Following observations can be made from these results:

- Cold fraction becomes positive when flow transition takes place from Reverse to T-flow.
- In the T-flow region, even if the cold fractions are positive, observed temperature gradients are almost zero meaning no energy separation.
- In the transitional region, even if the cold fractions are significantly positive (~8 to 15%); the achieved energy separation effect is nominal.

Figure 28 shows required critical back pressures (P_b) to achieve flow transitions from Reverse, Elbow and T-type of flows to the VT-type of flow structure for different inlet pressures (P_i).

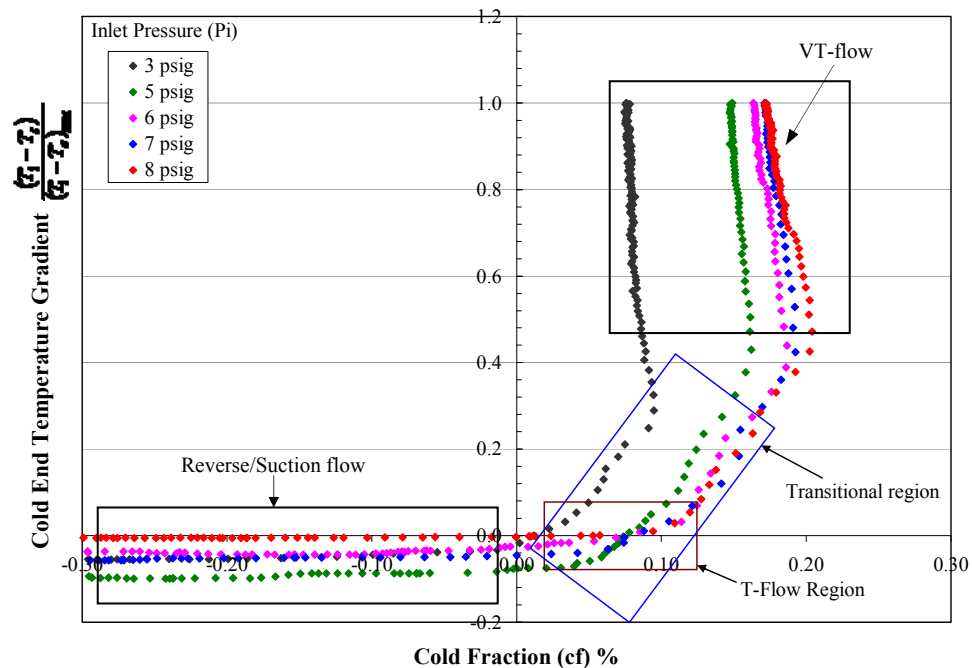


Figure 27: Multiple flows and the critical cold fractions

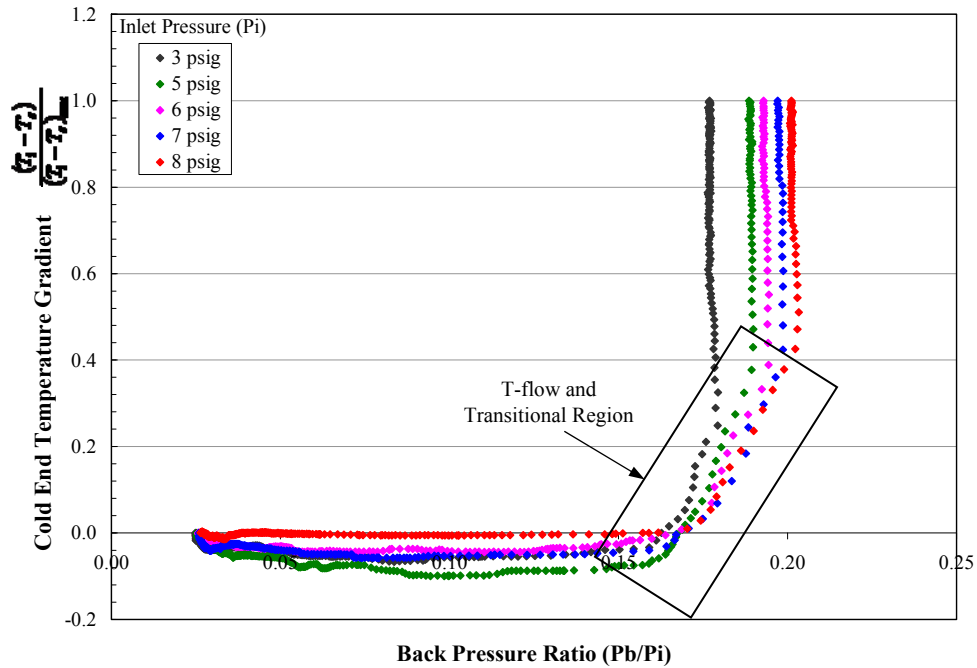


Figure 28: Multiple flows and the critical back pressures

As inlet pressure increases, the back pressure needed to start vortex type of flow increases. This effect could be collapsed with a non-dimensionalization as shown in figure 28. What seems of interest here is the transitional region as shown in figure 27 and 28. It can be observed that depending upon the inlet pressure, not only does the point where energy separation occurs change, but the length of the transitional region also changes. We need an appropriate one dimensional theoretical model to explain multiple flow modes and the transition from one mode to another.

Figure 29 shows the actual time experiment conducted in the lab to observe multiple flow structures inside the vortex tube. As discussed earlier, cold end flux separation efficiency is simply the product of cold fraction (cf) and the cold end temperature gradient ($T_i - T_c$) divided by the compressor work (CW). When there is a Reverse/Suction flow inside the vortex tube, temperature gradient ($T_i - T_c$) is either positive, negative or zero as T_c is

atmospheric temperature and it can be anything ($T_c < T_i$ or $T_c \geq T_i$). Cold fraction is also negative. Hence the cold end flux separation is positive during the Reverse/Suction flow.

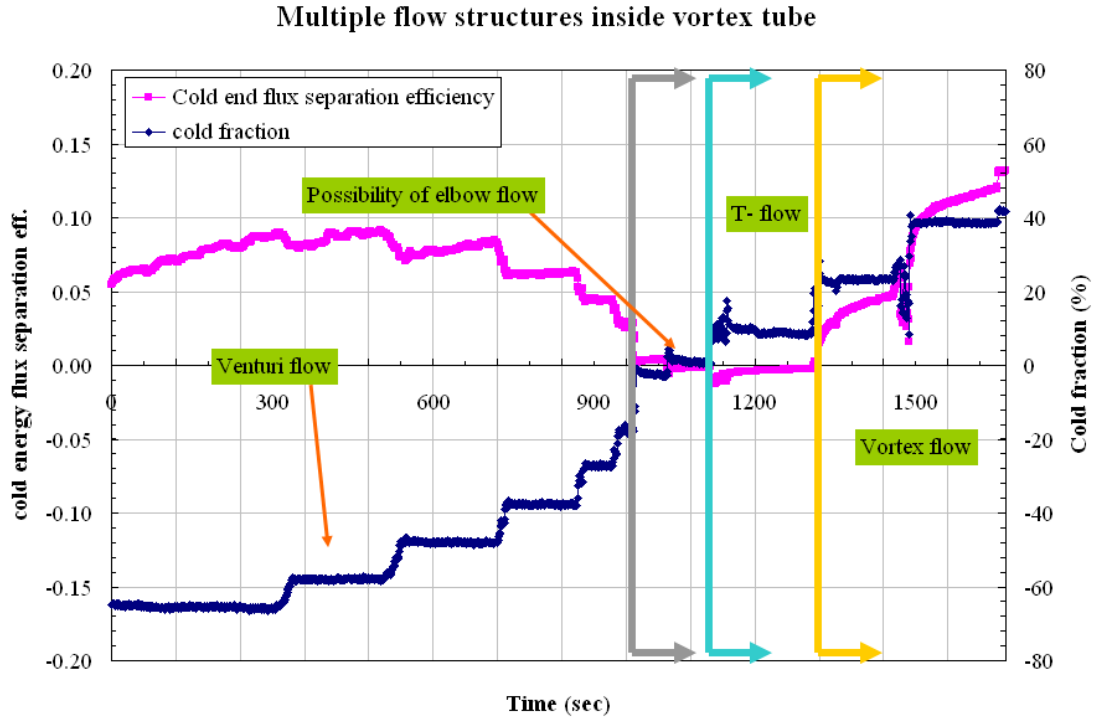


Figure 29: Observing multiple flow structures inside vortex tube – time plot

If the cold flux separation efficiency and the cold fraction both are zero, we get Elbow type of flow inside the vortex tube. If the separation efficiency is zero even if the cold fraction is positive, we have T-flow inside the vortex tube. If both the separation efficiency and the cold fraction are positive, we get VT-flow inside the vortex tube.

Cold End Energy Separation Efficiency	Cold Fraction (cf)	Flow Type
Positive, Negative or Zero	Negative	Reverse/Suction Flow
Zero	Zero	Elbow Flow
Zero	Positive	T-flow
Positive	Positive	Transition or VT-flow

Table 5: Thermo-physical Conditions for the multiple flow structures inside vortex tube

3.6 Hysteresis behavior of the vortex tube & the thermal time constant

Many of our earlier experiments showed sign of hysteresis behavior inside vortex tube. During those experiments we observed that temperature gradients obtained while increasing the inlet pressure (P_i) from zero to some positive value were different than those obtained while decreasing the inlet pressure from some positive value to zero. We called it dual valued behavior of the vortex tube.

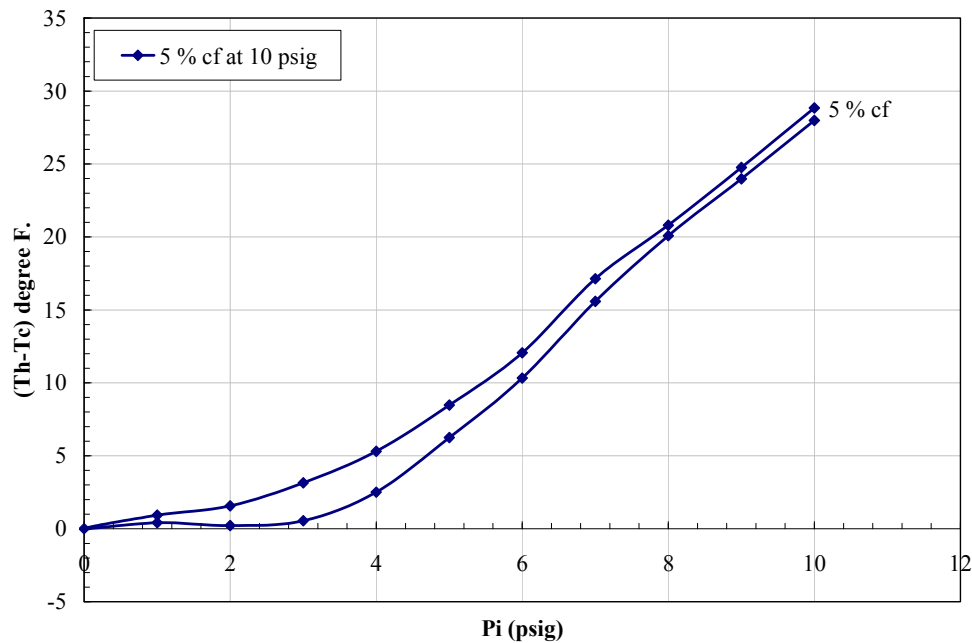


Figure 30: Dual valued behavior in temperature gradient

Hysteresis nature of curves showed in figure 30 and 31 indicates a delayed response by the cold end side flow to changes in the forces acting at the entrance. Figure 31 shows dual valued behavior in cold fractions.

We believe that thermal properties of the vortex tube are secondary in nature and are mainly governed by the type of flow structure. To test this hypothesis, we conducted a simple experiment on vortex tube by replacing a tapered valve with a movable wall. For a

fixed inlet needle valve position, we changed the back pressure by moving the wall closer or away from the hot end. (See figure 32).

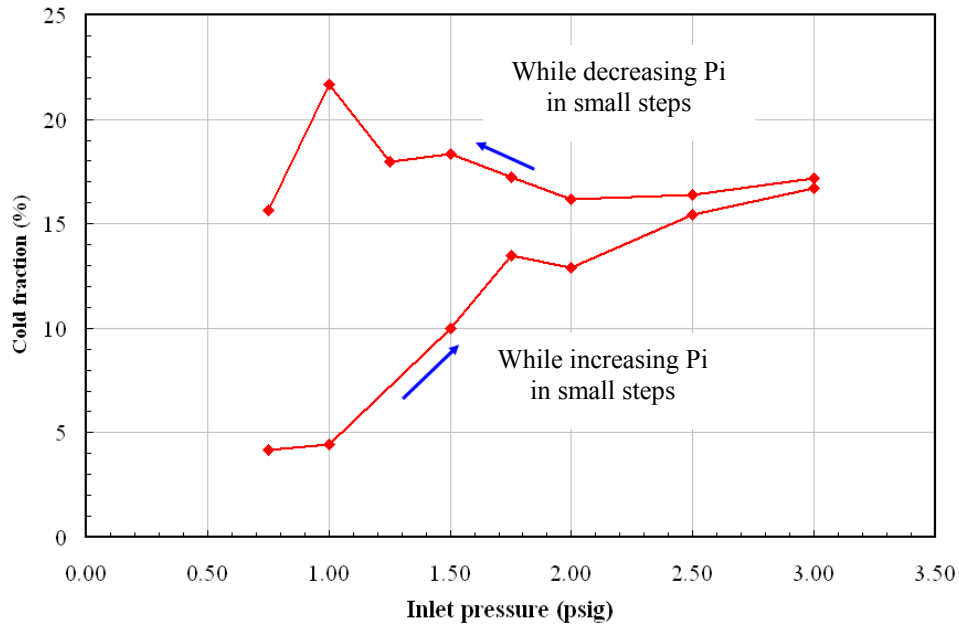


Figure 31: Dual valued behavior in cold fraction

In figure 32, red data points are showing the measurements taken while increasing the back pressure (P_b) or moving the wall closer to the hot end. Green data points are taken while decreasing the back pressure or moving the wall away from the hot end. Two sets of readings were taken for two fixed inlet needle valve positions (~ 3.5 and 4 psig inlet pressures at $P_b = 0$).

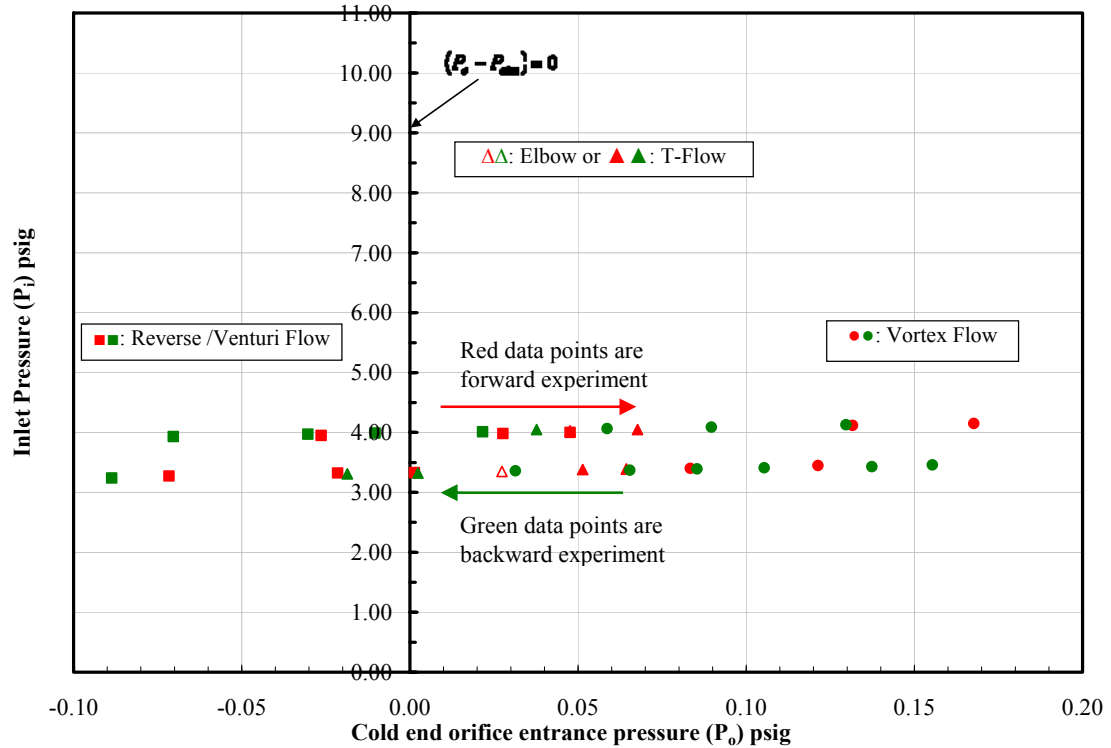


Figure 32: Hysteresis behavior of the vortex tube and the flow transition

Initially we thought that while moving the wall closer and away from the hot end, the flow transitions from T-flow to VT-flow take place at different back pressures (see figure 32). For example at inlet pressure 4 psig, reverse flow was observed until $P_o - P_{atm} = 0.05$ while moving the wall away from the hot end. But while moving the wall closer to the hot end, reverse flow didn't occur until $P_o - P_{atm} \approx 0.02$.

Experiment shown in figure 33 and 34 is very similar to the aforementioned experiment except the results are shown in different form. In figure 33, temperature differences are plotted against the cold fraction and in figure 34, frequency outputs from the inlet and hot end mass flow meters are plotted against the inlet pressure.

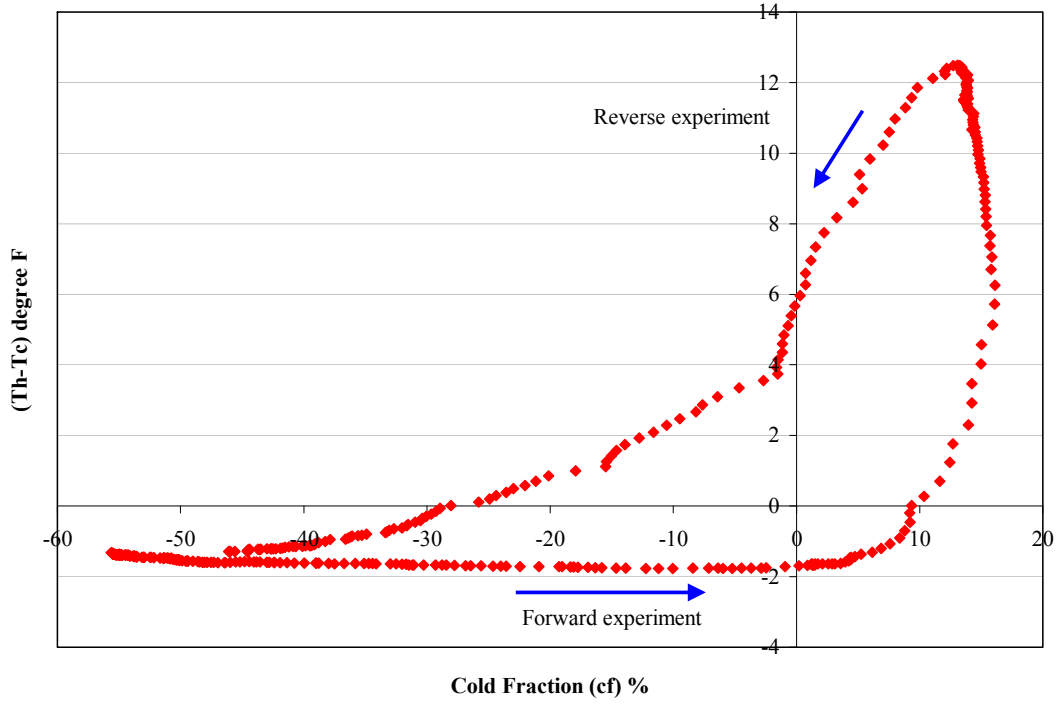


Figure 33: Hysteresis behavior in temperatures and the flow transition

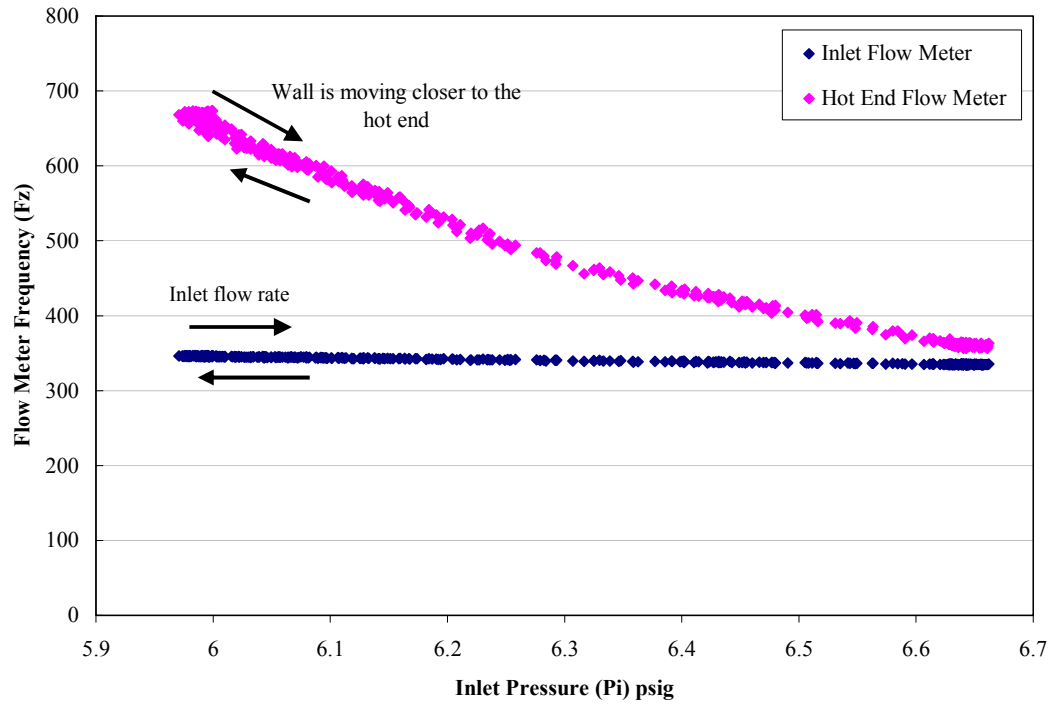


Figure 34: Linear (non-dual valued) behavior of flow meter raw data

Following observations can be made from the figures 33 and 34:

- Hysteresis behavior can only be observed in terms of temperature gradients. Temperature gradients observed while moving the wall closer to the hot end are different from those observed while moving the wall away from the hot end. It is because of the unsteadiness of the temperatures as it takes almost one hour to achieve thermal steady state.
- No dual valued behavior is observed in inlet or hot end frequencies obtained from the mass flow meters. As the volumetric flow rates are proportional to the frequencies, we can conclude that no hysteresis behavior is observed in terms of volumetric flows.

Different Approach:

For supporting above arguments, we conducted exactly opposite experiments (see figure 35 & 36) in the laboratory. During these experiments, we kept the movable wall position fixed and changed the inlet pressure from 3 to 10 psig and back to 3 psig. Cold fraction and raw flow meter data is shown in figures 32 and 33. From the results it can be concluded that the observed dual valued behavior in cold fractions is due to the unsteadiness of the temperatures and not because of the changes in flow structures inside the vortex tube. Figure 36 shows that flow meter frequencies behaved consistently linear during all these experiments.

In summary, dual valued behavior observed in the past is due to the unsteadiness of the temperatures or not reaching the thermal steady state and not because of the flow structure changes inside the vortex tube.

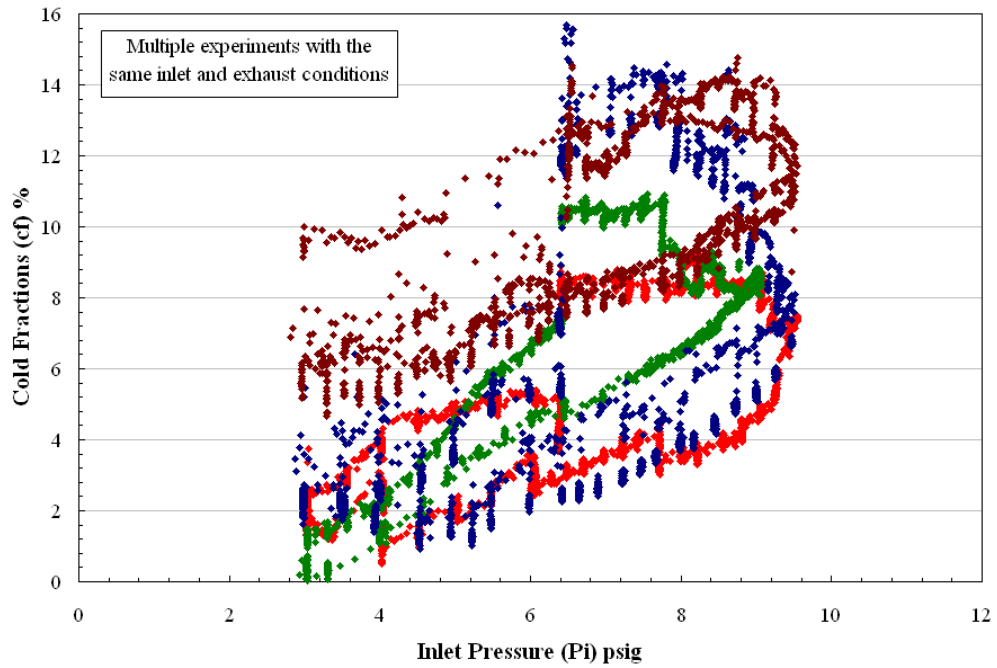


Figure 35: Non-linear (dual valued) behavior in cold fractions due to unsteady temperatures

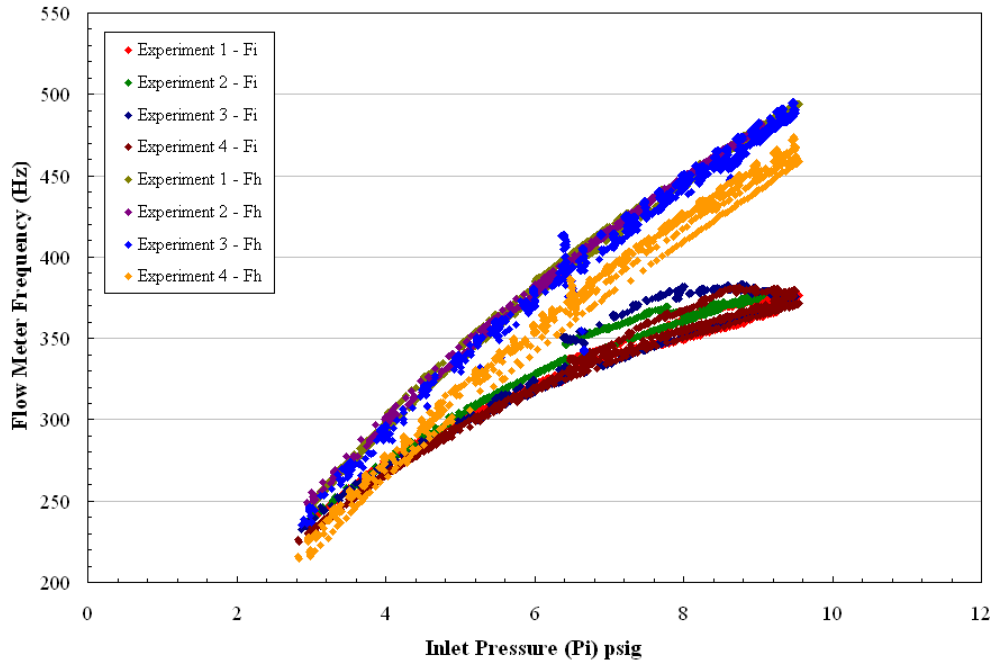


Figure 36: Linear (non-dual valued) behavior of flow meter

Chapter 4 Analytical Modeling and Application of Modeling to Experimental Results

In this section, we are going to relate the back pressure (P_b) exerted by the moving wall with the cold end orifice entrance pressure (P_o). As shown in figure 37, flow conditions at the cold end are decided by the cold end orifice entrance pressure.

- If P_o is greater than the atmospheric pressure, we should get the flow coming out of the cold end side – required condition for T-flow, Transition or VT-flow,
- If P_o is less than P_{atm} , there should be a suction effect at the cold end and air should get drawn inside the vortex tube – Suction/Venturi flow, and
- If P_o is equal to P_{atm} , air should not get drawn out or in and we should get Elbow type of flow inside vortex tube – Elbow flow.

4.1 Cold end orifice entrance pressure and multiple flow structures

Let's find out the relationship between the absolute pressure at the entrance of cold end orifice (P_o) to the inlet pressure (P_{in}) and the back pressure (P_b) at the hot end side.

As shown in figure 37,

P_{in} = Inlet pressure,

P_b = Hot end back pressure,

P_w = Pressure near the wall of the vortex tube,

P_m = Pressure at the intermediate location on the axis of the vortex tube,

P_o = Pressure at the entrance of cold end orifice,

r_o = Radius of the vortex tube.

4.2 A theoretical model explaining multiple flow modes

Let's start with the continuity and the momentum equations inside vortex tube,

Continuity equation:

$$\frac{1}{r} \left(\frac{\partial(r \cdot U)}{\partial r} \right) + \frac{\partial W}{\partial z} = 0$$

where,

U = Radial velocity component (9)

W = Axial velocity component

V = Tangential velocity component

Radial momentum equation:

$$\rho \left(\frac{U \partial U}{\partial r} + \frac{W \partial U}{\partial z} \right) = - \frac{\partial p}{\partial r} + \rho \frac{V^2}{r} + \left\{ \begin{array}{l} \text{Turbulence or} \\ \text{wall shear stress terms} \end{array} \right\} \dots (10)$$

Assumptions:

1. Flow variations in the radial direction are small. Therefore $U \approx 0$ and $\frac{\partial U}{\partial z} \approx 0$.
2. Wall shear stress is negligible.
3. The vortex flow at any axial position is forced vortex (or irrotational) with the exception of the close vicinity of the tube wall.

Hence, $V \cong V_o(z) \left(\frac{r_o}{r} \right)$

Therefore, radial momentum equation becomes,

$$\frac{\partial p}{\partial r} = \rho \left(\frac{V^2}{r} \right) \dots (11a)$$

$$\frac{\partial p}{\partial r} = \rho \left(\frac{r_o^2 V_o^2(z)}{r^3} \right) \dots (11b)$$

By integrating equation (11b) from $r = 0$ to $r = r_o$, we get,

$$(p_w - p_o) = s_1 \rho \left(\frac{V_o^2}{2} \right)$$

where, (12)

$s_1 = \text{constant}$

If we assume there is a negligible pressure drop along the length of the vortex tube, back pressure P_b is simply average of P_o and P_w .

$$\frac{P_o + P_w}{2} \cong P_b \text{ (13)}$$

For limiting cases (like Reverse, Elbow and T-flow), flow inside vortex tube is nearly laminar and can be treated as a simple pipe flow as they occur at very low Reynolds numbers. Hence, overall pressure drop along the length of vortex tube can be obtained by using Bernoulli's equation,

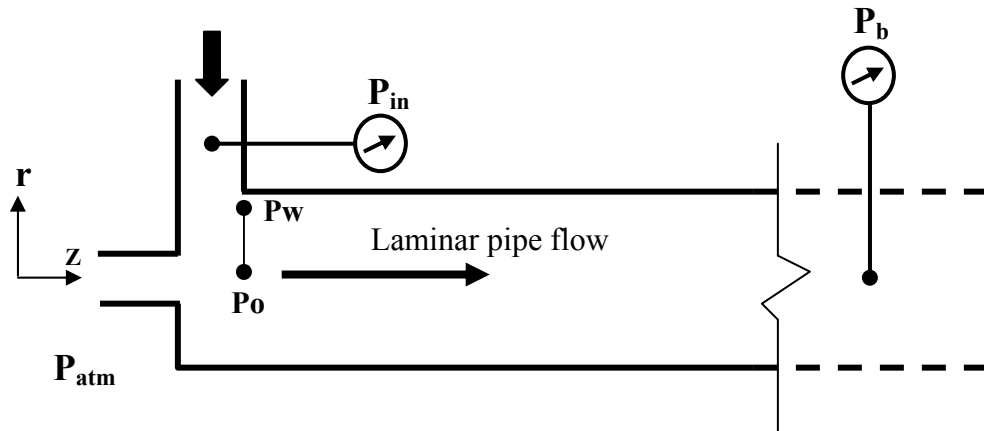


Figure 37: Laminar flow assumption and Bernoulli's equation

$$(p_m - p_b) = s_2 \rho \left(\frac{W^2}{2g_c} \right)$$

where, (14)

$s_2 = \text{constant}$

As for Reverse, Elbow and T-flow, rotational component of the velocity is negligible, we can assume $V_o = W$. Hence, equation becomes:

$$(p_{in} - p_b) \cong s_2 \rho \left(\frac{V_o^2}{2g_c} \right) \dots (15)$$

Up to this point, we have derived following three equations (12), (13) & (15):

$$(p_w - p_o) = s_1 \rho \left(\frac{V_o^2}{2} \right)$$

where,

$s_1 = \text{constant}$

$$P_o + P_w \cong 2P_b$$

$$\text{And, } (p_{in} - p_b) \cong s_2 \rho \left(\frac{V_o^2}{2g_c} \right)$$

If we simplify above equations and solve for P_o , we get,

$$P_o \cong P_b - \frac{s_2 g_c}{2s_1} (P_{in} - P_b) \dots (16)$$

Where, $g_c = 386.4 \text{ inch/sec}^2$, s_1 and s_2 are the constants determined from the experimental data. After simplifying equation (16) even more, we get relationship between P_{in} and P_b ,

$$P_{in} \cong \left(\frac{2s_1}{s_2 g_c} + 1 \right) P_b - \left(\frac{2s_1}{s_2 g_c} \right) P_{atm} \dots (17)$$

To get values for s_1 and s_2 , let's use experimental data. In figure 38, multiple flow modes are plotted in the back pressure (P_b) and the inlet pressure ($P_i = P_{in}$) parametric space. Reverse/Suction flow is shown by solid squares (■), Elbow flow is shown by empty triangles (Δ), T-flow by solid triangles (▲) and VT-flow by using solid circles (●). On the left side of the solid line shown in figure 38, we always found Reverse flow. Again Reverse flow means suction at the cold end side, which causes atmospheric air to enter into the vortex tube chamber through the cold end.

Limiting case of Reverse/Suction flow is Elbow type of flow, where you do not get anything out of cold end side. Again these limiting cases are shown by hollow triangles in figure 38. If we add trend line to these cases, we get relationship between P_{in} and P_b as:

$$P_{in} = 6.0096 \cdot P_b - 0.0742 \dots (18)$$

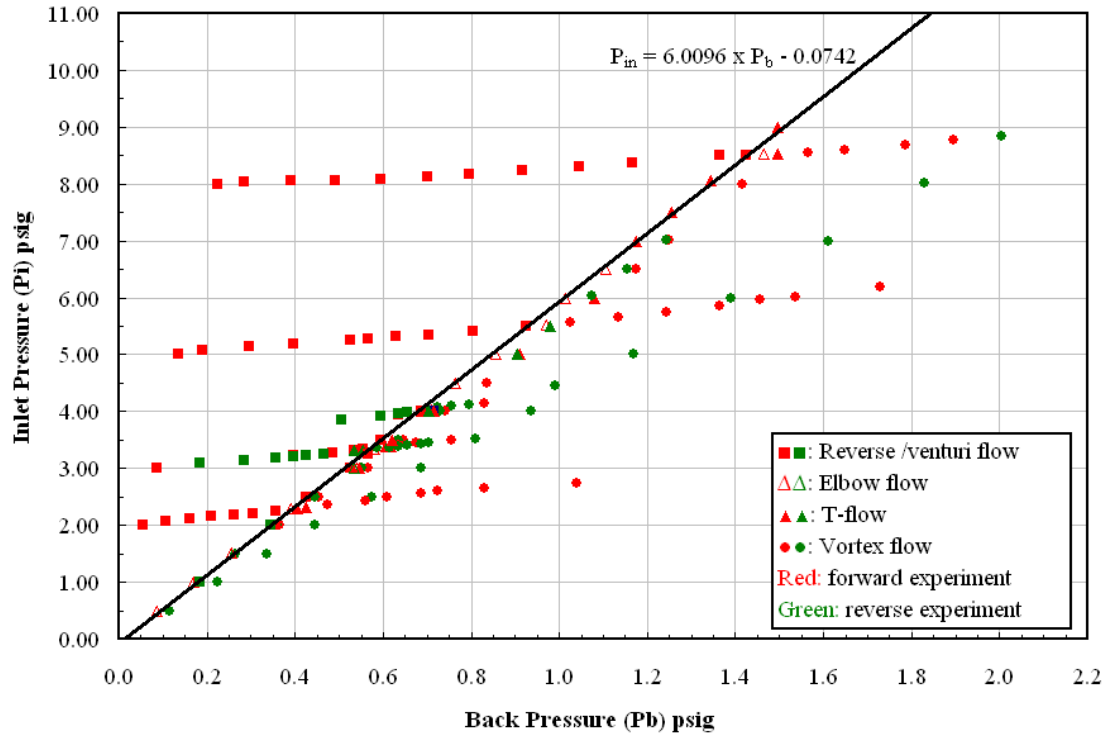


Figure 38: Mapping multiple flow structures on inlet pressure and back pressure parametric plane

By solving equations 17 and 18, we get values of the coefficients as follows,

$$s_1 = 67.515 \text{ and } s_2 = 0.06975$$

Therefore, P_o becomes,

$$P_o \cong P_b - 0.20(P_{in} - P_b) \dots (19)$$

By subtracting P_{atm} from both sides, we get

$$(P_o - P_{atm}) \cong P_b - 0.20(P_{in} - P_b) - P_{atm} \dots (20)$$

4.3 Criteria for different flow structures

Case 1: Reverse/Suction flow

$$(P_o - P_{atm}) \cong P_b - 0.20(P_{in} - P_b) - P_{atm} < 0 \dots (21)$$

Case 2: Elbow flow

$$(P_o - P_{atm}) \cong P_b - 0.20(P_{in} - P_b) - P_{atm} = 0 \dots (22)$$

Case 3 and 4: T-flow and VT-flow

$$(P_o - P_{atm}) \cong P_b - 0.20(P_{in} - P_b) - P_{atm} > 0 \dots (23)$$

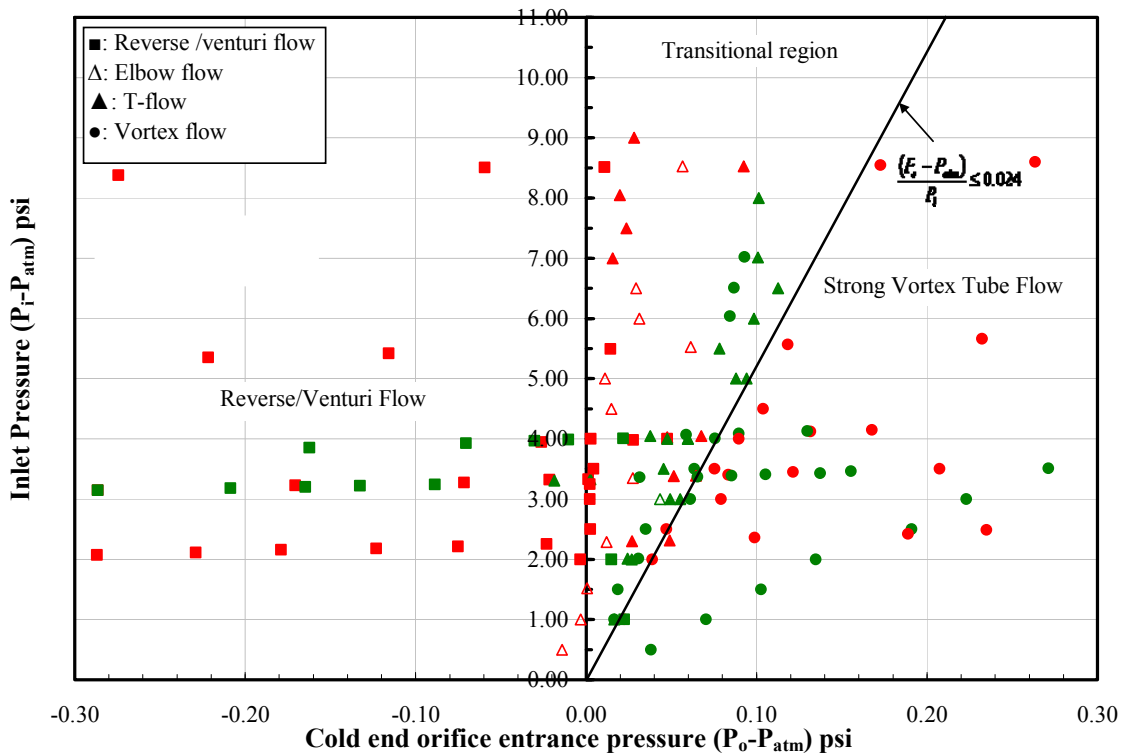


Figure 39: Relating back pressure (P_b) with cold end orifice entrance pressure (P_o)

4.4 Transition from T-flow to VT-flow

In the previous sub-section, we saw transition from Reverse flow (or Suction flow) to Elbow type of flow. When $P_o = P_{atm}$, we get Elbow type of flow. As shown in figure 39, to the left of $P_o - P_{atm} = 0$ line, we always observed Reverse flow or Suction flow at the cold end side. Along with the mass flow meter readings, the multiple flow modes were also confirmed by using a smoke technique. If the smoke gets drawn in at the cold end side that means we have a Reverse flow. If it gets gusted away from the cold end, that's the T or VT type of flow. But if it goes straight up (no suction or blowing) we have an Elbow type of flow inside vortex tube.

It is obvious that when P_o becomes greater than atmospheric pressure, air starts coming out of cold end side. Fascinatingly, we observed another transitional region ($P_o - P_{atm} > 0$) on the right side of the critical line ($P_o - P_{atm} = 0$) as shown in figure 39.

In this region, defined by $\frac{(P_o - P_{atm})}{P_i} \leq 0.024$ approximately, we observed strong vortex tube type of flow (VT-flow) everywhere. In the region enclosed by the lines defined by ($P_o - P_{atm} = 0$) and $\frac{(P_o - P_{atm})}{P_i} \leq 0.024$, we obtained either T-flow or weak VT type of flow.

In this transitional region, even at higher inlet pressures (6-9 psig), vortex tube failed to produce any/adequate amount of energy separation.

This transition from T-flow to VT-flow is a very intriguing phenomenon and needs more experimental and theoretical understanding. Following propositions and the facts can be used as the stepping stones to explain the transition from “no energy separation” to “energy separation”:

- We believe that the flow transition from T-flow to VT-flow is accompanied by the relocation of an axial stagnation point.
- We also believe that the axial pressure distribution inside the vortex tube plays a very responsible role during the relocation of an axial stagnation point.
- Axial and radial pressure gradients inside the vortex tube are controlled by inlet pressure (P_i) and the back pressure (P_b) exerted by the hot fraction control valve.
- Many studies (M. A. Herrada 2003 [50], J. J. Keller 1985 [51]) shows that axial and radial pressure distributions inside the rotating pipe flows are linked with the phenomenon of “vortex breakdown”. Vortex breakdown inside the vortex tube can be defined as an abrupt and drastic change of vortex structure, initiated by a variation in inlet pressure or the back pressure exerted by the tapered valve.

4.5 Location of axial stagnation point inside vortex tube

4.5.1 Carriage and slider method

In trying to map out axial flow direction in the vortex tube, we had trouble reducing the effect that the swirl had on our results. The flow was too turbulent for threads, and probes inserted into the tube were too easily caught up in the swirl and affected the cold fraction.

Our solution to this problem was Carriage & Slider Method (CSM): setting up a horizontal wire in the clear section of the vortex tube with a short section of thin tubing, called the slider, which could freely slip to either end of the wire.

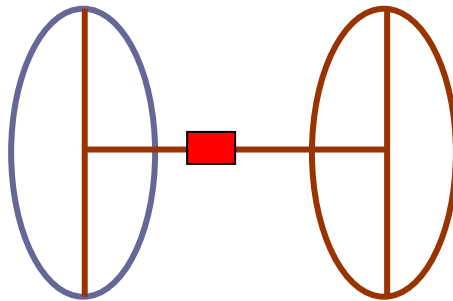


Figure 40: Carriage and slider method

The ends of the horizontal wire were soldered to bisect a vertical wire, which were in turn soldered across a metal ring with a diameter just under that of the clear tube. One ring was often made out of stainless steel, so that the carriage, seen in figure 40, could be moved around in the tube by using neodymium magnets. All other parts were made of copper wire, for ease of soldering and therefore better accuracy. The purpose of this method was to find stagnation points along the center axis, and it benefits from the slider's inability to move in any direction except for axial.

4.5.2 Experimental Setup and Procedure

We introduced the carriage into the system through the cold end side by removing the generator. After having replaced the generator, we positioned the carriage either with magnets or with a probe stuck through the hole in the generator. Tests were run at a whole range of cold fractions and inlet pressures. When moving the carriage, if the slider didn't change location, the probe was used to move it to check whether or not the slider was at a point of stagnation.

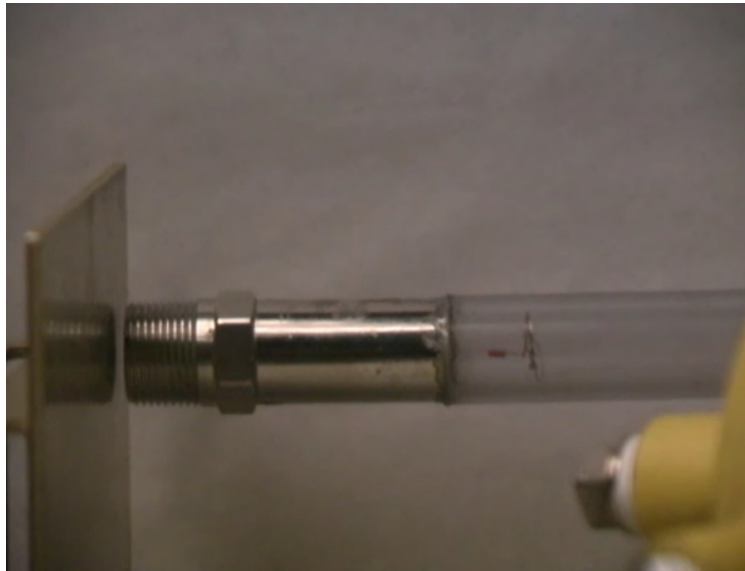


Figure 41: Flow visualization by carriage and slider method

4.5.3 Axial Stagnation Point Test Results

No matter what the inlet pressure or location of the carriage in the clear tube, the slider slid towards the cold end side. This held true for all cold fractions except for zero; when the valve was removed entirely, the slider slid towards the hot end side, as is to be expected. Even when the valve was still attached but at its fully open state, the slider slid towards the cold end side, although one could cause an axial stagnation point by holding the valve up to the end of the pipe without fully inserting it. To test this last

phenomenon, we removed the valve and set up a wall at the end of the tube instead, to examine a more simplistic end condition. With the pressure at 1.5 psig, we started the wall at 16 mm away from the tube, and slowly moved it forward until we saw the slider start to move at 9 mm from the end. When the wall was 6.5 mm from the end of the tube, the stagnation point was 52.4 mm from the detwister. At 5 mm, the slider was stable at 100 mm from the detwister, and by 4mm, the stagnation point had passed the generator (127 mm from the detwister), and so reverse flow as expected in a vortex tube had developed. Overall, this seems to indicate that for low cold fractions (more precisely during T or Transition flow) the axial stagnation point is located somewhere near the inlet region of the vortex tube and as we move the wall closer to the hot end axial stagnation point moves downstream continuously and in the end stabilizes at the valve (and we get VT-flow inside the vortex tube) (Figure 42).

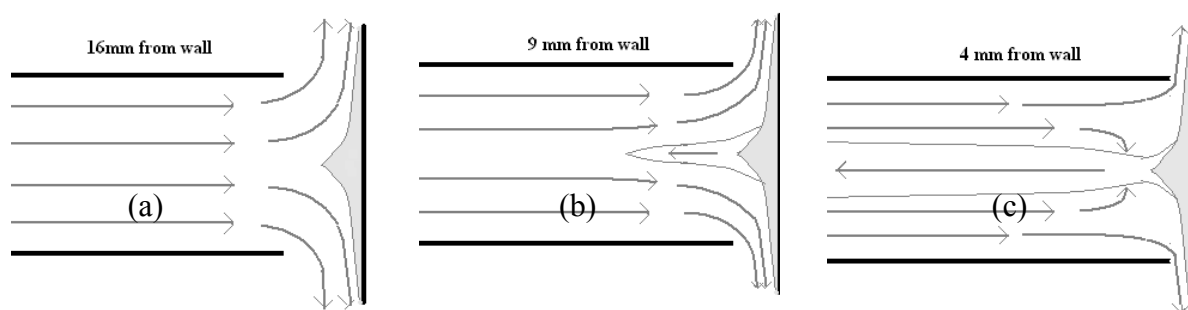


Figure 42: Theorized axial flow structures when the wall is at different positions the tube end.
 [For case (a) and (b), axial stagnation point is located somewhere near the inlet region of the vortex tube.
 For case (c) axial stagnation point is located at the end wall. Figure shows the grey area indicating the stagnant boundary region next to the wall. A reverse flow region begins to grow out of it, and eventually extends to the other end of the tube]

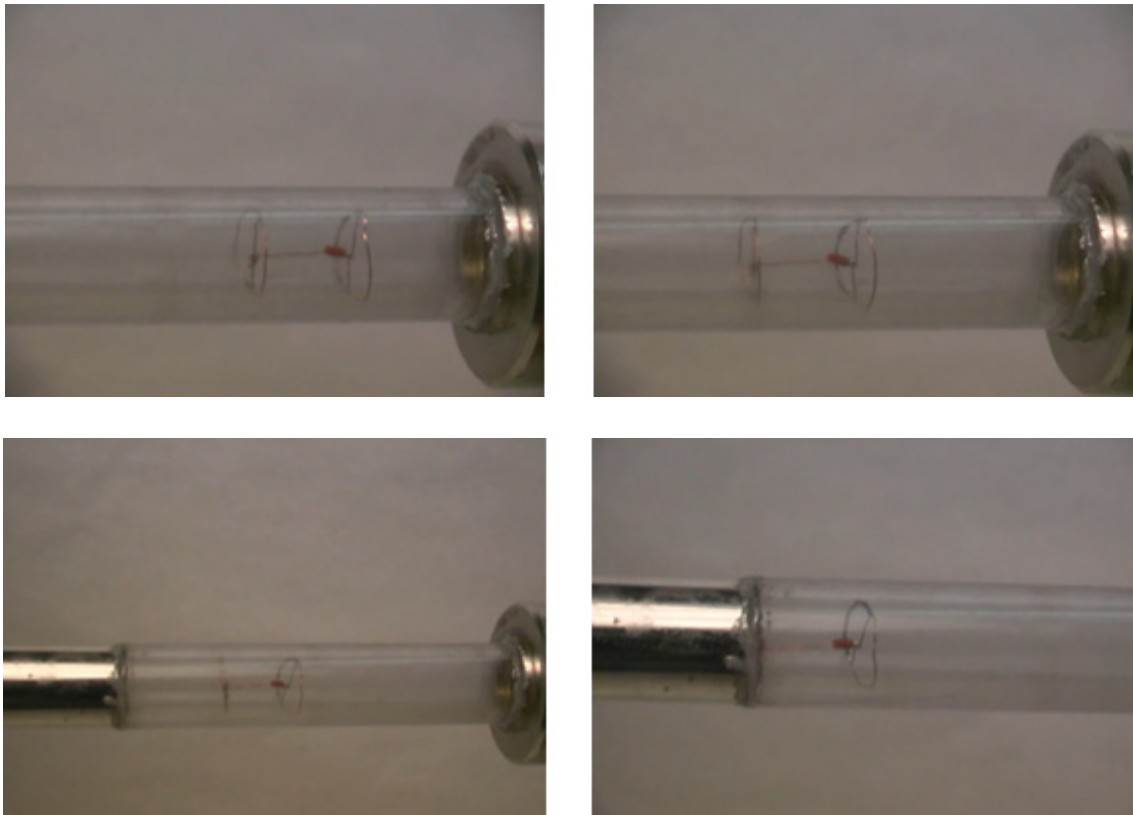


Figure 43: Flow visualization experiment
[Carriage and slider placed at different locations along the length of the vortex tube]

4.6 A theoretical model to predict the location of an axial stagnation point

point

As discussed before (section 4.4), based on our experimental results, we hypothesize that the flow transition from T-flow to VT-flow is accompanied by the relocation of an axial stagnation point. As shown in figure 44, for Reverse, Elbow and T-flow, the axial stagnation point is possibly located near the inlet region of the vortex tube.

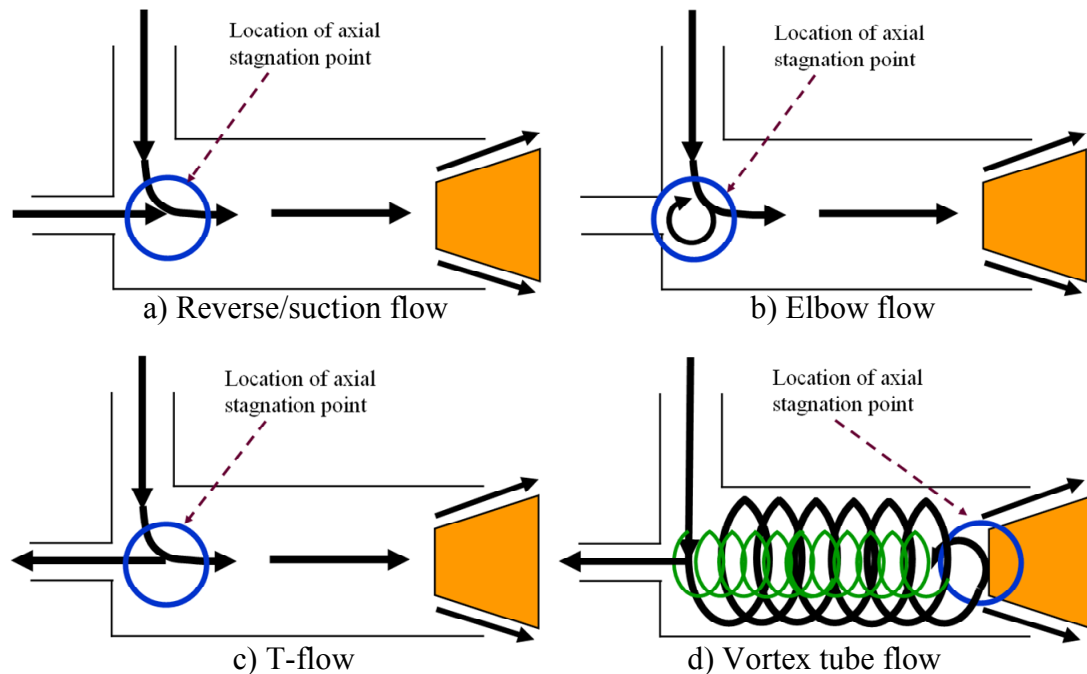


Figure 44: Observed multiple flow structures and the probable axial stagnation point locations.

In the transitional region (a region between T-flow and strong VT-flow), the axial stagnation point is located somewhere in between inlet and the hot end of the vortex tube. But when the flow transition takes place from T-flow to VT-flow completely, the axial stagnation point moves downstream and becomes stable against the surface of the tapered valve or the movable wall. Flow visualization tests conducted in the lab using the slider

and carriage method show that for a vortex tube type of flow, axial stagnation point always occurs at the tapered hot fraction control valve.

To support this argument, we also developed an analytical solution governing several important features of the swirling flow inside vortex tube based on F. Hussain's (1997) work [52]. F. Hussain (1997) developed a new class of analytical solutions of the Navier-Stokes equations and suggested ways to predict and control complex swirling flows. He developed a five-parameter solution family that describes a large variety of flow patterns and models fluid motion in a cylindrical can, whirlpools, tornadoes, and cosmic swirling jets. The resulting composite solutions describe flows, consisting of up to seven separation regions, and model flows in the Ranque-Hilsch tube, in vortex breakdown, and in an industrial vortex burner. His analytical solutions allow a clear understanding of how different control parameters affect the flow and guide selection of optimal parameter values for desired flow features.

We used F. Hussein's generalized vortex sink solution to explain multiple flow structures inside the vortex tube because:

- It has a compact algebraic representation and a clear physical explanation.
- It has a capability to elucidate the intriguing mechanisms in the swirling flows like vortex breakdown and dual valued behavior.

By using stream function and the pressure distribution relations from F. Hussein's work [52], we developed a following relation to obtain the pressure drop across the cold end side. For detailed derivation please see the Appendix 4.

$$(P_0 - P_{atm}) = \left\{ \sqrt{(P_{in} - P_{atm}) - c_1 \cdot z} \cdot \left\{ c_2 L^{\frac{5}{2}} \right\} - c_1 \cdot z \right\} \dots \quad (24)$$

Where, c_1 is integration constant and c_2 is given by,

$$c_2 = \left\{ \frac{128\pi^2 \rho^3 v A_h r_0}{3K_h} \sqrt{\frac{g_c K_c}{cK_r \rho}} \right\}$$

By using $(P_o - P_{atm})$ relation (equation 24), we get following expression for the cold fraction (cf).

$$\text{Cold fraction (cf)} = \left[\frac{K_c}{K_{VT}(P_{in} - P_{atm})} \left\{ \sqrt{(P_{in} - P_{atm}) - c_1 \cdot z} \cdot \{c_2 \cdot z^{5/2}\} - c_1 \cdot z \right\} \right]^{\frac{1}{2}} \dots (25)$$

If we plot the pressure drop expression (24), for different values of z on the top of the experimental results shown in figure 45 we get following results.

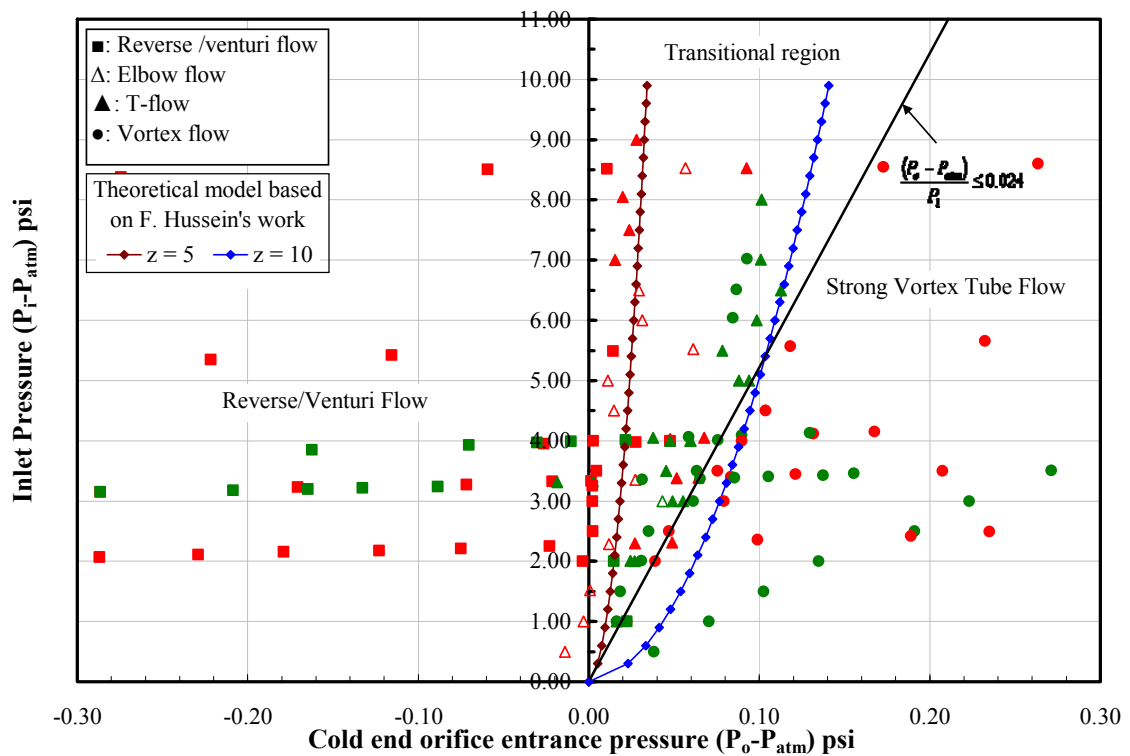


Figure 45: Transition from T to VT-flow and the effect of axial stagnation point location on the pressure drop across the cold end side.
 $[z = \text{the location of the axial stagnation point from inlet in inches, Vortex tube length is 10 inches}].$

- For a constant inlet pressure (P_i), as we move the axial stagnation point downstream (by increasing z in equation 24), we see increase in pressure drop across the cold end side. This means; depending upon the location of an axial stagnation point, cold fraction changes.
- For a fixed axial stagnation point location (constant z), ($P_o - P_{atm}$) and P_i (equation 24) behave qualitatively similar to the experimental data. As shown in figure 45, at higher inlet pressures we require higher and higher ($P_o - P_{atm}$) (or simply P_b) to achieve stronger energy separation inside the vortex tube.

4.7 T to VT-flow transition – A theoretical understanding

Transition from T-flow to VT-flow is a very intriguing phenomenon and needs more experimental and theoretical understanding. We believe that the flow transition from T-flow to VT-flow is accompanied by the relocation of an axial stagnation point. We also believe that the axial pressure distribution inside the vortex tube is responsible for the relocation of the axial stagnation point. Axial and radial pressure gradients inside the vortex tube are controlled by inlet pressure (P_i) and the back pressure (P_b) exerted by the hot fraction control valve.

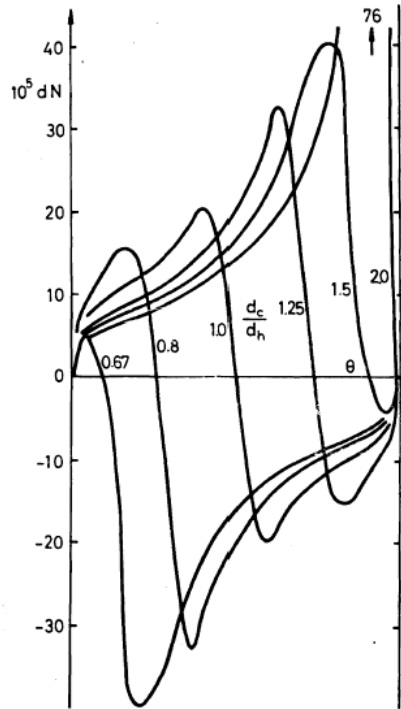
For better understanding of this phenomenon, work published by Linderstrom-Lang [18] during 1960's can be used as the springboard to explain T to VT-flow transition. Similar to our findings, they observed S-flow (in our language T-flow) at low cold fractions and U-flow (VT-flow in our case) at high cold fractions. To support the T to VT-flow transition argument; similar to Linderstrom-Lang, we recommend future researchers to measure the wall pressures, along the periphery of the vortex tube.

4.7.1 T to VT-flow transition and Linderstrom-Lang's work

In 1964, Linderstrom-Lang [18] studied in detail the effect of cold and hot end valve opening conditions (cold/hot fractions) on the gas separation taking place in the vortex tube. They found that the separation effect as a function of cold fraction varies with constructional parameters like:

- The ratio of the diameters of the two orifices (cold and hot end openings) d_h/d_c through which the gas escapes from the tube.
- Cold and hot end opening sizes relative to the tube diameter (d_h/D or d_c/D)

- Tube length (L) and
- Nozzle diameters of the generator (d_n or l and w of nozzles).



[dN = No. of heavy molecules – No. light molecules]

Figure 46: Effect of d_h/d_c on the gas separation effect.
 [d_h = Hot end opening diameter, d_c = cold end opening diameter]

Depending upon the relative magnitudes of aforementioned parameters, Linderstrom-Lang observed U and S-type of flows as shown in figure 47. They used U and S types of flow structures to explain ineffective gas separation inside vortex tube.

As per Linderstrom-Lang, the U-shaped flow pattern (equivalent to VT-flow in our case) of figure 47 (a) existed under conditions which favored a positive separation effect ($dN = N_h - N_c = +ve$) (figure 46) while flow ratios corresponding to conditions favoring negative effects gave an S-shaped flow pattern (T or Transition flow in our case) in agreement with figure 47 (b).

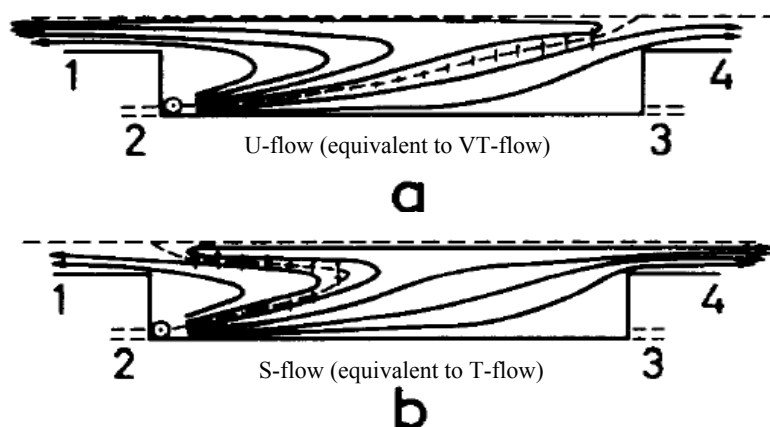


Figure 47: Flow patterns; visualized by Linderstrom-Lang.
 [(a) Hot flow heavier than cold. (b) Cold flow heavier than hot.]

They found that the gas separation takes place along the line or rather surface that separates the two streams which afterwards emerge through the exit ducts. For U-type of flow, a radial diffusion of a net amount of the lighter component takes place inward and the heavier component outward. For S-type of flow, they observed the lighter component outward and heavier component inside.

In conclusion, sign of the gas separation effect depends upon the cold and hot end opening conditions relative to the tube diameter.

Later in 1967, Linderstrom-Lang tried to explain U-flow to S-flow transition based on internal pressure changes due to the changes in cold and hot end valve opening conditions. To do that they measured the peripheral (along the wall of the vortex tube) pressures for different cold fractions (see figure 48). They observed that when one valve is partly closed, a pressure increase in the corresponding exit duct results; this must be felt more strongly at the center than at the periphery of the exit duct. Indeed the flow will be quite easily stopped and reversed near the center before any large change in the flow

fraction has taken place; this will lead to a shift of the stagnation point on the axis towards, and perhaps into, the partly closed exit duct, as indicated in figure 48.

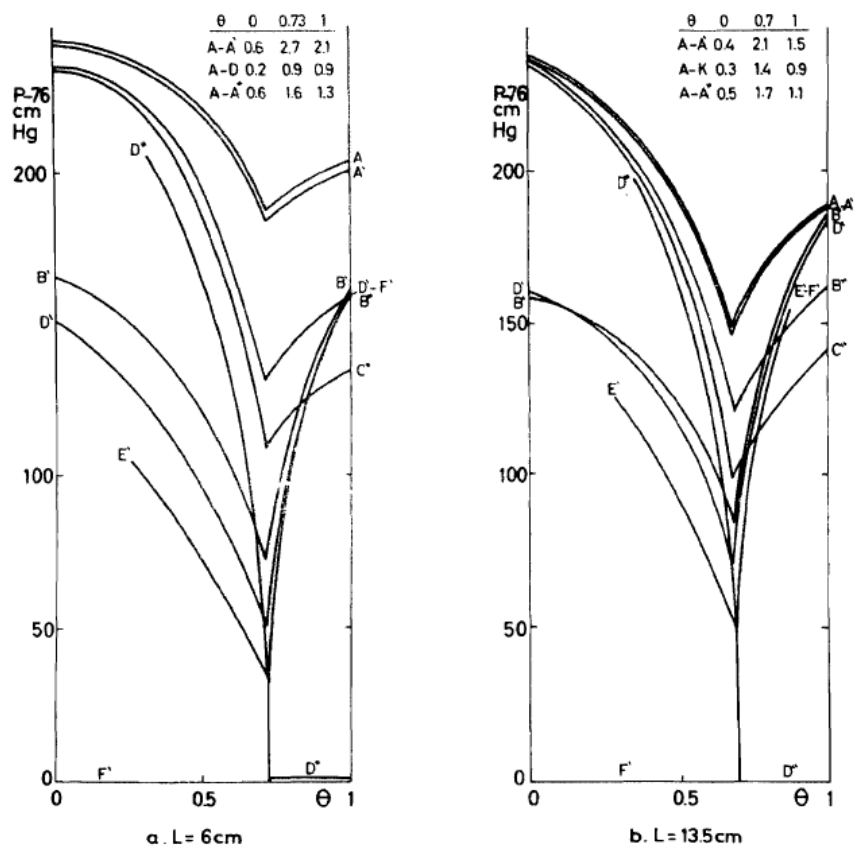


Figure 48: Wall pressures as functions of hot fraction ($\theta = 1 - \text{cold fraction}$)

4.7.2 T to VT-flow transition and the traveling vortex breakdown

As mentioned before, many studies shows (M. A. Herrada 2003 [50], J. J. Keller 1985 [51]) that axial and radial pressure distributions inside the swirl flows in pipes are governed by the phenomenon of “vortex breakdown”. Vortex breakdown can be defined as an abrupt and drastic change of vortex structure, initiated by a variation in the characteristic ratio of tangential to axial velocity components. When the adverse pressure gradient reaches the threshold value at the vortex centerline along the length of the pipe and overpasses the streamwise momentum flux, we get vortex breakdown.

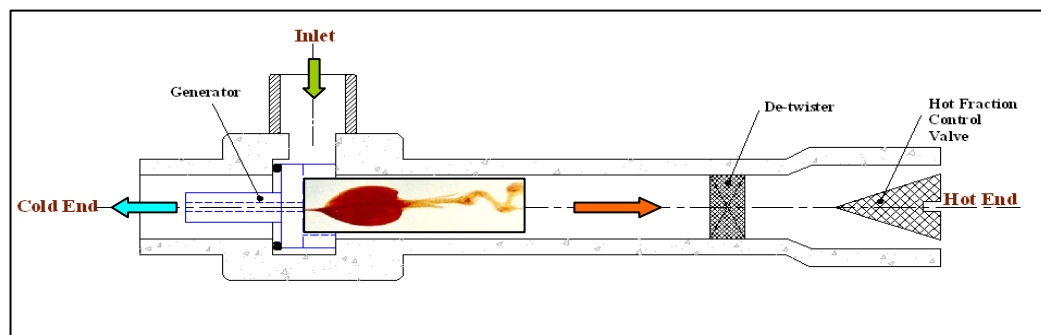


Figure 49: The possibility of vortex breakdown inside vortex tube

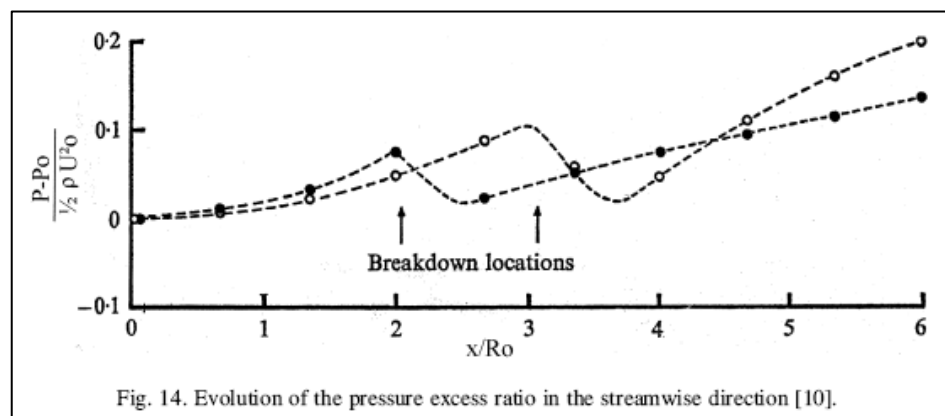


Fig. 14. Evolution of the pressure excess ratio in the streamwise direction [10].

Figure 50: The effect of an axial pressure distribution inside the pipe on the location of vortex breakdown bubble or vice versa, Sarpkaya (1971)

We believe that T-flow to vortex tube flow transition seen inside the vortex tube is linked with the traveling vortex breakdown studied by Sarpkaya in 1971 [53] (figure 50). To understand the phenomenon of vortex breakdown and its existence in compressible swirl flows inside the pipes, we reviewed the studies undertaken on this subject over the past 52 years. Our findings which can be useful to explain T-flow to VT-flow transition are summarized below:

- Vortex breakdown can exist in a swirling air flow,
- Vortex breakdown involves an abrupt transition from uniform state of swirling flow (supercritical) to a turbulent state of swirling flow (subcritical).
- When inlet swirl intensity increases, vortex breakdown moves upstream and when decreased, vortex breakdown moves downstream,
- When the flow was decelerated by constricting the exit hole at the downstream end of the test tube, the breakdown rapidly moved upstream and often reached the center-body in the form of a reversed turbulent core.

Chapter 5 Conclusions and Discussion

5.1 Using vortex tube for utilizing industrial waste pressure energy

- Similar to waste heat, waste pressure can also be characterized as a reclaimable form of energy and there are many opportunities to utilize it in industrial systems.
- Vortex tube technology for recovering waste pressure and heat simultaneously is a relatively new concept that has not been explored completely in the commercial market.
- However our research shows that there are many potential sources of waste pressure energy that could be utilized using vortex tube technology.

5.2 Appropriate non-dimensionalization of energy separation effect

Isentropic compression work seems an appropriate scale to non-dimensionalize the energy separation effect. Energy separation and energy flux separation efficiencies are suitable measuring parameters to recover characteristic properties of the vortex tube.

5.3 Thermal and fluid dynamical time-scales

The time constants required for the temperature and the flow data to achieve a steady state condition, were measured experimentally in the laboratory. It was observed that the thermal time scale for the vortex tube is larger (~22 minutes) than the fluid dynamical timescale (<3 minutes).

5.4 Quantitative observations on multiple flow modes inside vortex tube

- Experimental observations show that in the low inlet pressure regime (<10 psig) and low cold fraction (<10%); vortex tubes behave differently and produce multiple flow structures rather than expected re-circulating cold stream and the columnar hot stream type of flow (or simply “Vortex Tube or VT-flow”).
- It was observed that the back pressure (P_b) exerted by the hot fraction control valve has more dominant effect on the cold fractions as compared to the inlet pressure (P_i). Opening or closing the hot fraction control valve by just a small amount shows more dramatic effect on the flow patterns as compared to the inlet pressure.
- One dimensional model developed based on our experimental results shows that the flow conditions at the cold end side are decided by the cold end orifice entrance pressure (P_o) as follows:
 - If $(P_o - P_{atm}) < 0$, we get Reverse/Venturi type of flow and there is a suction effect at the cold end.
 - If $(P_o - P_{atm}) = 0$, we get Elbow type of flow inside the vortex tube. This is a limiting case of Reverse/Venturi type of flow where we do not get anything out of cold end side.
 - If $(P_o - P_{atm}) > 0$, we get a T or VT type of flow inside the vortex tube depending upon the magnitude of the back pressure (P_b).

- Transition from T-flow to VT-flow is a very intriguing phenomenon and needs more experimental and theoretical understanding.
- Following propositions and the facts can be used as the stepping stones while explaining the transition from T-flow (no energy separation) to VT-flow (energy separation):
 - We believe that the flow transition from T-flow to VT-flow is accompanied by the relocation of an axial stagnation point.
 - We also believe that the axial pressure distribution inside the vortex tube is responsible for the relocation of the axial stagnation point.
 - Axial and radial pressure gradients inside the vortex tube are controlled by inlet pressure (P_i) and the back pressure (P_b) exerted by the hot fraction control valve.
 - Work published by Linderstrom-Lang during 1960's can be used as the springboard to explain T to VT-flow transition. Similar to our findings, they observed S-flow (equivalent to T-flow) at low cold fractions and U-flow (equivalent to VT-flow) at high cold fractions. To support the T to VT-flow transition argument; similar to Linderstrom-Lang, we recommend future researchers to measure the wall pressures, along the periphery of the vortex tube.
 - We believe that T-flow to VT-flow transition seen inside the vortex tube is somehow linked with the traveling vortex breakdown studied by Sarpkaya in 1971 [53].

Chapter 6 Future Work

There are several issues with regard to multiple flow modes observed inside the vortex tube which should be further investigated. Probing deeper, the results in this thesis provide a strong foundation for the future work in intriguing science of energy separation inside vortex tube:

- Transition from T-flow to VT-flow is a very intriguing phenomenon and needs more experimental and theoretical understanding. It would be valuable to use current experimental setup for further data collection and refinement to understand the basic science behind the flow transitions.
- What triggers the flow mode selection and what are the operating conditions to avoid reverse, elbow or T-flow? Is it because of the relocation of an axial stagnation point, or because of the traveling vortex breakdown or both effects combined? Transparent vortex tube and the flow visualization using the carriage and the carrier technique would help us to answer these questions.
- Not only experimentally but understanding T-flow to VT-flow transition theoretically is equally important. F. Hussein's work and similar literature would help us in developing appropriate theory to explain flow mode transitions.
- Numerical simulation of various flow modes inside the vortex tube is necessary. By numerical work, it is possible to simulate the pressure, velocity, temperature, density, fluctuation simultaneously and overcome the difficulties met in the experiments.

Chapter 7 Appendix

7.1 Appendix 1: Catalogue of vortex tube applications

Application	Motivation	Mode	Reference
Spot cooling of machine tools and instrumentation in high temperature environments.	Low capital and maintenance cost, easy to install , very localized cooling needed.	Cold side	Readily available commercially. (Exair Corp., ITW Vortec, Pelmer Inc. etc.)
Cabinet or enclosure cooling: VT coupled with thermostat cools electrical cabinets.	Low capital and maintenance cost, easy to install .	Cold side	Readily available commercially. (Exair Corp., ITW Vortec, Pelmer Inc. etc.)
Diaphragm Valve De-icing.	Provide necessary heating to combat Joule Thomsen cooling of CH ₄	Hot Side	Brown R. (1995). "Free pre-heat, the vortex tube option". Gas Engineering and Management. [21]
Geothermal Reboilers.	Waste pressure from non-condensable exhaust gases.	Both	Our work.
Chiller Economizer.	Vortex tube as an expansion valve, to replace the (irreversible) adiabatic & isenthalpic process by an exothermal process.	Cold Side	Our work.
Deep sea breathing apparatus or in airline respirators.	Provide necessary heating to combat Joule Thomsen cooling of breathable gasses.	Hot Side	North Safety Products, USA.
The vortex tube separator.	For gas dew pointing, gas dehydration and condensate recovery or removal.	Both	I.L.Khodorkov (2003), "The VT: A universal device for heating, cooling, cleaning & drying gases and separating gas mixtures". Chemical & Petroleum Engineering. [22]
A Vortex Contactor for CO₂ separation.	For the separation of carbon dioxide from natural gas and flue gases.	Cold	Kevin Raterman, Brian Stokes etc. (1999) Idaho National Engg. & Environmental Lab, pacific Gas & Electric Company.
Enrichment of Methane.	Enrichment of Methane via separation of gases using vortex tube.	Both	Manohar Kulkarni (2002), Journal of Energy Engineering. [21]
Compressed Air Energy Storage in Hard Rock	Cooling of compressed air during the charging phase, and heating the air during the discharging phase.	Both	Y. Zimmels (2002), "Design criteria for compressed air storage in hard rock" – Energy & Environment, Vol.13, No.6. [89]

Table 6: Catalogue of vortex tube applications.

7.2 Appendix 2: Instrumentation for Vortex Tube Experiments

A block diagram (figure 51) of the experimental setup shows locations of vital instruments used for measuring pressures, temperatures and flow rates.

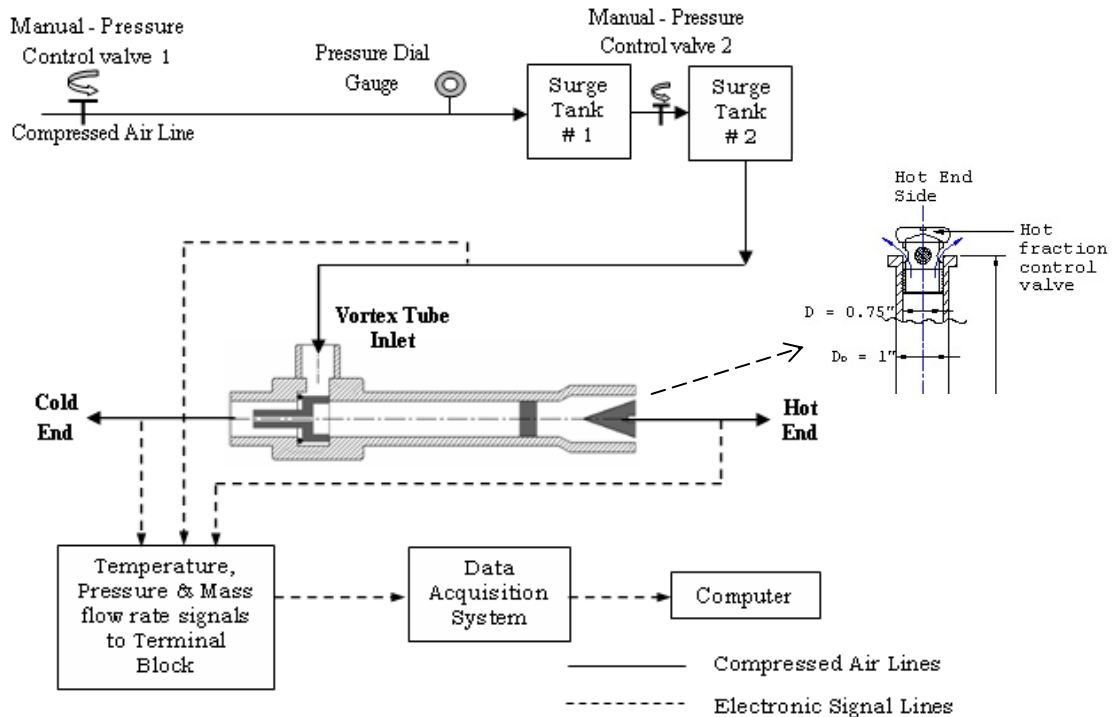


Figure 51: Schematic diagram of the experimental apparatus

Some details about these instruments are given below:

7.2.1 Thermistors

In our experiments we used Omega precision thermistors (Model 44005) with resistance-versus-temperature mode of operation. Figure 52 shows constructional details of these thermistors and their operational circuit. Technical specifications of Omega precision thermistor 44005 are as follows:

- Interchangeability: ± 0.2 °C.
- Maximum operating temperature: 150 °C.

- Time constant, maximum: 1 second in well stirred oil and 10 seconds in still air.

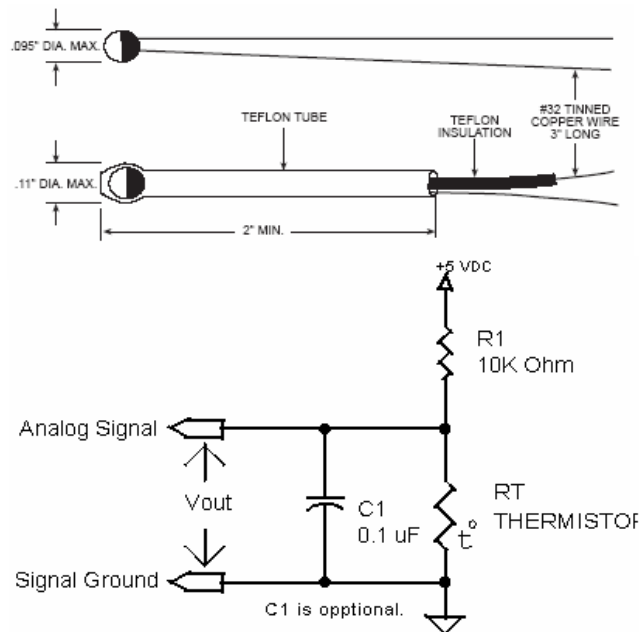


Figure 52: Omega precision thermistor (Model 44005)

7.2.2 Pressure Transducer: (211-B-RF-7/CR/GA-GP-50)

The Model 211 is a bonded strain gauge type transducer with internal signal conditioning to provide a 0-5 Vdc output signal in direct proportion to input pressure.



Figure 53: Pressure transducer (211-B-RF-7/CR/GA – GP-50)

Internal voltage regulation on this unit allows operation on an unregulated power supply from 9-40 Vdc. The units have a single-ended output with a common ground between

input and output, so that multiple units may be easily powered by a common power supply.

Technical features:

- Pressure range: 0-300 psig.
- Accuracy: $0 \pm 5 \text{ Vdc} \pm 2\% \text{ FSO}$.
- Excitation: 9.0 to 40 Vdc.

7.2.3 Precision Turbine Flow-meters with direct signal conditioner

(FTB 936, FTB 933 and FLSC-64)

The precision turbine flow meter is a volumetric flow measuring device. The flowing fluid engages the vaned rotor causing it to rotate at an angular velocity proportional to the flow rate. The angular velocity of the rotor results in the generation of an electrical signal (AC sine wave type). Summation of the pulsing electrical signal relates directly to the flow rate. The OMEGA ® FTB-930 & FTB-940 Series turbine meters have male NPT end fittings for easy connections. They are suitable for use with gases with a minimum density of 0.025 lb/ft³ (air at STP is 0.0752 lb/ft³).



Figure 54: Precision turbine flow meter with signal conditioner

These units come supplied with a mating 2-wire connector and can be supplied with integrally mounted FLSC-60 Series signal conditioners to provide 4-20 mA, 0-5 V, or amplified pulse outputs. These turbine flow meters are intended for clean service only.

Technical features:

FTB 936: 4-60 Max Linear Range (ACFM); 1 End Connections MNPT (in).

FTB 933: 1-10 Max Linear Range (ACFM); 1/2 End Connections MNPT (in).

Common features:

- **Accuracy:** ± 1.0 % of reading
- **Repeatability:** ± 0.25 %
- **Materials of Construction:** Body: 304 stainless steel; Rotor: 17 to 4 pH SS;

Bearings: 440C stainless steel

- **Max. Temp. Range:** -268 to 232°C (-450 to 450°F)
- **Maximum Pressure Drop:** Gas density in lb/ft³ x 4 (psid)

7.2.4 Direct signal conditioner (FLSC-64)

The FLSC-64 amplifies and conditions low-amplitude signals such as those developed by a magnetic pickup coil. The amplitude of the square wave output equals the input supply voltage of the FLSC-64. A sensitivity adjustment permits the FLSC-64 to discriminate between an input signal and noise. The FLSC-64 contains a built-in test oscillator that enables the operator to verify the amplifier's operation without a signal source.



Figure 55: Direct signal conditioner (FLSC-64)

Signal conditioners can be directly mounted on turbine type of flow-meters as shown in figure 55. Frequency of square wave coming out of signal conditioner will be proportional to flow rate of air through turbine flow-meter.

7.2.5 Vortex Tube: (Model # 3499)

EXAIR vortex tubes are available in three sizes. Each size can produce a number of flow rates, as determined by a small internal part called a generator. If flow and temperature requirements are known, the appropriate vortex tube can be chosen according to the specification information or the performance charts available online at www.exair.com

3400 series vortex tubes provide lowest cold air temperatures, but at low cold airflow (when less than a 50% cold fraction is used)



Figure 56: Vortex tube (Model # 3499)

Generally 3400 series vortex tubes are used when temperatures below 0 °F (-18 °C) are desired.

7.2.6 Vortex Tube performance

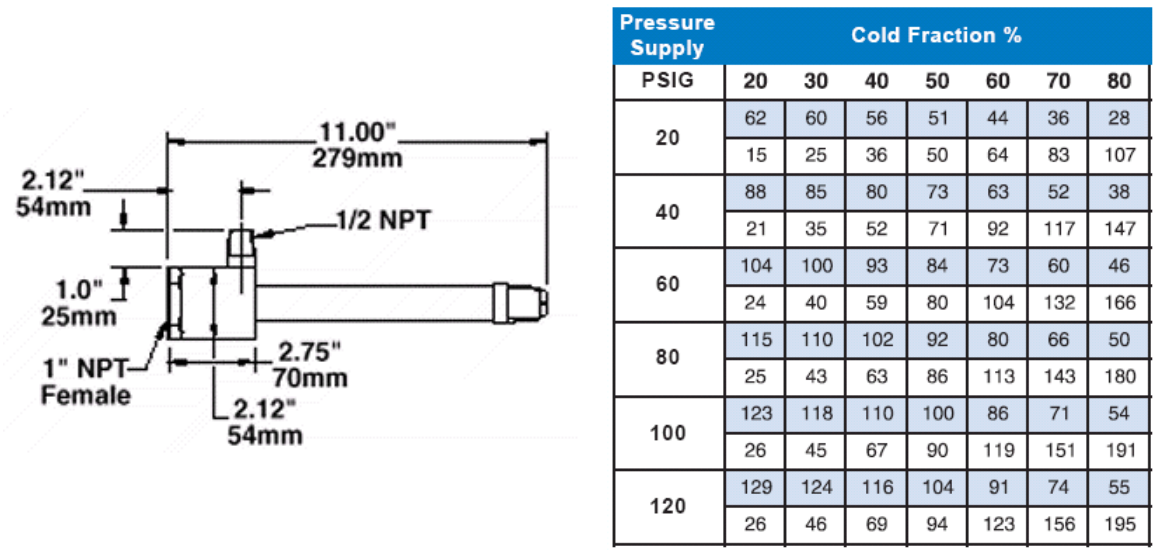


Figure 57: Model # 3499 – dimensions and performance chart.

[Numbers in shaded area give temperature drop of cold air, °F. Numbers in white area give temperature rise of hot air, °F.]

While dealing with Exair vortex tubes, the use of clean and dry air is essential. A vortex tube provides a temperature drop or rise from supply air temperature hence inlet air

temperature is another important parameter. Elevated inlet temperatures will produce a corresponding rise in cold air temperatures.

7.2.7 Data acquisition and signal conditioning

(E Series multifunction DAQ PCI-6024E)

The National Instruments PCI-6024E is a data acquisition board that uses E Series technology to deliver high-performance, reliable data acquisition capabilities in a wide range of applications. You get up to 200,000 samples/sec sampling and 12-bit resolution on 16 single-ended analog inputs. Depending on your type of hard drive, the NI PCI-6024E can stream to disk at rates up to 200 kS/s. They are ideal for applications ranging from continuous high speed data logging to control applications to high voltage signal or sensor measurements when used with NI signal conditioning.



Figure 58: E Series multifunction DAQ PCI-6024E

Technical features:

- 16 analog inputs at up to 200 kS/s, 12 or 16-bit resolution.
- Up to 2 analog outputs at 10 kS/s, 12 or 16-bit resolution.

- 8 digital I/O lines (TTL/CMOS); Two 24-bit counter/timers.
- Input signal range 10 V (Software selectable).
- Digital triggering.
- 4 analog input signal ranges.
- NI-DAQ driver simplifies configuration and measurements.

7.2.8 Lab-view program

The LabVIEW Full Development System for Windows includes all functionality of the Base Package plus additional features. It provides extensive hardware support for platforms such as data acquisition, instrument control, and distributed I/O.

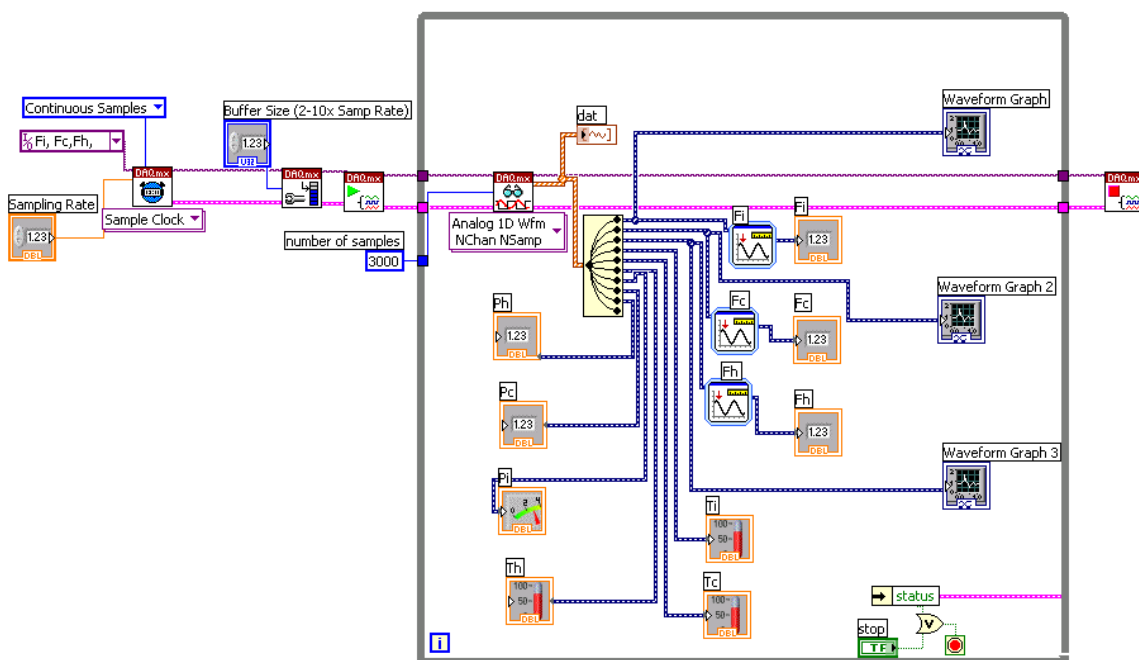
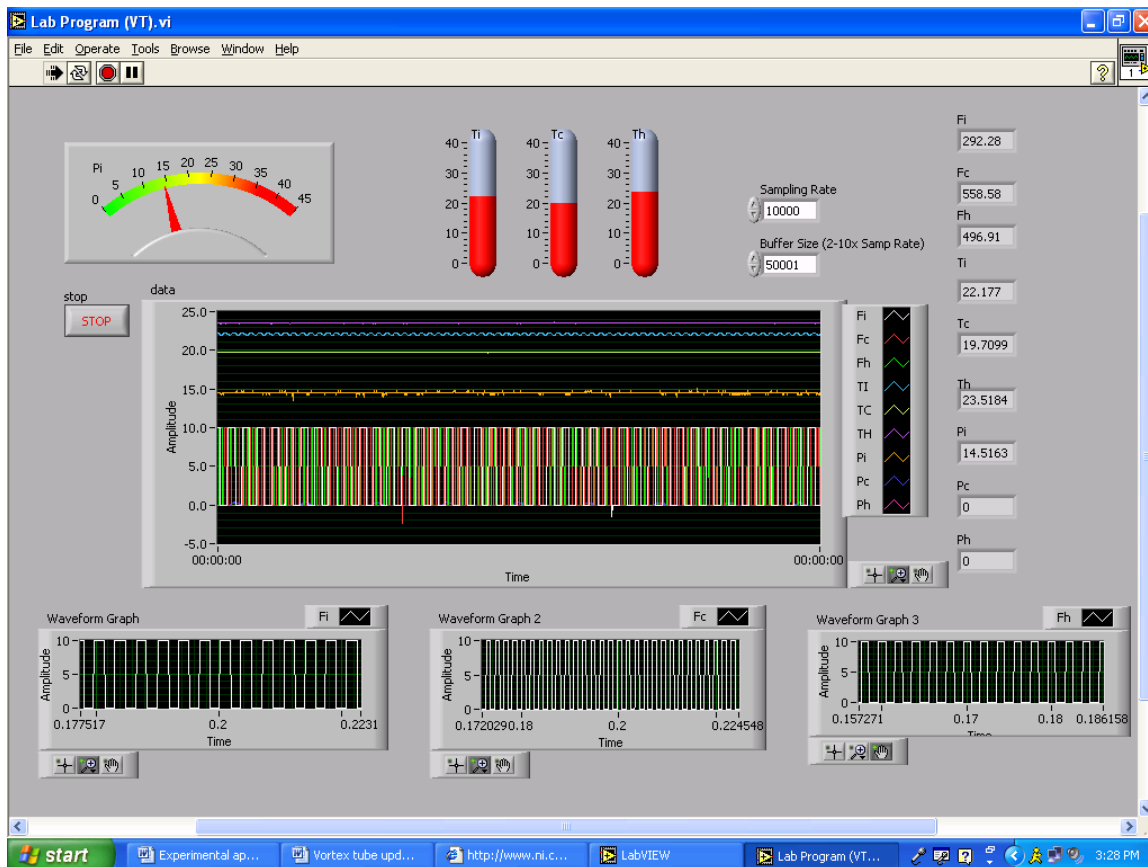


Figure 59: Lab-view program – Front panel and program.

7.3 Appendix 3: Experimental Procedures

7.3.1 Experiment 1 - Thermal and fluid dynamical time scales

Observation: The thermal time constant of the vortex tube apparatus is larger (~22 minutes) than the fluid dynamical time constant (<3 minutes).

Experimental Procedure (Refer to figure 51):

- Turn on all the instruments (thermistors, pressure transducers, and the flow meters) including the lab-view program.
- Hot fraction control valve position: For time scale experiment we do not care about the amount of cold fraction or the intensity of energy separation hence keep the hot fraction control valve open by at least 4 to 5 turns. That way you will get sufficient amount of air from both the ends and the adequate energy separation.
- Start the data acquisition system and keep running it for at least 30 minutes at inlet pressure equal to zero. After some time you will not see any changes in the cold and hot end side temperatures.
- After 30 minutes, suddenly change the inlet pressure to 6 psig from 0 psig by using the needle valve. Again keep the data loggers running for at least 30 minutes.
- During both the experiments you are going to measure inlet, cold and hot end temperatures, flow rates and pressures.
- Calculate thermal and fluid dynamical time constants as shown in section 3.2 of chapter 3.

Total time required for the experiment: 70 minutes.

7.3.2 Experiment 2 - Flow meter calibrations

Observation: Factory calibration numbers were inaccurate. Inlet, cold and hot end flow meters re-calibrated in the laboratory.

Experimental Procedure (Refer to figure 51):

During all of the experiments mentioned in this report, precision turbine flow meters were used to measure the mass flow rates. Inside the turbine flow meters, the flowing fluid engages the vaned rotor causing it to rotate at an angular velocity proportional to the flow rate. The angular velocity of the rotor results in the generation of an electrical signal (AC sine wave type). Summation of the pulsing electrical signal relates directly to the flow rate. Both the turbine flow meter models (1-10 and 4-60 scfm) were factory calibrated. As the thermal and fluid dynamical properties of the vortex tube are sensitive to the flow rate data (S. Nimbalkar, [3], [54]), we decided to re-calibrate these flow meters in the lab.

Calibration method used in the lab is very straightforward.

- To calibrate hot end side flow meter, cold end side was closed by using a metal cap and all the flow was directed towards the hot end side. (10 minutes)
- To calibrate cold end side flow meter, hot end side was closed and all the flow was directed towards the cold end side. (10 minutes)
- If cold end side is closed, hot end mass flow rate must match with the inlet mass flow rate ($m_h = m_i$). Similarly, when we close hot end side, cold mass flow rate must match the inlet mass flow rate ($m_c = m_i$).

Figure 60 is showing the frequency raw data taken from hot end and inlet turbine flow meters. Periodic fluctuations in the data are due to the line pressure variations. In the next

figure (figure 61) scaled mass flow rates are shown. Flow data is converted into mass flow rate data by using following parametric relations:

$$\dot{m}_i = 0.000410903 \times \frac{P_i}{T_i} \times f_i$$

$$\dot{m}_h = 0.00046747 \times \frac{P_h}{T_h} \times f_h$$

Similar kinds of experiments were conducted to calibrate the hot end side flow meter. Following relations were obtained to convert frequency data into the mass flow rate data by using the calibration data:

$$\dot{m}_i = 0.000410903 \times \frac{P_i}{T_i} \times f_i$$

$$\dot{m}_c = 0.000414325 \times \frac{P_h}{T_h} \times f_h$$

Total time required for the experiment: 30 minutes

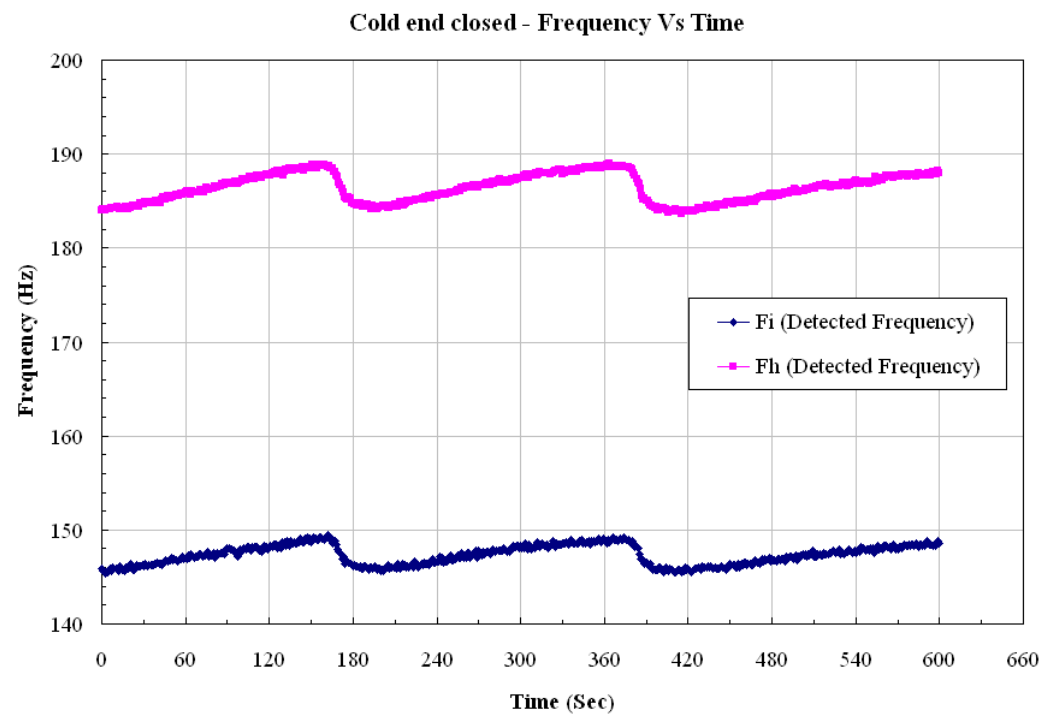


Figure 60: Flow meter raw frequency data

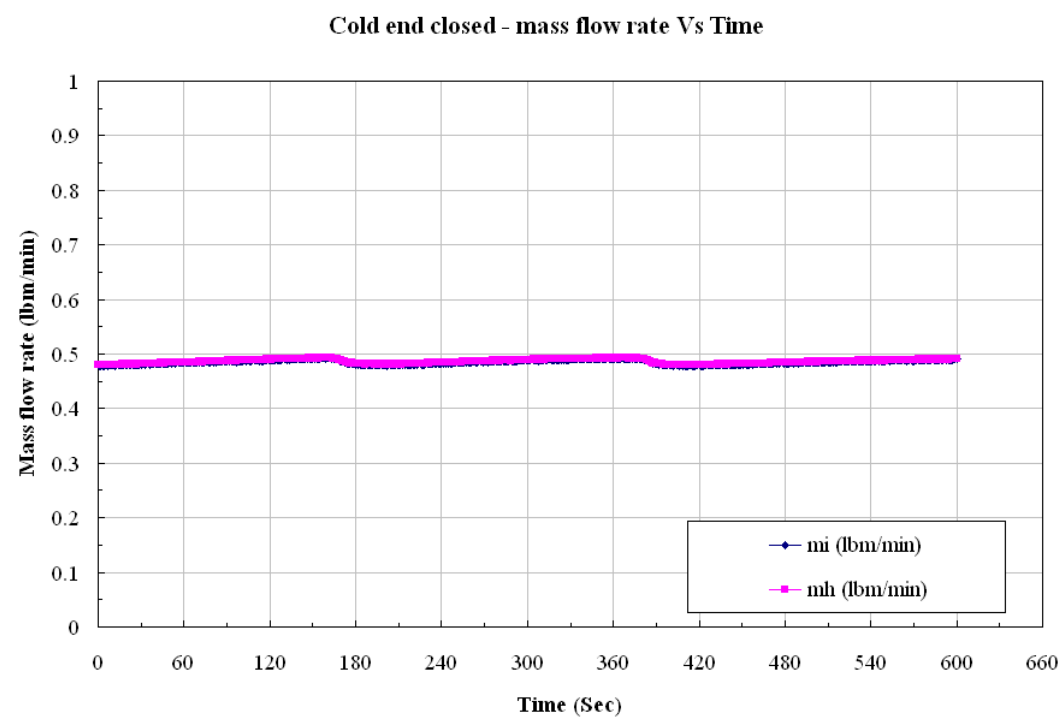


Figure 61: Calibrated mass flow rate data

7.3.3 Experiment 3 - The frictional coefficient (k value) of the hot fraction control valve

Based on the literature review and our past experimental results (S. Nimbalkar, 2005 [3]), we argue that there are mainly two critical independent parameters govern the energy separation characteristics of the vortex tube with a fixed geometry:

1. Inlet pressure (P_i),
2. 'k' value (frictional coefficient) of the tapered hot fraction control valve.

Inlet pressure can be easily measured and controlled but the problem is with the 'k' value of the tapered valve. Not a single researchers or a manufacturer ever published frictional coefficients for the tapered valve for various opening positions. Tapered valve controls the hot fraction coming out of the hot end side. If we close the valve, for the same inlet pressure, hot end mass flow rate drops. And if we open it, hot end mass flow rate increases.

To calculate frictional coefficient (k) of the tapered valve, it is necessary to measure pressure drop (ΔP) across the valve and the hot end mass flow rate (m_h). Then 'k' value of the valve can be calculated by using the following equation:

$$k = \frac{\Delta P}{(\dot{m}_h)^2}$$

Where,

$\Delta P = P_v - P_h$, P_v = Pressure before the valve and P_h is the pressure after the valve, psi

m_h = hot end mass flow rate, lbm/min. As shown in figure 62, tests were conducted for 4, 4.5, 5, 6, 7 and 8 turns open of the tapered valve. For different opening positions,

pressures before and after the valve were measured. Hot end mass flow rate was measured by using the turbine type of flow meter.

After calculating 'k' values for the aforementioned opening positions, 'k' values for other opening positions (like 2, 2.5, 3 and 8.5) were extra or interpolated (see figure 63).

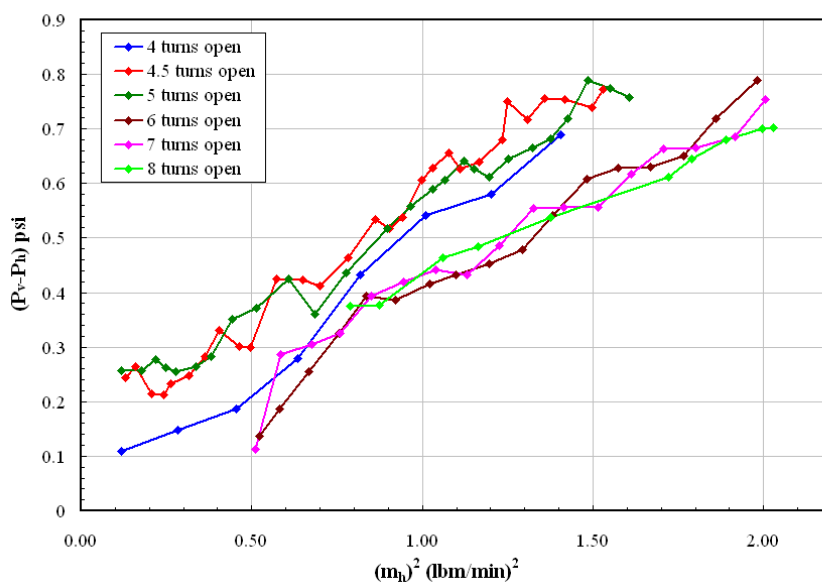


Figure 62: Pressure drops and mass flow rates across the tapered valve for different opening positions

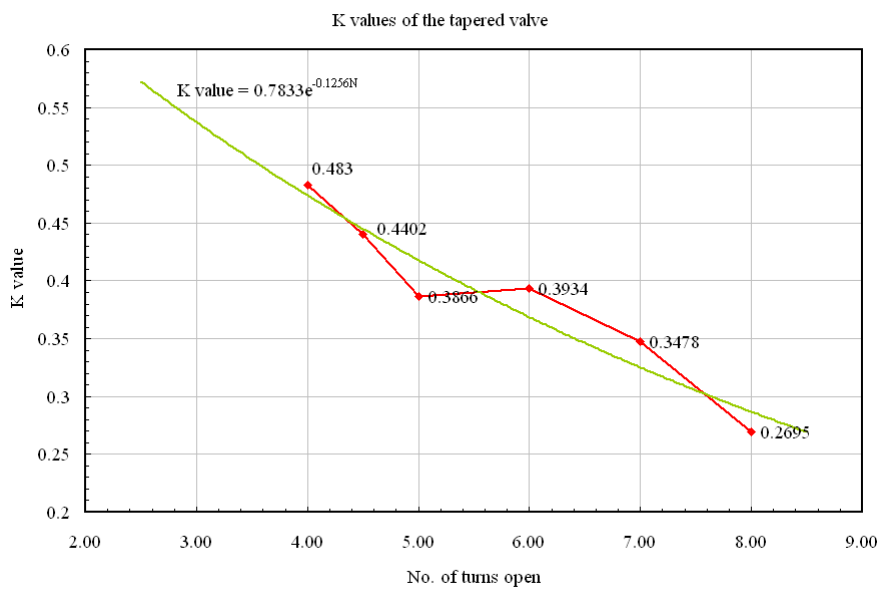


Figure 63: Frictional coefficients (k) of the tapered valve for different opening positions

Exponential fit to the experimental data gives us parametric relationship between the numbers of turn open of the hot fraction control valve to the frictional coefficient of the valve.

$$k = 0.7833e^{-0.1256N}$$

Although the aforementioned relation is specifically applicable to the vortex tube model used in the lab, the procedure to obtain such kind of relation for any other setup will remain the same.

Total time required for the experiment: 7 hours

7.3.4 Experiment 4 - Quantitative observations on multiple flow structures

Observation: Required critical back pressures (P_b) to achieve flow transitions from Reverse, Elbow and T-type flow structures to the VT type of flow structure for different inlet pressures.

Experimental setup:

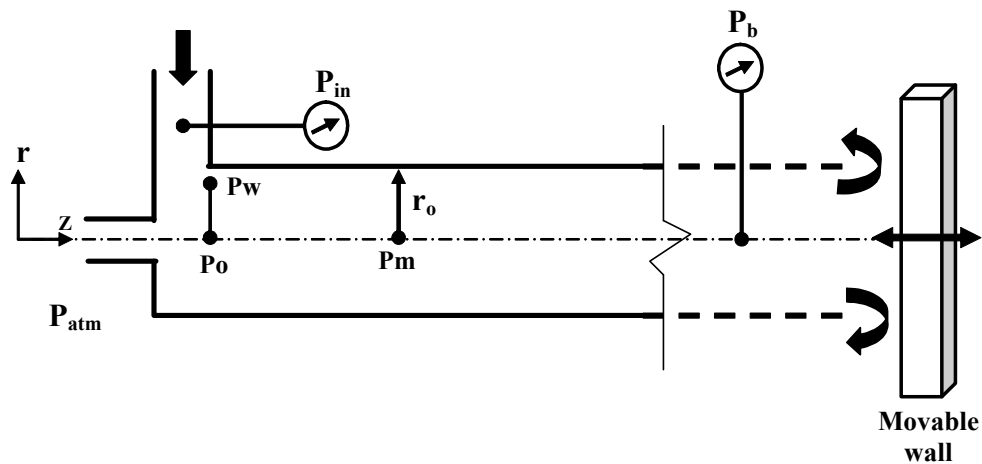


Figure 64: Quantitative observations on multiple flow structures inside vortex tube

Experimental Procedure:

As shown in figure 64, for various constant inlet pressures ($P_i = 3, 5, 6, 7$ and 8 psig), the back pressure (P_b) was changed by moving the wall closer or away from the hot end. Flow transitions from Reverse to Elbow, Elbow to T and from T to VT-flow were observed respectively.

Experimental steps:

- Turn on all the instruments (thermistors, pressure transducers, and the flow meters) including the lab-view program.
- Initially keep the movable wall far away from the hot end.

- Adjust inlet pressure to certain constant value ($P_i = 3, 5, 6, 7$ and 8 psig) using the needle valve.
- Start recording the pressure, temperature and the flow data using the lab-view data logger program.
- Slowly start bringing the movable wall closer and closer to the hot end. At each given wall location wait for at least 3 minutes to achieve fluid dynamical steady state. Back pressure (P_b) exerted by the wall will start increasing. Initially you will observe the suction effect at the cold end side because of the less back pressure (P_b).
- At certain position of the movable wall you will observe elbow type of flow inside vortex tube. For elbow type of flow, air will not drain out or in from the cold end side.
- If you will keep moving the wall closer and closer to the hot end, at certain back pressure value you will observe T type of flow. During the T-flow, air drains out from both the ends but without any energy separation. You will observe that the cold and hot end temperatures almost equal to inlet temperature.
- At critical back pressure, you will observe the transition from T-flow to VT-flow. As shown in figure 45, there is a transitional region in between Elbow and VT-type of flow where you observe either T-flow or weak VT-flow.
- If you will keep moving the wall closer and closer, you will observe the increase in cold fraction numbers and you will get stronger and stronger energy separation.

Total time required for the experiments: 5 – 6 hours

7.3.5 Experiment 5 – Hysteresis behavior of the vortex tube

Observation:

Hysteresis (dual valued) of the vortex tube behavior observed in the past (during M.S. research) is due to the unsteadiness of the temperatures or not reaching the thermal steady state and not because of the flow structure changes inside the vortex tube.

Experimental Procedure:

Approach 1: Constant inlet pressure and movable wall.

- Turn on all the instruments (thermistors, pressure transducers, and the flow meters) including the lab-view program.
- Initially keep the movable wall far away from the hot end.
- Adjust inlet pressure to certain constant value ($P_i = 2, 3, 4, 6$ and 7 psig) using the needle valve.
- Start recording the pressure, temperature and the flow data using the lab-view data logger program.
- Slowly start bringing the movable wall closer and closer to the hot end in steps. Wait at least for 3 minutes between each step. In this study we don't care about the thermal steady state as we are going to plot raw flow data to check hysteresis behavior.
- After bringing the wall to the closest position from the hot end, start moving it away from the hot end in small steps as mentioned above.
- Plot the temperature and flow data separately.

Total required time for the experiment: 60 minutes.

Approach 2: Varying inlet pressure and constant wall position.

- Turn on all the instruments (thermistors, pressure transducers, and the flow meters) including the lab-view program.
- Keep the movable wall at a fixed location from the hot end in such a way that you will get energy separation at any particular inlet pressure.
- Start the experiment with inlet pressure equal to 3 psig and start recording the pressure, temperature and the flow data using the lab-view data logger program.
- Vary the inlet pressure from 3 psig to 10 psig using the needle valve in small steps and wait for at least 3 minutes between each step.
- Again in this study we don't care about the thermal steady state as we are going to plot raw flow data to check hysteretic behavior.
- Now start lowering the inlet pressure from 10 psig to 3 psig in small steps.
- Plot the temperature and flow data separately.

Total required time for the experiment: 60 minutes.

7.4 Appendix 4: Multiple flow structures – A theoretical model

7.4.1 Multiple flow structures - A theoretical model

The goal of this chapter is to develop analytical solutions governing several important features of the swirling flow inside vortex tube based on F. Hussein's work [52].

F. Hussein (1997) developed a new class of analytical solutions of the Navier-Stokes equations and suggested ways to predict and control complex swirling flows. He developed a five-parameter solution family that describes a large variety of flow patterns and models fluid motion in a cylindrical can, whirlpools, tornadoes, and cosmic swirling jets. The resulting composite solutions describe flows, consisting of up to seven separation regions, and model flows in the Ranque-Hilsch tube, in vortex breakdown, and in an industrial vortex burner. His analytical solutions allow a clear understanding of how different control parameters affect the flow and guide selection of optimal parameter values for desired flow features.

There are a few characteristics (governed by conservation laws) whose values are crucial for explaining flow patterns inside vortex tube, including the entrainment rate along the radial direction (or radial Reynolds number Re) and the angular momentum (the swirl Reynolds number Γ). Using just these characteristics – Re and Γ , for the radial and swirl velocity – we find that only three more parameters are required to specify the axial velocity (and the cold fraction) in an axisymmetric flow inside the vortex tube. These parameters characterize contributions to the velocity profile from an outer free stream, due to:

- An outer free stream or uniform flow along the periphery,

- An axial pressure gradient, and
- Radial convergence or advection of the flow.

7.4.2 A generalized vortex sink solution

We are using F. Hussein's generalized vortex sink solution to explain multiple flow structures inside the vortex tube because:

1. It has a compact algebraic representation and a clear physical explanation.
2. It will also help us to elucidate the intriguing mechanisms in the swirling flows like vortex breakdown and dual valued behavior.

7.4.3 Introduction to the generalized vortex sink solution

The generalized vortex sink is singular on the entire z axis (see equations 26a, b & c), thus necessitating an inner solution encompassing the entire axis. Therefore, to match the vortex sink, one has to construct a solution describing a weakly swirling jet flowing from its origin in both the positive and negative z directions; this is the bipolar jet.

Applying the work of F. Hussein (1997) to the velocity field inside the vortex tube leads to the following results:

$$v_r = \text{Re} \frac{V}{r} \dots \text{(Radial velocity) } \dots \text{ (26a)}$$

$$v_\phi = \Gamma \frac{V}{r} \dots \text{(Circumferential velocity) (26b)}$$

$$v_z = \left[W_c + W_p \left(\frac{r}{r_0} \right)^2 + W_r \left(\frac{r}{r_0} \right)^{\text{Re}} \right] \frac{V}{r_0} \dots \text{(Axial velocity) } \dots \text{ (26c)}$$

Equation 26 (a, b, and c) is the generalized vortex sink solution, which satisfies the Navier-Stokes equations and includes five dimensionless parameters: Re , Γ , W_c , W_r , and W_p .

Re = Radial Reynolds number,

Γ = Swirl Reynolds number,

W_c = is a free parameter characterizing the uniform part of the axial flow.

W_p = characterize the non-uniform shear of the axial velocity induced by the axial pressure gradient,

W_r = characterize the non-uniform shear of the axial velocity induced by the radial advection.

The axial part includes a parabolic part [the first two terms in (26c)], which is similar to pipe flow and is independent of the vortex-sink component. The last term in (26c) depends on the radial flow rate Re and is interpreted below as the entrainment effect of a near axis jet.

To visualize flow patterns for comparison with experiments, it is convenient to use the Stokes stream function Ψ . According to F. Hussein (1997) [52], the dimensionless stream function,

$\psi = \frac{\Psi}{r_0 Re}$, has the form:

$$\psi = a \left(\frac{r}{r_0} \right)^2 + b \left(\frac{r}{r_0} \right)^{Re+2} + c \left(\frac{r}{r_0} \right)^4 - \frac{z}{r_0} \dots (27)$$

Where,

$$a = \frac{W_c}{2Re} \dots \left\{ \begin{array}{l} W_c \text{ is a free parameter characterizing the uniform part of the axial flow.} \\ Re = \text{Radial Reynold's number and indicated radial advection.} \end{array} \right\}$$

$$b = \frac{W_r}{\text{Re}(\text{Re} + 2)} \dots \left\{ \begin{array}{l} W_r \text{ characterizes the non - uniform shear of the axial velocity} \\ \text{induced by the radial advection.} \end{array} \right\}$$

$$c = \frac{W_p}{4\text{Re}} \dots \left\{ \begin{array}{l} W_p \text{ characterizes the non - uniform shear of the axial velocity} \\ \text{induced by the axial pressure gradient.} \end{array} \right\}$$

Finally, the pressure p for this solution family has the distribution:

$$p = p_\infty - \frac{1}{2} \rho \left(\frac{v}{r} \right)^2 (\text{Re}^2 + \Gamma^2) + \rho \left(\frac{v}{r_0} \right)^2 P \frac{z}{r_0} \dots \quad (28)$$

Where,

$$P = \frac{r_0^3}{\rho v^2} \frac{\partial p}{\partial z}$$

According to (28), the pressure decreases as $r \rightarrow 0$. Since, as shown below, $\Gamma^2 \gg \text{Re}^2$ typically in practical applications, the pressure drop near the axis is mainly an effect of swirl. The pressure can also decrease or increase in the axial direction, depending on the sign of P .

7.4.4 Need for an inner solution

Since the velocity is singular at $r = 0$, solution (26) is not useful near the axis for practical flows. However, the vortex sink can serve as an outer solution, to be matched with an inner solution valid near the axis (i.e. near $r=0$). That means, the inner solution must rapidly decay as r increases to match the outer solution. Therefore, v_z has its maximal value near the axis, with jet like flow in the inner (“core”) region. The core radius is typically small in comparison with that of the outer region, where (26) is valid. For this reason, one can apply the boundary layer approximation for the near-axis jet. The inner solutions can be swirl-free, weakly or strongly swirling jets, but for vortex tube we are

going to consider weakly swirling bipolar jet. Bipolar jet means a jet flowing from its origin in both the positive and negative z directions.

$$\psi = a \left(\frac{r}{r_0} \right)^2 - \frac{Br^2}{(zr_0) \left[1 + B \left(\frac{r}{z} \right)^2 \right]} + c \left(\frac{r}{r_0} \right)^4 \dots (29)$$

Where,

$$B = \frac{3J}{64\pi\rho\nu^2} \dots \left\{ \begin{array}{l} B \text{ characterizes the axial momentum flux } J \text{ through a plane normal to} \\ \text{the jet axis, mostly governed by the adverse pressure gradient} \end{array} \right\}$$

Above solution remains singular at the origin, $z = r = 0$. To avoid this singularity, one needs to match (29) and a stagnation flow near $z = r = 0$.

By differentiating the relation for stream function with respect to z and r , we can find out the radial and axial velocities respectively.

$$\begin{aligned} V_r &= -\frac{1}{r} \frac{d\psi}{dz} \\ V_z &= \frac{1}{r} \frac{d\psi}{dr} \end{aligned} \dots (30)$$

Where, $\Psi = (vr_0 \text{ Re})\psi$

As we know, for an axial stagnation point on the axis of the vortex tube ($r = 0$), both axial and radial velocities are going to be zero. Hence, the condition for the location of an axial stagnation point is:

$$V_z|_{r=0} = V_r|_{r=0} = 0 \dots (31)$$

If we solve equations (29), (30) and (31) we get two solutions:

$$\begin{aligned} \frac{z}{r_0} &= 0 \\ \frac{z}{r_0} &= -\frac{B}{a} = -\frac{3J}{32\pi\rho\nu^2} \cdot \frac{\text{Re}}{W_c} \dots (32) \end{aligned}$$

Where,

J = The axial momentum flux through a plane normal to the jet axis,

Re = Radial Reynolds numbers which defines radial advection (+ve if source, -ve if sink)

W_c = A free parameter characterizing the uniform part of the axial flow,

ρ = Density of the fluid under consideration,

ν = Kinematic viscosity of the fluid under consideration.

J, the axial momentum flux can be obtained as follows:

$$\begin{aligned}
 J &= \frac{\text{Initial axial momentum} - \text{Final axial momentum}}{\text{Length of the vortex tube}} \\
 &= \frac{\left[\dot{m}_i V_{zi} - \dot{m}_h V_{zh} \right]}{L} = \frac{\left[0 - \dot{m}_h V_{zh} \right]}{L} = -\frac{\dot{m}_h}{L} \cdot \frac{\dot{m}_h}{\rho A_h} \quad \dots (33) \\
 J &= \frac{K_h (P_b - P_{atm})}{L \rho A_h}
 \end{aligned}$$

Where,

P_b = Back pressure controlled by tapered valve or the wall,

K_h = Frictional coefficient of the tapered valve.

Re, Radial advection or entrainment rate can be given as,

$$\begin{aligned}
 \text{Re} &= \text{Radial Reynolds number,} \\
 &= \frac{\text{Average radial velocity (from } z = 0 \text{ to } z = L) \cdot \text{radius}}{\text{Kinematic viscosity}} \\
 &= \frac{\left[\frac{V_r|_{z=0} + V_r|_{z=L}}{2} \right] r_0}{\nu} \quad \dots (34) \\
 &= \frac{V_r|_{z=0} r_0}{2\nu} = \frac{\dot{m}_r|_{z=0}}{4\pi\rho r_0 L} \\
 \text{Re} &= \frac{\sqrt{K_r (P_w - P_0)}}{4\pi\rho r_0 L}
 \end{aligned}$$

Where,

K_r = Frictional coefficient corresponding to the radial flow,

P_w = Absolute pressure near the vortex tube wall,

P_0 = Absolute pressure at the entrance of cold end orifice.

W_c characterizes the uniform part of the axial flow, $V_z = \left[W_c + W_p \left(\frac{r}{r_0} \right)^2 + W_r \left(\frac{r}{r_0} \right)^{\text{Re}} \right] \frac{v}{r_0}$

As it's just the uniform part of the axial flow, we can apply Bernoulli's equation to get it,

$$W_c = \frac{r_0}{v} \sqrt{\frac{2g_c}{\rho} K_c (P_{in} - P_b)} \dots (35)$$

Where, K_c = Frictional coefficient of the cold end orifice.

After simplifying equation (32), by using equations (33), (34) and (35), we get,

$$(P_0 - P_{atm}) = \sqrt{\frac{(P_{in} - P_b)}{(P_b - P_0)}} \cdot \left\{ \frac{128\pi^2 \rho^3 L^3 v A_h r_0}{3K_h} \sqrt{\frac{g_c K_c}{K_r \rho}} \right\} - (P_b - P_0) \dots (36)$$

To simplify equation (36), we need to use a relation for an absolute pressure inside the vortex tube given by F. Hussein (1997).

$$P = P_{atm} - \frac{1}{2} \left(\frac{v}{r} \right)^2 (\text{Re}^2 + \Gamma^2) + \rho \left(\frac{v}{r_0} \right)^2 \frac{P_z z}{r_0}$$

... (37)

where,

$$P_z = \frac{\partial P}{\partial z} \cdot \frac{r_0^3}{\rho v^2}$$

After putting P_z in the equation (37) and simplifying, we get,

$$P - P_{atm} + \frac{1}{2} \left(\frac{v}{r} \right)^2 (\text{Re}^2 + \Gamma^2) = c \cdot L \dots (38)$$

where, c = constant

Case 1: If $z = r = 0$, $P = P_0$.

$$P_0 - P_{atm} = \lim_{r \rightarrow 0} \left\{ \frac{1}{2} \left(\frac{v}{r} \right)^2 (\text{Re}^2 + \Gamma^2) \right\}$$

Case 2: If $r = 0$ and $z = L$, $P = P_b$.

$$P_b - P_{atm} = c \cdot L + \lim_{r \rightarrow 0} \left\{ -\frac{1}{2} \left(\frac{v}{r} \right)^2 (\text{Re}^2 + \Gamma^2) \right\}$$

Hence,

$$P_b - P_0 = c \cdot L \dots (39) \text{ and}$$

$$P_b = P_{atm} + c \cdot L + \lim_{r \rightarrow 0} \left\{ -\frac{1}{2} \left(\frac{v}{r} \right)^2 (\text{Re}^2 + \Gamma^2) \right\} \dots (40)$$

After simplifying equation (36) with equation (39) and (40), we get,

$$(P_0 - P_{atm}) = \left\{ \sqrt{(P_{in} - P_{atm}) - c \cdot L + \lim_{r \rightarrow 0} \left\{ -\frac{1}{2} \left(\frac{v}{r} \right)^2 (\text{Re}^2 + \Gamma^2) \right\}} \cdot \left\{ \frac{128\pi^2 \rho^3 L^{5/2} v A_h r_0}{3K_h} \sqrt{\frac{g_c K_c}{cK_r \rho}} \right\} - c \cdot L \right\} \dots (41)$$

For low inlet pressures, we can neglect radial advection and swirl intensity term from equation (41).

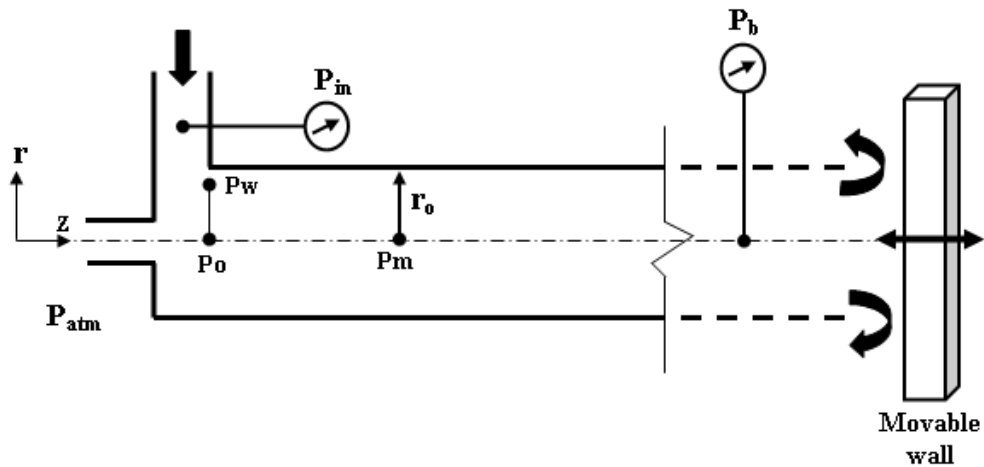


Figure 65: The effect of axial stagnation point location on the pressure drop across the cold end side

$$(P_0 - P_{atm}) = \left\{ \sqrt{(P_{in} - P_{atm}) - c \cdot L} \cdot \left\{ \frac{128\pi^2 \rho^3 L^{5/2} v A_h r_0}{3K_h} \sqrt{\frac{g_c K_c}{cK_r \rho}} \right\} - c \cdot L \right\} \dots (42)$$

Or in simplified form,

$$(P_0 - P_{atm}) = \left\{ \sqrt{(P_{in} - P_{atm}) - c_1 \cdot L} \cdot \left\{ c_2 L^{\frac{5}{2}} \right\} - c_1 \cdot L \right\} \dots \text{(43), where,}$$

$$c_1 = c \text{ and}$$

$$c_2 = \left\{ \frac{128\pi^2 \rho^3 v A_h r_0}{3K_h} \sqrt{\frac{g_c K_c}{cK_r \rho}} \right\}$$

As $(P_0 - P_{atm})$ is a pressure drop across the cold end side, by using equation (42), we can easily find out an expression for the cold fraction.

$$\text{Cold fraction (cf)} = \left[\frac{K_c}{K_{VT}(P_{in} - P_{atm})} \left\{ \sqrt{(P_{in} - P_{atm}) - c \cdot L} \cdot \left\{ \frac{128\pi^2 \rho^3 L^{5/2} v A_h r_0}{3K_h} \sqrt{\frac{g_c K_c}{cK_r \rho}} \right\} - c \cdot L \right\} \right]^{\frac{1}{2}} \dots \text{(44)}$$

If we plot the pressure drop expression (43), for different values of L on top of the experimental results we get following trend (figure 66).

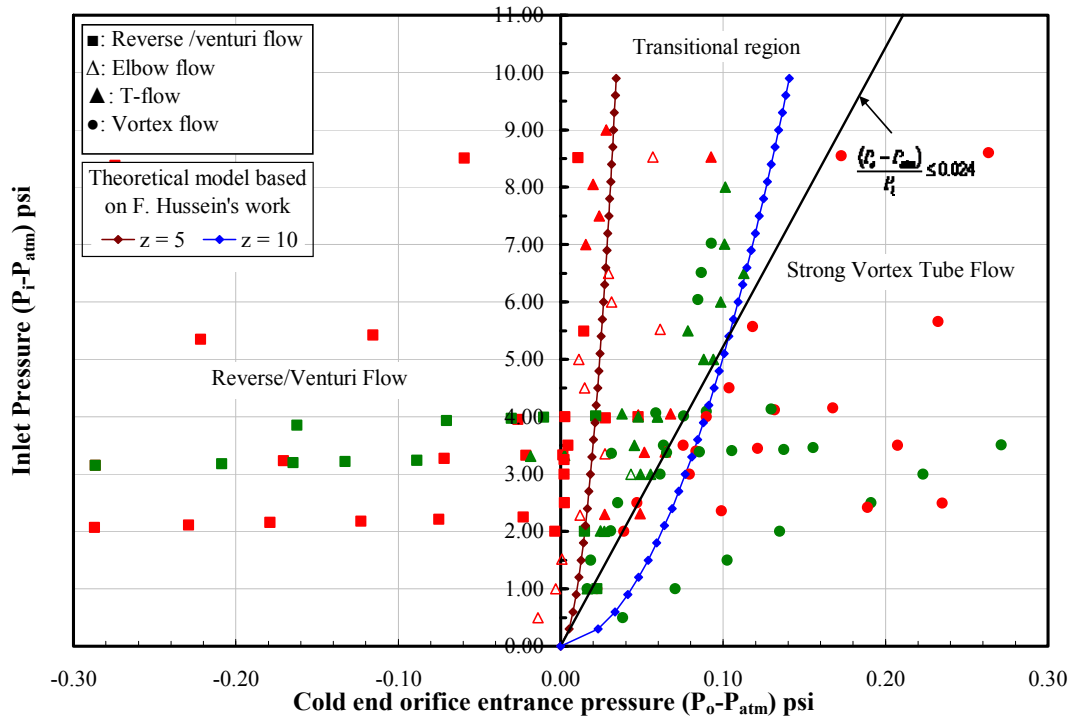


Figure 66: The effect of axial stagnation point location on the pressure drop across the cold end side. [z = the location of the axial stagnation point from inlet in inches, Vortex tube length is 10 inches].

- For a constant inlet pressure (P_i), as we move the axial stagnation point downstream (by increasing z in equation 42), we see increase in pressure drop across the cold end side. This means; depending upon the location of an axial stagnation point, cold fraction changes.
- For a fixed axial stagnation point location (constant z), ($P_o - P_{atm}$) and P_i (equation 42) behave qualitatively similar to the experimental data. As shown in figure 66, at higher inlet pressures we require higher and higher ($P_o - P_{atm}$) (or simply P_b) to achieve stronger energy separation inside the vortex tube.

Chapter 8 Bibliography

1. Piotr A. Domanski: Theoretical evaluation of the vapor compression cycle with a liquid-line/ suction-line heat exchanger, economizer, and ejector, NISTIR 5606, March 1995.
2. Selin Arslan: Vortex tube applications in Micro-Power generation, Rutgers University, Master's dissertation, 2002
3. Sachin U. Nimbalkar: Optimizing vortex tube performance, Dept. of Mechanical & Aerospace Engineering, Rutgers University, Master's dissertation, 2005.
4. Keller, J. U., et al. The Vortex Tube : A Note on its Physical Foundations and New Applications in Energy- and Chemical Engineering, Int. J. of Thermal Sciences, in Vorbereitung, 2002.
5. T. Amitani, T. Adachi, T.A. Kato, Study on temperature separation in a large vortex tube, Transactions of the Japan Society of Mechanical Engineers 48 (1983), pp-877-884.
6. H. Takahama. Studies on vortex tubes (1) experiments on efficiency of energy separation (2) on profiles of velocity and temperature. Bulletin of JSME, 8(31):433–440, 1965.
7. H. Takahama, H. Kawamura, S. Kato, and H. Yokosawa. Performance characteristics of energy separation in a steam-operated vortex tube. Int. J. Engng Sci., 17:735–744, 1979.
8. H. Takahama and H. Yokosawa. An experimental study of vortex tubes (where the vortex chamber includes a divergent tube). Research, 1981.
9. M. Sibulkin. Unsteady, viscous, circular flow part 3. application to the Ranque-Hilsch vortex tube. J. Fluid Mech., 12:269–293, 1961.
10. Bruun H. H, Experimental Investigation of the Energy Separation in Vortex Tubes. Journal of Mechanical Engineering Science 11 (6) 1969, 567 - 82.
11. K. Stephan, et. al. An investigation of energy separation in a vortex tube, International J. of Heat and Mass Transfer, Vol. 26, No.3, pp. 341-348, 1983.
12. M.H. Saidi, M.S. Valipour: Experimental modeling of vortex tube refrigerator, App. Thermal Engg. April 2003.
13. Exair.com. <http://www.exair.com/vortextube/vt page.htm>.
14. B. A. Kashiwa and Corey B. Kashiwa, The solar cyclone: A solar chimney for harvesting atmospheric water, Energy, Vol.33, Issue 2, 2008, pp-331-339.
15. J. Schlaich, The solar chimney: electricity from the sun, Edition Axel Menges, Stuttgart (1995).
16. T.G. Kreutz, R.H. Williams: Production of Hydrogen and electricity from coal with CO₂ capture. 6th Greenhouse Gas Tech. Conf., Kyoto, Japan, September 2002.
17. Piralishili, Sh. A and Fuzeeva, A. A., Hydraulic characteristics of Ranque-Hilsch energy separators, High Temperature, Vol. 43, No. 6, 2005, pp-900-907.
18. C.U. Linderstrom-Lang. On gas separation in Ranque-Hilsch vortex tubes. Z. Naturforsch., 22(a):835–837, April 1967.

19. J. Marshall. Effect of operating conditons, physical size and fluid characteristics on the gas separation performance of a Linderstrom-Lang vortex tube. *Int. J. Heat Mass Transfer*, 20:227–231, 1977.
20. K.T. Raterman, M. Mckellar, A. Podgomey, D. Stacey, and T. Turner. A vortex contactor for carbon dioxide separations. In *First National Conference on Carbon Sequestration*. National Energy Technology Laboratory, U.S.A., [http://www.netl.doe.gov/publications/proceedings/01/carbon seq/7b3.pdf](http://www.netl.doe.gov/publications/proceedings/01/carbon%20seq/7b3.pdf), May 2001.
21. M.R. Kulkarni and C.R. Sardesai. Enrichment of Methane concentration via separation of gases using vortex tubes. *J. Energy Engrg*, 128(1):1–12, April 2002.
22. N.V. Poshernev and I.L. Khodorkov. Natural-gas tests on a conical vortex tube (CVT) with external cooling. *Chemical and Petroleum Engineering*, 40(3-4):212–217, March 2004.
23. R.L. Collins and R.B. Lovelace. Experimental study of two-phase propane expanded through the Ranque-Hilsch tube. *Trans. ASME, J. Heat Transfer*, 101:300–305, May 1979.
24. R.T. Balmer. Pressure-driven Ranque-Hilsch temperature separation in liquids. *Trans. ASME, J. Fluids Engineering*, 110:161–164, June 1988.
25. T. Cockerill. Ranque-Hilsch vortex tube. Master thesis, University of Cambridge, 1995.
26. R. Hilsch. The use of the expansion of gases in a centrifugal field as cooling process. *Rev. Sci. Instrum.*, 18(2):108–113, 1947.
27. Ahlborn B, Groves S. Secondary flow in a vortex tube, *Fluid Dynamics Research*, Volume 21, 1997, pp. 73-86.
28. C.M. GAO, K.J. Bosschaart, J.C.H. Zeegers, and A.T.A.M. de Waele. Experimental study on a simple Ranque-Hilsch vortex tube. *Cryogenics*, 45(3):173, 2005.
29. H. Takahama and K. Kawashima. An experimental study of vortex tubes. *Research*, 1960.
30. J.P. Hartnett, E.R.G. Eckert, Experimental study of the velocity and temperature distribution in a high velocity vortex tube flow, *Trans. Am. Soc. Mech. Engrs., Series C, J. Heat Transfer* 79 (1976) 751–758.
31. Smith Eiamsa-ard and P. Promvonge, Numerical simulation of flow field and temperature separation in a vortex tube, *International communications in Heat and Mass Transfer*, Vol 35, 2008, pp-937-947.
32. A. Gutsol. The Ranque effect. *Physics-Uspekhi*, 40(6):639–658, 1997.
33. A.I. Leont'ev. Gas-dynamic methods of temperature stratification (a Review). *Fuild Dynamics*, 37(4):512–529, 2002.
34. M.G. Ranque. Method and apparatus for obtaining from a fluid under pressure two currents of fluid at different temperatures. US Patent No. 1952281, March 1934.
35. C.D. Fulton. Comments on the vortex tube. *J. ASRE Refrigerating Engng*, 58:984, 1950.
36. G.W. Scheper. The vortex tube–internal flow data and a heat transfer theory. *J. ASRE Refrigerating Engng*, 59:985–989, 1951.
37. J.E. Lay. An experimental and analytical study of vortex-flow temperature separation by superposition of spiral and axial flow, part II. *Trans. ASME J. Heat Transfer*, 81:213–222, Aug. 1959.

38. F. Kreith and D. Margolis. Heat transfer and friction in turbulent vortex flow. *Flow, Turbulence and Combustion*, 8(1):457 – 473, January 1959.
39. R.Z. Alimov. Flow friction and heat and mass transfer in a swirled flow. *Journal of Engineering Physics and thermophysics*, 10(4):251 – 257, April 1966.
40. A.J. Reynolds. Studies of Rotating fluids a) Plane Axisymmetric Flow, b) Forced Oscillations in a Rotating fluid, c) The Ranque-Hilsch Vortex Tube. PhD dissertation, University of London, September 1960.
41. A.J. Reynolds. A note on vortex-tube flow. *J. Fluid Mech.*, 14:18–20, 1962.
42. R.G. Deissler and M. Perlmutter. Analysis of the flow and energy separation in a turbulent vortex. *Int. J. Heat Mass Transfer*, 1:173–191, 1960.
43. J.J. van Deemter. On the theory of the Ranque-Hilsch cooling effect. *Appl. Sci. Res.*, 3:174–196, 1951.
44. W.S. Lewellen. A solution for three-dimensional vortex flows with strong circulation. *J. Fluid Mech.*, 14:420–432, 1962.
45. B B Parulekar. The Short Vortex Tube.. *Journal of Refrigeration*, vol 4, 1961, pp 74-80.
46. M. Kurosaka. Acoustic streaming in swirling flow and the Ranque-Hilsch (vortex-tube) effect. *J. Fluid Mech.*, 124:139–172, 1982.
47. G.F. Nellis N.F. Aljuwayhel and S.A. Klein. Parametric and internal study of the vortex tube using a cfd model. *International Journal of Refrigeration*, 28(2):442–450, 2005.
48. J.J. van Deemter. On the theory of the Ranque-Hilsch cooling effect. *Appl. Sci. Res.*, 3:174–196, 1951.
49. Sachin U. Nimbalkar, Michael R. Muller, An experimental investigation of the optimum geometry for the cold end orifice of a vortex tube, *Applied Thermal Engineering*, In Press, Corrected Proof, Available online 25 March 2008,
50. Herrada M. A. and et. al, Vortex breakdown in compressible flows in pipes, *Physics of fluids*, Vo. 15, 2003, pp. 2208-2218.
51. B. Ahlborn, J. Camire, and J.U. Keller. Low-pressure vortex tubes. *J. Phys. D: Appl. Phys.*, 29:1469–1472, 1996.
52. F. Hussain, et.al. Vortex sinks with axial flow: solutions and applications, *Physics of fluids*, Vol. 9, 1997, pp. 2941-2959.
53. Sarpkaya, T., On stationary and traveling vortex breakdowns, *Journal of fluid mechanics*, vol. 45, pp. 545-559.
54. S. Nimbalkar, M. Muller, An experimental investigation of the optimum geometry for the cold end orifice of a vortex tube, *Applied Thermal Engineering*, Volume 29, issues 2-3, pp. 509-514.

References not directly referred in this thesis

55. B. Ahlborn and J.M. Gordon. The vortex tube as a classic thermodynamic refrigeration cycle. *J. Appl. Phys.*, 88(6):3645–3653, 2000.
56. G. Kh. Step and M. V. Petrovichev: Pressure swing adsorption for air separation and purification, *Chemical and Petroleum Engineering*, Vol.38, Nos. 3-4, 2002.
57. Khodorkov I.L.; Poshernev N.V.; Zhidkov M.A.: The vortex tube – a universal device for heating, cooling, cleaning and drying gases and separating gas mixtures, *Chemical and Petroleum Engineering*, Vol. 39, Issue 7-8, 2003.
58. Long Fu; Guoliang Ding: Steady-state simulation of screw liquid chillers, *Applied thermal engineering*, 22, 2002, 1731-1748.
59. R.F. Boucher and J.R. Tippetts. Vortex tube driven thermo-electricity. In Sixth triennial international symposium on Fluid Control, Measurement and Visualization, 6th, Sherbrooke, Canada, Paper 50, August 2000.
60. Method of natural gas liquefaction. Russia patent No. 2202078 C2, April 2003.
61. R. Westley. Vortex tube performance data sheets. Cranfield College Note 67, College of Aeronautics, 1957.
62. R. Westley. A bibliography and survey of the vortex tube. Cranfield College Note 9, College of Aeronautics, 1954.
63. K.G. Hellyar. Gas liquefaction using a Ranque-Hilsch vortex tube: Design criteria and bibliography. Report for the degree of Chemical Engineer, September 1979.
64. R. Westley. Optimum design of a Vortex Tube for achieving larger temperature drop ratios. Cranfield College Note 30, College of Aeronautics, 1955.
65. H. Takahama and N. Soga. Studies on vortex tubes (2nd report): Reynolds number. The effects of the cold air rate and the partial admission of nozzle on the energy separation. *Bulletin of JSME*, 9(33):121–130, 1966.
66. H. Takahama and etc. Studies on vortex tubes (3rd report): Variations of velocity, temperature and energy with axial distance, the mechanism of energy separation. *Bulletin of JSME*, 235:503–510, 1966.
67. H. Takahama and H. Yokosawa. An experimental study of vortex tubes (where the vortex chamber includes a divergent tube). *Research*, 1981.
68. H. Takahama and H. Yokosawa. Energy separation in vortex tubes with a divergent chamber. *Trans. ASME, J. Heat Transfer*, 103:196–203, May 1981.
69. Y.D. Raikii and L.E. Tunkel. Influence of vortex-tube configuration and length on the process of energetic gas separation. *Journal of Engineering Physics and Thermo-physics*, 27(6):1578 – 1581, December 1974.
70. A.I. Gulyaev. Investigation of conical vortex tubes. *Journal of Engineering Physics*, 10(3):193–195, 1966.
71. V.A. Safonov A.I. Borisenko and A.I. Yakovlev. The effect of geometric parameters on the characteristics of a conical vortex cooling unit. *Journal of Engineering Physics and Thermo-physics*, 15(6):1158–1162, 1968.
72. N.V. Poshernev and I.L. Khodorkov. Experience from the operation of a conical vortex tube with natural gas. *Chemical and Petroleum Engineering*, 39(9-10):602–607, September 2003.
73. L.M. Dyskin. Characteristics of a vortex tube with detwisting of cold flow. *Journal of Engineering Physics and Thermophysics*, 57(1):756–758, July 1989.

74. R.W. James and S.A. Mashall. Vortex tube refrigeration. Refrigeration and air conditioning, pages 69–88, June 1972. Part 2.
75. D.W. Guillaume and J.L. Jolly. Demonstrating the achievement of lower temperatures with two-stage vortex tubes. Review of Scientific Instruments, 72(8):3446–3448, August 2001.
76. J.G. Chu. Acoustic streaming as a mechanism of the Ranque-Hilsch effect. PhD dissertation, University of Tennessee, Knoxville, Dec. 1982.
77. H. Kuroda. An experimental study of temperature separation in swirling flow. PhD dissertation, University of Tennessee, Knoxville, Dec. 1983.
78. R. MacGee Jr. Fluid action in the vortex tube. J. ASRE Refrigerating Engng, 58:974–975, 1950.
79. J.L. Smith Jr. An experimental study of the vortex in the cyclone separator. Trans. ASME, J. B. Engng, 84:602–608, Dec. 1962.
80. J.L. Smith Jr. An analysis of the vortex flow in the cyclone separator. Trans. ASME, J. B. Engng, 84:609–618, Dec. 1962.
81. W. A. Scheller and G. Martin Brown. The Ranque-Hilsch vortex tube. Fluid Mechanics in Chemical Engineering, 49(6):1013–1016, 1957.
82. J.P. Holman and G.D. Moore. An experimental study of vortex chamber flow. Trans. ASME, J. B. Engng, 83:632–636, Dec. 1961.
83. A.I. Leont'ev. Gas-dynamic methods of temperature stratification (a Review). Fluid Dynamics, 37(4):512–529, 2002.
84. C.D. Fulton [37]. Ranque's tube. J. ASRE Refrigerating Engng, 58:473–479, 1950.
85. A.J. Reynolds. On the dynamics of turbulent vortical flow. Z. angew. Math. Phys., 12:149–158, 1961.
86. Q.H. Wu. The internal process analysis and the experimental investigation on the Ranque-Hilsch vortex tube. Master thesis, Xi'an Jiaotong University, Xi'an, China, 1991.
87. J.B. Yang. Mathematical model of vortex tube and experimental study of optimizing performance parameters in vortex tube. Master thesis, Xi'an Jiaotong University, Xi'an, China, 1991.
88. Y.B. Zhang. The theoretical and experimental study on vortex tube. Master thesis, Xi'an Jiaotong University, Xi'an, China, 1993.
89. Y. Zimmels (2002), "Design criteria for compressed air storage in hard rock" – Energy & Environment, Vol.13, No.6.

CURRICULUM VITA

SACHIN UTTAMRAO NIMBALKAR

EDUCATION

May, 2009 - PhD (Doctor of Philosophy) in Mechanical & Aerospace Engineering, Rutgers, The State University of New Jersey, NJ.

May, 2005 - M.S. (Master in Science) in Mechanical & Aerospace Engineering, Rutgers, The State University of New Jersey, NJ.

May, 2001 - B.E (Bachelor of Engineering) in Mechanical Engineering, Government College of Engineering, Pune, India.

PRINCIPAL OCCUPATION & POSITIONS

March 2008 to present, Postdoctoral Research Associate, Oak Ridge Associated Universities (ORAU), Oak Ridge, TN

Jan 2003 to March 2008, Graduate Research Assistant, Center for Advanced Energy Systems (CAES), Rutgers University, NJ

Sept. 2007 to Dec. 2007, Teaching Assistant, Dept. of Mechanical & Aerospace Engineering, Rutgers University, NJ

PUBLICATIONS

- A note on an optimum cold end orifice diameter of a vortex tube, Applied Thermal Engineering, 2008, Volume 29, issues 2-3, pp. 509-514.
- CHP Project Design: Cost benefits of dispatching versus baseline mode of operations, ACEEE Conference, White Plains, New York –July 2007
- Utilizing “waste pressure” in industrial systems, Energy: Production, distribution and conservation, ASME-ATI Conference, Milan, Italy –May 2006